

---

# **Modellverifikation eines Zweiradfahrzeugs anhand Mehrkörpersimulationen und Experimente**

## **Model Validation for a Two-Wheeled Vehicle using Multibody Simulation and Experimental Data**

---

**Master Thesis LRS-MA18/05**

**Rizwan Ahmed Afzal**

**Department of Electrical and Computer Engineering  
Institute of Control Systems**

**Thesis advisor:**

**MSc. Alen Turnwald**



**December 20, 2018**



## Declaration

I, Rizwan Ahmed hereby declare that the thesis titled ***Model Validation for a Two-Wheeled Vehicle using Multibody Simulation and Experimental Data***, is the original work done by me. All the points taken from the published and unpublished writings are cited as such

Kaiserslautern, December 20, 2018

---

Rizwan Ahmed

## Acknowledgements

First and foremost I would like to thank my thesis advisor *MSc. Alen Turnwald* who has actively guided me through-out the thesis work. His advice and contributions made the successful completion of the objectives laid down in this thesis.

Furthermore, I would like to thank Prof. Steven Liu and all members of the *Institute of Control Systems, TU Kaiserslautern*.

Finally, I would like to thank my parents and brothers for the emotional support and everything else. Thank you.

# Contents

<b>List of figures</b>	<b>XII</b>
<b>List of tables</b>	<b>XIII</b>
<b>1 Introduction</b>	<b>5</b>
1.1 Objectives . . . . .	6
1.2 Outline of the Thesis . . . . .	6
<b>2 Preliminaries</b>	<b>9</b>
2.1 Time domain analysis of a first order system . . . . .	9
2.1.1 Step response . . . . .	9
2.1.2 Impulse response . . . . .	11
2.2 Stability analysis . . . . .	12
2.2.1 Stability in linear systems . . . . .	12
2.2.2 Stability in Non-linear systems . . . . .	14
2.3 MATLAB / SimMechanics toolbox . . . . .	16
2.3.1 Analysis in MATLAB / SimMechanics . . . . .	17
<b>3 State of the Art</b>	<b>19</b>
3.1 Literature review on bicycle models . . . . .	19
3.2 Tyre modeling and models in practice . . . . .	20
3.3 Sign convention . . . . .	23
3.4 Tyre material behaviour . . . . .	24
3.5 Generation of forces and moments in a tyre . . . . .	25
3.5.1 Rolling resistance . . . . .	25
3.5.2 Vertical loading in a bicycle wheel . . . . .	25
3.5.3 Longitudinal tyre forces (Brush model) . . . . .	27
3.5.4 Lateral tyre forces (Brush model) . . . . .	29
3.5.5 Self-Aligning Moment . . . . .	31
3.5.6 Turn slip . . . . .	32
3.5.7 Camber Thrust . . . . .	34
3.6 Cornering stability in a slip induced tyre . . . . .	35
3.7 Tyre relaxation length . . . . .	35
<b>4 Multibody modeling</b>	<b>37</b>
4.1 Wheel coordinate system . . . . .	38

---

4.2	Tyre model for generation of tyre forces and moments . . . . .	38
4.3	Body element simulation in SimMechanics . . . . .	39
4.4	Wheel geometry . . . . .	40
4.5	Defining plane normal . . . . .	40
4.6	Wheel vector calculation . . . . .	41
4.7	Tyre model for Multibody application . . . . .	42
4.7.1	Vertical tyre force . . . . .	42
4.7.2	Defining slips . . . . .	43
4.7.3	Longitudinal and lateral tyre forces . . . . .	44
4.7.4	Propagation speed . . . . .	45
4.8	Modeling tyre relaxation behavior . . . . .	46
4.8.1	Longitudinal slip with tyre relaxation . . . . .	46
4.8.2	Lateral slip with tyre relaxation . . . . .	47
4.8.3	Turn Slip with tyre relaxation . . . . .	47
4.8.4	Camber thrust . . . . .	50
4.9	Integrating tyre model in the simulator . . . . .	51
4.10	Construction of physical models in SimMechanics . . . . .	52
4.10.1	Construction of a single wheel model . . . . .	52
4.10.2	Construction of a Tricycle model . . . . .	53
4.10.3	Construction of a Bicycle model in SimMechanics . . . . .	55
<b>5</b>	<b>Multibody Simulation Results</b>	<b>59</b>
5.1	Single wheel model . . . . .	59
5.2	Tricycle model . . . . .	64
5.3	Bicycle validation from linear benchmark model . . . . .	68
5.4	Investigations for testing SimMechanics models . . . . .	69
5.4.1	Investigation 1: With no self-aligning tyres . . . . .	70
5.4.2	Investigation 2: With self-aligning tyres . . . . .	77
5.4.3	Investigation 3: Testing with different bicycle parameters .	80
5.4.4	Investigation 4: Scenarios using feedback . . . . .	88
<b>6</b>	<b>Experimental Investigation</b>	<b>91</b>
6.1	Challenges in measuring the experimental data . . . . .	91
6.2	Experimental setup . . . . .	92
6.3	Experimental tests on a real bicycle . . . . .	95
6.3.1	Investigation 1 . . . . .	95
6.3.2	Investigation 2 . . . . .	97
6.3.3	Investigation 3 . . . . .	100
6.4	Summarizing the observations from experimental investigations .	101
<b>7</b>	<b>Conclusion and Outlook</b>	<b>103</b>
7.1	Future work . . . . .	105

<b>A Appendix: Single Wheel Simulator</b>	<b>107</b>
A.1 Tyre model library . . . . .	109
<b>B Appendix: Tricycle Simulator</b>	<b>115</b>
<b>C Appendix: Bicycle Simulator</b>	<b>119</b>
<b>Bibliography</b>	<b>129</b>



# List of Figures

2.1	Step response of a first order system . . . . .	10
2.2	Impulse response of a first order system . . . . .	11
2.3	Neighborhood of a non-linear system stability . . . . .	14
2.4	Lagrange Stability . . . . .	15
2.5	Lyaponov Stability . . . . .	15
2.6	Asymptotic stability . . . . .	16
3.1	Various tyre models in practice . . . . .	21
3.2	Sign convention used in SimMecahnics environment . . . . .	23
3.3	Equivalent radius of the tyre under compression . . . . .	24
3.4	Pressure variations under the contact patch . . . . .	26
3.5	Vertical loading in a bicycle wheel . . . . .	26
3.6	Brush model for longitudinal tyre force calculation [Pac] . . . . .	27
3.7	Lateral slip angle for a steered wheel . . . . .	31
3.8	Defining lateral slip angle . . . . .	31
3.9	Lateral force and Self-Aligning moment . . . . .	32
3.10	Condition of pure turn slip [Lu13] . . . . .	33
3.11	Lateral compression due to road camber . . . . .	34
4.1	Wheel coordinate frames . . . . .	38
4.2	Tyre model for tyre forces and moments . . . . .	39
4.3	Wheel model in SimMechanics environment . . . . .	40
4.4	Plane normal . . . . .	41
4.5	Wheel element showing vectors along the contact point . . . . .	42
4.6	Horizontal forces at the contact point . . . . .	44
4.7	Plots showing the variation of $C_{M_\phi}$ with $\phi_t$ . . . . .	49
4.8	Plot showing the deviations in wheel trajectories for various stiffness $C_{M_\phi}$ . . . . .	50
4.9	Wheel trajectory for $C_{M_\phi} = 0$ . . . . .	50
4.10	Simulation Data flow in SimMechanics . . . . .	53
4.11	Figures showing the single wheel model built in SimMechanics . . . . .	53
4.12	Figures showing the tricycle model built in SimMechanics . . . . .	54
4.13	Figures showing the bicycle model built in SimMechanics . . . . .	57
5.1	Comparison of wheel trajectories at $v_0 = 1.5m/s$ . . . . .	60
5.2	Comparing cycles at $v_0 = 1.5m/s$ . . . . .	61

---

5.3	Comparing wheel trajectories at $v_0 = 2.5m/s$ . . . . .	61
5.4	Comparing wheel trajectories at $v_0 = 5.0m/s$ . . . . .	62
5.5	Comparing wheel trajectories with friction at $v_0 = 2.0m/s$ . . . . .	63
5.6	Comparing wheel trajectories with friction at $v_0 = 5.0m/s$ . . . . .	63
5.7	Construction of SimMechanics tricycle model with a pendulum attached . . . . .	64
5.8	Input steering torque and output steering angle . . . . .	65
5.9	Trajectory of a tricycle for tyre with $M_\phi$ . . . . .	65
5.10	Pendulum angle and measured torque for tricycle with $M_\phi$ . . . . .	66
5.11	Trajectory of a tricycle for tyre with no $M_\phi$ . . . . .	66
5.12	Input steering torque and output steering angle for tyre with no $M_\phi$ . . . . .	67
5.13	Pendulum angle and measured torque of tricycle for tyre with no $M_\phi$ . . . . .	67
5.14	Phase lag between $\varphi$ and $\delta$ . . . . .	71
5.15	Investigation 1: Weave mode at $v = 4.3m/s$ . . . . .	71
5.16	Investigation 1: Stabilization of weave motion at $v_w = 4.4m/s$ . . . . .	72
5.17	Investigation 1: Self-stable mode at $v_0 = 4.5m/s$ . . . . .	72
5.18	Investigation 1: Self-stability at higher velocities . . . . .	73
5.19	Investigation 1: Capsize velocity at $v_0 = 6.5m/s$ . . . . .	74
5.20	Investigation 1: Capsize mode at higher velocities . . . . .	75
5.21	Investigation 1: Bicycle trajectory at higher capsizing velocities . . . . .	75
5.22	Investigation 1: Non-minimal phase behavior . . . . .	76
5.23	Investigation 1: Trajectory of non-minimal phase behavior . . . . .	76
5.24	Investigation 2: Weave mode instability at $v_0 = 4.4m/s$ . . . . .	77
5.25	Investigation 2: Trajectory at weave velocity $v_0 = 4.4m/s$ . . . . .	78
5.26	Investigation 2: Weave velocity at $v_0 = 4.6m/s$ . . . . .	78
5.27	Investigation 2: Capsizing mode at $v_0 = 9.5m/s$ . . . . .	79
5.28	Investigation 2: Capsizing mode trajectory at $v_0 = 9.5m/s$ . . . . .	79
5.29	Investigation 2: Self-stability at $v_0 = 5.0m/s$ . . . . .	79
5.30	Investigation 2: Increase in weave velocity with stiffer tyres . . . . .	80
5.31	Construction of blue bike in SimMechanics . . . . .	80
5.32	Blue bike: Weave velocity stabilization at $v_w = 5.9m/s$ . . . . .	81
5.33	Blue bike: Stable capsizing mode at higher velocities . . . . .	82
5.34	Blue bike: Capsizing velocity $v_w = 11.5m/s$ for tyre with $M_\phi = 0$ . . . . .	82
5.35	Construction of the red bike in SimMechanics . . . . .	84
5.36	Red bike: Stabilization of weave mode at $v_w = 2.4m/s$ . . . . .	85
5.37	Red bike: Stable capsizing velocity of $v_c = 3.8m/s$ . . . . .	85
5.38	Red bike: Self-Stability at $v = 2.5m/s$ . . . . .	85
5.39	Red bike: Trajectory of non-minimal phase behavior at $v_0 = 2.5m/s$ . . . . .	86
5.40	Red bike: Non-minimal phase behavior at $v_0 = 2.5m/s$ . . . . .	86
5.41	CMG model in SimMechanics for Red bike . . . . .	87
5.42	Scenario 1: Bicycle trajectory with $T_\delta$ as input . . . . .	88
5.43	Scenario 1: Feedback using $T_\delta$ . . . . .	89

---

5.44 Scenario 2: Trajectory of bike while controlling $\varphi$ by applying $T_\varphi$	89
5.45 Scenario 2: Feedback using $T_\varphi$	90
5.46 Scenario 3: Balance of bike at $v = 0m/s$ by applying $T_\delta$	90
6.1 Rotary sensor attached to the front steering handle [Fra17, p.40]	92
6.2 IMU lean sensor attached to the rear frame of the bicycle [Fra17, p.20]	92
6.3 Bicycle showing sensors and measurement unit [Fra17, p.4]	93
6.4 Track where tests for investigations 1 and 2 were conducted	94
6.5 Track where tests for investigations 3 were conducted	94
6.6 Experimental Investigation 1: Full range of experimental data	95
6.7 Experimental Investigation 1: Plots indicating the onset of bicycles self-stability	96
6.8 Experimental Investigation 2: Full range of experimental data	97
6.9 Experimental Investigation 2: Onset of self-stability is highlighted with green ellipse	98
6.10 Experimental Investigation 2: Plots indicating the onset of bicycles self-stability	98
6.11 Experimental Investigation 2: Phase lag between $\delta$ and $\varphi$	99
6.12 Experimental Investigation 2: Full range of experimental data	100
6.13 Experimental Investigation 2: Red box highlights onset of self-stability	101
A.1 Single Wheel: Model overview	108
A.2 Single Wheel: Tyre slips, forces and moment calculation	109
A.3 Single Wheel: Forces and Moments actuation to body element using a Force element	110
A.4 Single Wheel: Wheel vector calculation and slip velocity	111
A.5 Single Wheel: Initial conditions for the simulation	112
A.6 Single Wheel: Initializing wheel geometrical parameters	112
A.7 Single Wheel: Initializing tyre parameters	112
A.8 Single Wheel: Initializing friction at the wheel bearings	113
A.9 Single Wheel: Results from the scope block	113
B.1 Overview of a tricycle model built in SimMechanics	115
B.2 Tricycle: Initializing simulation initial conditions	116
B.3 Tricycle: Initializing tyre parameters	116
B.4 Tricycle: Actuating steering	117
B.5 Tricycle: Steering Torque	117
B.6 Tricycle: Visualizing simulation in Mechanics explorer	118
C.1 Blue bike: Model overview	119
C.2 Blue bike: Fundamental construction of a bicycle	120
C.3 Blue bike: Ground parameters	120

C.4 Blue bike: Adjusting tyre parameters . . . . .	120
C.5 Blue bike: Initial condition on velocity . . . . .	121
C.6 Blue bike: Input lateral disturbance . . . . .	121
C.7 Bicycle: Feedback using $T_\varphi$ . . . . .	122
C.8 Bicycle: Feedback using $T_\delta$ . . . . .	122
C.9 Bicycle: Feedback using $T_\delta$ for balance at $v = 0m/s$ . . . . .	123
C.10 Bicycle: Feedback using $T_\varphi$ for hands free riding in a curve . . . . .	123
C.11 Bicycle: Feedback using $T_\delta$ for riding in a curve . . . . .	124
C.12 Bicycle: Calculation of leaning angle $\varphi$ . . . . .	125
C.13 Blue bike: Visualization in Mechanics explorer . . . . .	126

# List of Tables

4.1	Benchmark Parameters for bicycle model in SimMechanics . . . . .	56
4.2	Tyre Parameters for bicycle model in SimMechanics . . . . .	57
5.1	Wheel parameters for a single wheel simulation . . . . .	59
5.2	Tyre parameters considered for a single wheel simulation . . . . .	60
5.3	Eigen modes of the bicycle . . . . .	68
5.4	Summary of various investigations to be carried out with SimMechanics models . . . . .	70
5.5	Design parameters of blue bike . . . . .	81
5.6	Design parameters of red bike . . . . .	83
5.7	Tyre parameters for the red bike . . . . .	84



# Nomenclature

## Abbreviations

<b>3D</b>	Three dimensional
<b>CAD</b>	Computer Aided Design
<b>CMG</b>	Control moment gyroscope
<b>DAE</b>	Differential Algebraic Equations
<b>DOF</b>	Degrees of freedom
<b>EoM</b>	Equations of motion
<b>ODE</b>	Ordinary Differential Equations

## Small letters

$a_N$	Centripetal acceleration	$m/s^2$
$c$	Trail of the bicycle	$m$
$d$	Wheel penetration	$m$
$e_{\text{long}}$	Longitudinal direction unit vector	$m$
$e_{\text{lat}}$	Longitudinal direction unit vector	$m$
$e_{\text{Axis}}$	Wheel axis unit vector	$m$
$g$	Acceleration due to gravity	$m/s^2$
$m_B$	Mass of rear frame	$kg$
$m_H$	Mass of front frame	$kg$
$m_{FW}$	Mass of front wheel	$kg$
$m_{RW}$	Mass of rear wheel	$kg$
$p$	Contact point of the wheel on the ground	
$q$	Generalized coordinates	$m$
$\dot{q}$	Generalized velocities	$m/s$
$r_e$	Effective radius of the tyre	$m$
$w$	Wheel base of the bicycle	$m$
$x$	Body-coordinate	$m$
$y$	Body-coordinate	$m$
$z$	Body-coordinate	$m$

## Big letters

$B_{xyz}$	Body-fixed frame of reference	
$C_{F_\alpha}$	Lateral stiffness	$N/m$
$C_{F_\kappa}$	Longitudinal stiffness	$N/m$
$C_{M_\phi}$	Self-Aligning stiffness due to turn slip $\phi_t$	$N/m/(rad/m)$
$\mathbf{F}_{\text{camber}}$	Camber force	$N$
$\mathbf{F}_{\text{long}}$	Longitudinal force	$N$
$\mathbf{F}_n$	Normal force	$N$
$\mathbf{F}_{\text{lat}}$	Lateral force	$N$
$I_{xyz}$	Inertial frame of reference	
$I_B$	Inertia tensor of rear frame	$kg - m^2$
$I_H$	Inertia tensor of front frame	$kg - m^2$
$\mathbf{M}_\phi$	Self-aligning moment due to turn-slip	$N/m$
$P$	Pressure	$Pa$
$V_s$	Slip velocity	$m/s$
$V_x$	Velocity of the center of wheel	$m/s$
$V_{px}$	Propagation velocity	$m/s$
$X$	Reference coordinate in $I_{xyz}$	$m$
$Y$	Reference coordinate in $I_{xyz}$	$m$
$Z$	Reference coordinate in $I_{xyz}$	$m$
$Z_{xyz}$	Body-fixed frame of reference but non-rotating	

## Greek letters

$\alpha$	Lateral slip	
$\delta$	Steering angle	<i>rad</i>
$\dot{\delta}$	Steering rate	<i>deg/s</i>
$\dot{\eta}$	Rear wheel velocity in body fixed frame	<i>m/s</i>
$\kappa$	Longitudinal slip	
$\gamma$	Camber angle	<i>rad</i>
$\lambda$	Steer axis tilt	<i>deg</i>
$\omega$	Angular velocity	<i>rad/s</i>
$\phi_t$	Pure turn-slip ratio	<i>rad/m</i>
$\psi$	Orientation angle	<i>deg</i>
$\dot{\psi}$	Wheel spinning rate about axis normal to the contact point	<i>deg/s</i>
$\sigma$	Tyre relaxation length	<i>m</i>
$\varphi$	Lean or camber angle	<i>deg</i>
$\dot{\varphi}$	Leaning rate	<i>deg/s</i>



# Abstract

This thesis aims at developing a multibody simulator for a bicycle by progressively developing a single wheel model, a tricycle model and finally a bicycle model in Matlab / SimMechanics. The wheel model is validated with the results from no-slip solid disc mathematical model. The tricycle model is used as an intermediate model to investigate the forces that maintain the nonholonomic constraints by the wheels. Finally, the bicycle model is developed which is flexible to be used for investigating bicycles with different design parameters and tyre parameters. The results from the SimMechanics bicycle model is compared with the results from the *Benchmark Bicycle model* and the deviations from the *Benchmark Bicycle model* is compared with the results from Bulsinki et al.,. Finally, the various modes of bicycle's motion are also verified through experimental investigations conducted on a real bicycle.



# Zusammenfassung

Ziel dieser Arbeit ist die Entwicklung eines Mehrkörpersimulators für ein Fahrrad durch allmählich Entwickeln eines Einzelradmodells, eines Dreiradmodells und schließlich eines Fahrradmodells in Matlab / SimMechanics. Das Radmodell wird mit den Ergebnissen aus dem mathematischen Model einer festen Platte ohne Slip validiert. Das Dreiradmodell wird als Zwischenmodell verwendet, um die Kräfte zu untersuchen, die die nicht-holonomischen Beschränkungen durch die Räder aufrechterhalten. Schließlich wird das Fahrradmodell entwickelt, das flexibel für die Untersuchung von Fahrrädern mit unterschiedlichen Design- und Reifenparametern eingesetzt werden kann. Die Ergebnisse aus dem SimMechanics-Fahrradmodell werden mit den Ergebnissen des *Benchmark-Fahrradmodells* und die davon resultierenden Abweichungen mit den Ergebnissen aus Bulsinki et al., verglichen. Schließlich werden die verschiedenartigen Weisen der Bewegung des Fahrrads durch experimentelle auf einem echten Fahrrad geführte Untersuchungen verifiziert.



# 1 Introduction

Since the introduction of safety bicycles in the late 19th century with pneumatic tyres and a chain drive, it was well known in practice that a bicycle can be balanced with a rider. Further a Cambridge undergraduate Francis Whipple used rigid body dynamics to show in theory that some bicycle could essentially balance themselves when moving at right speed range. Typically, a bicycle's balance is well known by two scenarios. One with a rider, when the rider adjusts the steering of the bicycle in the direction of undesired lean, which moves the ground contact points under the rider. In another case, a bicycle balances itself if moving at right speed range, the front steering oscillates damping the oscillation progressively as it stabilizes the lean to zero. In order to investigate such behavior of a bicycle, as well as, other modes such as weave mode and capsize mode along with lateral perturbations, a computerized model is developed in this thesis. Primarily, a multibody model of a bicycle is developed that has two wheels connected through two rigid links as described by a four-body model in *Benchmark Bicycle model* [MPRS07, p.2] by employing a numerical solver **Matlab / SimMechanics**.

With the help of the computerized models, it is easier to run simulations and investigate the motions of complex dynamical systems such as bicycles. Particularly, multibody systems constructed in a simulation environment such as SimMechanics have an advantage over mathematical modeling in the level of complexity that they reduce. The flexibility offered by SimMechanics for physical modeling of mechanical systems in terms of joints and rigid bodies connected through physical connections (also called acasual modeling) hides away the level of complexities through series of abstractions that are otherwise required in mathematical formulations.

Though Matlab's library has a motorcycle model already made available, it is built on the previous version of SimMechanics that is no longer used actively. As a matter of fact, Matlab has also stopped any updates to SimMechanics first generation library, also adding to that fact that it does not provide the user with the visualization that SimMechanics second generation provides. Also, in the popular literature for bicycle modeling, there are various models available that are modeled mathematically [MPRS07], [TL18a] or symbolically [EL00] among others. Additionally, SimMechanics second generation contains a general purpose contact forces library [Mil], the library still lacks a torus to plane type of contact

which is important to establish the tyre-road contact, also the slips used in the library are more general and different than that described specifically in tyre mechanics (Brush Model). Therefore, a custom contact library was created in order to establish this important tyre-road contact. The tyre models developed in this thesis have extensively utilized the theories from [DD10], [den], [Pac]. Particularly, the vector calculus for defining the wheel unit vectors in SimMechanics and *Brush Model* used to develop the slip quantities and the forces associated with them was utilized extensively from [Pac], which were simplified later to fit into the domain of this thesis.

The three SimMechanics models are developed in this thesis. The tyre model is validated with the no-slip mathematical model previously developed at the *Institute of Control Systems, TU Kaiserslautern*. The tricycle model is used as an interim model to help investigate the nonholonomic constraints in the rolling wheels. Finally, the simulations from SimMechanics bicycle model is compared with the *Benchmark Bicycle model* and the observed deviations with different tyre parameters are compared with the results from [BDBK15].

## 1.1 Objectives

The main objective of this thesis is to develop a simulator for bicycle motion simulations with the following objectives:

- Literature research on existing bicycle models and their verifications as well as nonholonomic systems and multibody simulations.
- Development of a multibody simulation of a four-body bicycle model, the wheels are modeled to follow the nonholonomic constraints.
- The self-stabilization behavior of the bicycle to be maintained by the simulation.
- Devising simulation and experimental scenarios for multibody simulation model and Experimental investigations for a real bicycle.
- Validation of multibody model and documentation of the thesis.

## 1.2 Outline of the Thesis

The thesis has been structured into the following chapters:

- **Chapter 2 - Preliminaries:** Analysis on the first order systems required

to describe tyre relaxation length, Formally defining stability analysis for linear and nonlinear systems and Review on SimMechanics Toolbox.

- **Chapter 3 - State of the Art:** Literature review on various bicycle models, Establishes the literature on tyre modeling.
- **Chapter 4 - Multibody Modeling:** Modeling of a single wheel, a tricycle and a bicycle in SimMechanics utilizing the literature established in chapter 3.
- **Chapter 5 - Multibody Simulation Results:** Simulation and validation of the SimMechanics models of a single wheel, tricycle and bicycles of various design parameters and tyre parameters.
- **Chapter 6 - Experimental Investigation:** On conducting experimental investigations on a real bike and generating results of bicycle's motion through sensor data.
- **Chapter 7 - Conclusion and Outlook:** Conclusion of the thesis, summarizing the results and ideas for the future work.
- **Appendices A,B and C - SimMechanics Models:** A user manual for the SimMechanics models: (A) single wheel, (B) tricycle and (C) bicycle.



## 2 Preliminaries

The dynamic behavior of the tyres for generating tyre forces and moments, called *Tyre Relaxation Length* is modelled as a first order response of the system as described in [MP97]. In order to understand the response of the first order systems, a brief description is given in this section on their modeling and analysis.

Further, as the thesis covers the topics on bicycle self-stability, stability analysis for linear and non-linear systems is formally defined later in this section. Also, a description of SimMechanics toolbox is given which is used as a numerical tool to build and analyze various models described in this thesis.

### 2.1 Time domain analysis of a first order system

The dynamic behavior due to tyre relaxation length can be studied by analyzing the response of a first order system described by equation (3.24). First order systems are the simplest form of dynamic systems. The canonical form of the first order system is expressed as [MT18]:

$$\tau \dot{y}(t) + y(t) = k_{dc} u(t) \quad (2.1)$$

the above equation can be expressed as transfer function in the Laplace domain [MT18]:

$$G(s) = \frac{Y(s)}{U(s)} = \frac{k_{dc}}{\tau s + 1} \quad (2.2)$$

where,  $\tau$  and  $k_{dc}$  are the parameters that completely define the response characteristics of a first order system and are called time constant and DC gain respectively.

#### 2.1.1 Step response

The object is to find the solution to the differential equation  $y(t)$  as given by the equation (2.1). This system with a unit step input  $u(t) = 1$  can be expressed in the Laplace domain as:

$$Y(s) = G(s)U(s) = \frac{k}{\tau s + 1} \frac{1}{s} \quad (2.3)$$

where  $k$  is the DC gain of the system, simplifying the above equation for the two poles  $s$  and  $(s + 1)$  and taking the inverse Laplace leads to the following solution:

$$y(t) = k - ke^{-t/\tau} \quad (2.4)$$

where the first term is the particular solution and the second term is the null solution of the differential equation (2.1). From the solution (2.4), it can be seen that at time  $t = \infty$  the particular solution remains constant at  $k$  and the null solution should approach an exponential decay to *zero*. For an example system with  $k_{dc} = 5$  and  $\tau = 10$ , a plot from numerical solution in MATLAB exhibits results as expected for a unit step input as shown in figure 2.1.

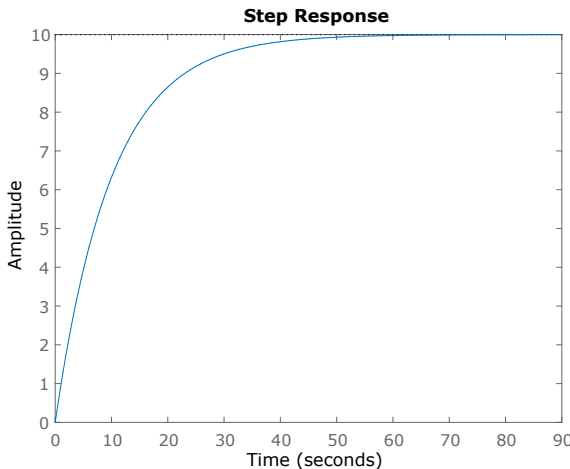


Figure 2.1: Step response of a first order system

From the plot 2.1, the DC gain can be inferred from the steady-state value reached by the system. For a unit step input, the DC gain is given by the step-up value at which the output of the system's response settles down, in this case,  $k = 5$  which is evident from the system value chosen to generate this plot. The time constant  $\tau$  can be inferred from plot and equation (2.4), for time  $t = \tau$ :

$$y(t) = k(1 - e^{-1}) = 0.632k \quad (2.5)$$

therefore, at one time constant  $\tau$ , the systems response settles down to about 63.2% of the steady-state vale. Generally, a steady-state response is fixed when this value reaches 98% of steady-state value, which from the plot and equation (2.1) can be inferred as at time  $t = 4\tau$ :

$$y(t) = k(1 - e^{-4}) = 0.98k \quad (2.6)$$

### 2.1.2 Impulse response

Consider a unit impulse as input to the first order system. The Laplace transform of the impulse signal is given by  $L(s) = 1$ . Therefore, the first order system with an impulse input is expressed as:

$$Y(s) = G(s)U(s) = \frac{k}{\tau s + 1} \cdot 1 \quad (2.7)$$

the inverse Laplace of the equation (2.7) will express the solution of the equation of the differential equation (2.1) with an unit impulse input:

$$y(t) = \frac{k}{\tau} e^{-\frac{t}{\tau}} \quad (2.8)$$

The above equation is the null solution of the differential equation (2.1) given as  $y = Ce^{at}$  with initial condition  $C = k/\tau$  and  $a = -1/\tau$ . From the solution (2.8) it can be inferred that for an unit impulse, the response of the system at time  $t = \infty$  is to settle down to zero with an exponential decay. From a numerical solution generated in MATLAB, the response decays to zero as shown in figure 2.2.

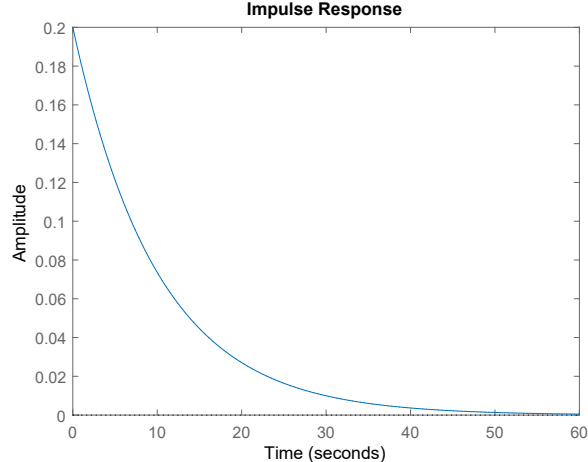


Figure 2.2: Impulse response of a first order system

## 2.2 Stability analysis

Once a model of a system has been established, it may be required to analyze the model in order to determine the response of the system, in this case in the time domain. In the perspective of a control design, the control system is often designed to improve the stability of the system, improve the speed of the response or the steady-state error, or prevent oscillations. Therefore, it is necessary to determine the dynamic properties of the system from the system model [MT18]. In this section, stability is defined formally for linear and non-linear systems (such as a bicycle), leading up to the asymptotic stability (self-stability) of the bicycle.

### 2.2.1 Stability in linear systems

For defining the important concepts in stability analysis, a simple second order linear and homogeneous system is considered as described below:

$$\ddot{y} + B\dot{y} + Cy = 0 \quad (2.9)$$

For a special case of the solution when  $y = e^{st}$ , the above equation can be re-written as:

$$s^2 + Bs + C = 0 \quad (2.10)$$

the roots of the above equation are given by:

$$\{s_1, s_2\} = \frac{-B \pm \sqrt{B^2 - 4C}}{2} \quad (2.11)$$

and the null (homogeneous) solution of the equation (2.9) can be expressed as:

$$y(t) = C_1 e^{s_1 t} + C_2 e^{s_2 t} \quad (2.12)$$

Alternatively, writing equation (2.9) in a matrix form:

$$\frac{d}{dt} = \begin{bmatrix} 0 & 1 \\ -C & -B \end{bmatrix} \begin{bmatrix} y \\ y' \end{bmatrix} \quad (2.13)$$

the above equation can be written in the form:

$$\frac{d}{dt} Z = [A] [Z] \quad (2.14)$$

where  $A$  is called the companion matrix, with roots of the equation found as the Eigen-Values of the matrix  $A$ :

$$\{\lambda_1, \lambda_2\} = \frac{-B \pm \sqrt{B^2 - 4C}}{2} \quad (2.15)$$

and the null solution of the second order differential equation:

$$y(t) = C_1 e^{\lambda_1 t} + C_2 e^{\lambda_2 t} \quad (2.16)$$

Both the null solutions predicted by the roots  $\{s_1, s_2\}$  and Eigen-Values  $\{\lambda_1, \lambda_2\}$  give the solution of the differential equation (2.9), however, with Eigen-values it is much easier to reach at the null solution. From the roots  $\{s_1, s_2\}$  or the Eigen-Values  $\{\lambda_1, \lambda_2\}$ , following cases can be drawn about the stability of the second order system:

Cases	Condition	Eigen-Values
Over-damped	$(B^2 > 4C)$	Negative Real Roots
Critically damped	$(B^2 = 4C)$	Real Roots
Under-damped	$(B^2 < 4C)$	Complex roots
Undamped	$B = 0$	Imaginary Roots

In the cases of system being damped and the real part of the roots lying in the negative real plane, the system is considered stable. In case of under-damped system, the system oscillates into a weave like wave-form and is stable. In case of undamped system, the motion is of purely oscillatory nature with constant wave length.

### 2.2.2 Stability in Non-linear systems

With linear systems, if the system is already in the stable condition, then regardless of the initial conditions, the system will get back to its stable position. However, a non-linear system is stable only if the perturbations lie within a certain range of neighbourhood. Lets consider a non-linear autonomous system expressed as a first order system dependent on velocity:

$$\dot{x} = f(x) \quad (2.17)$$

The equilibrium states can be defined for a non-liner system if it satisfies the condition:

$$\dot{x} = f(x_e) = 0 \quad \forall t > t_0 \quad (2.18)$$

where  $x_e$  is the point at which the function  $f(x) = 0$  and  $x_e = \text{constant}$ . The neighborhood is defined as: Given  $\delta > 0$ , a state vector  $x(t)$  is said to be in the neighborhood  $B_b(x_r(t))$  of the state  $x_r(t)$  if:

$$\|x(t) - x_r(t)\| < \delta \quad (2.19)$$

then,

$$x(t) \in B_\delta(x_r(t)) \quad (2.20)$$

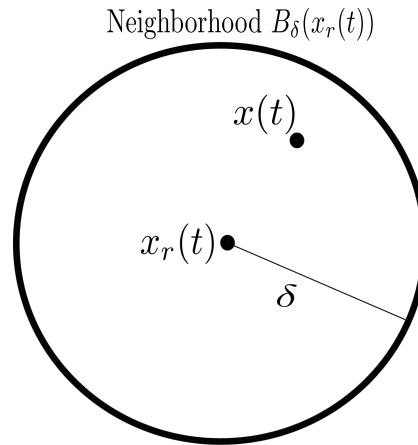


Figure 2.3: Neighborhood of a non-linear system stability

**Lagrange stability** is defined as: the state  $x(t)$  is said to be Lagrange stable (or bounded) relative to  $x_r(t)$  if there exists a  $\delta > 0$  such that:

$$x(t) \in B_\delta(x_r(t)) \quad \forall t > t_0 \quad (2.21)$$

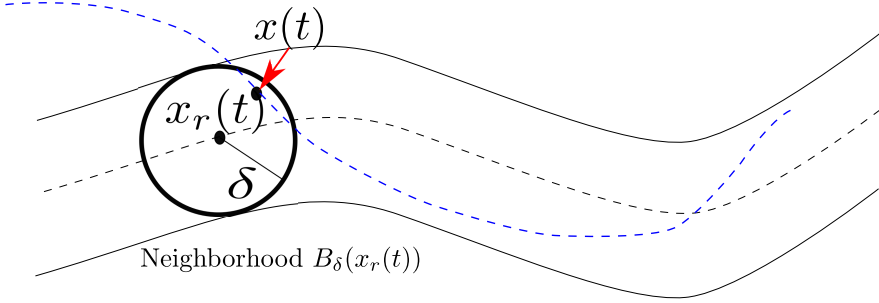


Figure 2.4: Lagrange Stability

**Lyapunov stability** of non-linear system is defined as: the state  $x(t)$  is said to be Lyapunov stable relative to  $x_r(t)$  if for each  $\epsilon > 0$  there exists a  $\delta(\epsilon) > 0$  such that:

$$x(t_0) \in B_\delta(x_r(t_0)) \quad (2.22)$$

$$x(t) \in B_\epsilon(x_r(t)) \quad \forall t > t_0 \quad (2.23)$$

Unlike Lagrange stability, in Lyaponov stability lets to define another neighborhood  $B_\epsilon(x_r(t))$  such that perturbations in the previous neighborhood  $B_\delta(x_r(t_0))$  would lead to  $B_\epsilon(x_r(t))$ , hence, unlike Lagrange stability which does not depend on the initial conditions (but on the physics of the problem) Lyapunov stability narrows down the initial states that could lead to stability in the motion in a later state. Also, unlike in the linear systems, the non-linear systems would lead to convergence just because the system is in the stable condition. The boundary  $B_\epsilon(x_r(t))$  could be very close to  $B_\delta(x_r(t_0))$  and the system would be stable in the  $\epsilon$ . For numerical simulation, it is required that the simulations are run for long enough time to prove that the stability remains within the conditions described by the Lyapunov conditions.

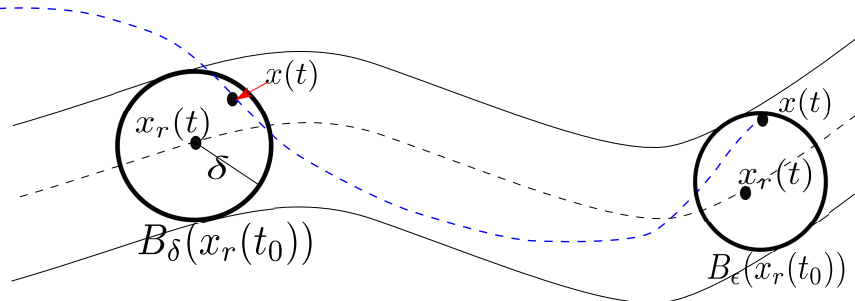


Figure 2.5: Lyapunov Stability

Once Lyapunov stability has been defined, an **Asymptotic stability** can be extended and defined as: the state  $x(t)$  is asymptotically stable relative to  $x_r(t)$  if  $x(t)$  is Lyapunov stable and there exists a  $\delta > 0$  such that:

$$x_0(t) \in B_\delta(x_r(t_0)) \text{ then,} \quad (2.24)$$

$$\lim_{t \rightarrow \infty} x(t) = x_r(t) \quad (2.25)$$

Therefore, in case of asymptotic stability, the boundary due to  $\epsilon$  goes to zero

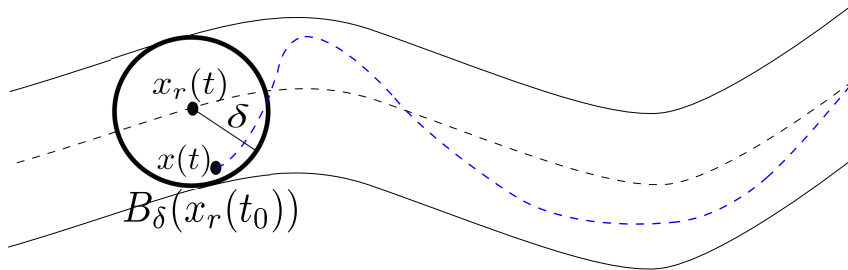


Figure 2.6: Asymptotic stability

and the boundary  $B_\epsilon(x_r(t))$  does not exists anymore, so now the motion  $x(t)$  converges to the reference  $x_r(t)$ . This is an ideal condition to converge to from controls perspective. Certain dynamic systems have shown to converge to this stability point in their natural modes of operation. A bicycle is one such example where under a certain range of velocities the weave motion of the bicycle converges to asymptotic stability by damping (not physically damping like in friction) the weave motion towards a zero lean and steering rates as described in later sections (5.4.1 and 5.4.1).

## 2.3 MATLAB / SimMechanics toolbox

MATLAB/SimMechanics multibody is a toolbox in MATLAB, that solves the equations of motion of dynamic systems based on the abstract representation of a physical model in the form of blocks similar to the ones used on MATLAB/Simulink. Contrary to Simulink where blocks represent mathematical operations, SimMechanics blocks represent the actual physical model of a mechanical system. The connection between the blocks in Simulink is unidirectional representing a causal modeling. In SimMechanics, however, the connections between the blocks are physical which means that the signals travel in either direction of the connection representing an actual physical connection. This makes the entire process of modeling more intuitive and less tedious as the equations of motion are assembled automatically by the solver internally. The environment of SimMechanics also enables direct integration of Simulink blocks as causal signals for implementing observer and control algorithms, mathematical constraints into the physical model and reading out SimMechanics sensor outputs.

### 2.3.1 Analysis in MATLAB / SimMechanics

Three kind of analysis is possible for mechanical systems in MATLAB / SimMechanics [Sch03]:

- **Forward dynamics:** Calculate the motion of the rigid-body / mechanism by the application of external forces and torques at the actuator joints.
- **Inverse dynamics:** Calculate the necessary forces and torques required in the actuator joints in order to produce the specified motion.
- **Kinematics:** Motion constraints can also be given to the actuator joints in terms of displacements.

The mechanics configuration solver interprets the systems mechanical assembly and constraints to SimMechanics. The mathematical aspects of the simulation are interpreted through Simulink's inbuilt solvers. Simulink's solvers interprets only ordinary differential equations (ODE's). The SimMechanics interpreter mechanism configuration solver interprets the mechanical aspects of the system and builds the mathematical model required for integration. The formulation of equations of motion (EoM's) in a multibody system can be expressed in general as follows:

$$g(t) = A(q)\dot{q} = 0 \quad (2.26)$$

$$M(q, t)\ddot{q} = Q(q, \dot{q}, t) + Q^c(q, \dot{q}, t) \quad (2.27)$$

$$\dot{g}(t) = A(q, \dot{q}, t)\ddot{q} - b((q, \dot{q}, t)) \quad (2.28)$$

where,

- Equation (2.26), is called the kinematic constraint equation, both the holonomic and nonholonomic constraints can be expressed in this form.
- $A(q)$  is the constraint coefficient matrix, which is a function of  $q$  (necessary and sufficient condition for holonomics but only necessary condition for nonholonomics)
- Equations (2.26 and 2.27) both described the dynamics of the system.
- Equation (2.28) is the derivative of the constraint equation, it is required for finding the Lagrange multiplier  $\lambda$ .

Equations (2.27 and 2.27) form the *Differential Algebraic Equations (DAE's)*. As Simulink's solvers only solves ODE's, in SimMechanics the DAE's are transformed into ODE's through various constraint reduction techniques. One of the techniques is to solve for *Lagrange Multiplier*  $\lambda$  using equation (2.28) [Sch03].



# 3 State of the Art

## 3.1 Literature review on bicycle models

Bicycles display intriguing dynamics such as being statically unstable at zero forward velocity similar to an inverted pendulum, displaying a non-minimal phase behavior (counter-steering) and also the self-stability against lateral perturbations while running at certain velocities. Intrigued with such dynamical behavior, scientists since the mid of 19th century have come up with various models describing the dynamics of the bicycles. One such early model is described in Drais [MPRS07] who is credited for inventing the two wheeled vehicle and showed that a rider could balance such a vehicle by controlling the steering. Also the Whipple model [Whi99] that describe the stability of the bicycle through deriving linearized equations of motion. Among the most recent available literature, a so-called *Linear Benchmark Model* from Meijaard et al. [MPRS07] described by a linear velocity parameter varying system. The *Linear Benchmark Model* serves as a basis for systematic analysis of the various modes of the bicycles motion as described by the four distinct Eigenmodes [MPRS07, p.15]. Further, from the linearized model, the controllability of the bicycles was analyzed by applying actuation to steering or the lean through a passive rider as described in [SMK12].

Linear models are generally limited for a range of parameters, for example, the balance of the bicycle at zero forward velocity and riding in a curve through hands free-riding cannot be described by the linear models [TL18c]. Getz [GM] introduced a nonlinear naive bicycle model applying nonholonomic contact constraints to the front and the rear wheels. In which a controller was derived by actuating the steering and the rear wheel torques, to implement a control of balance as well as converging the bicycle to the desired trajectory in the plane [GM]. However, the naive bike model cannot be used for balance at zero forward velocity. Extending from the naive nonlinear bike model from [GM], Turnwald [TL18c] developed a more general bicycle model that considers the shift of the center of mass of the bicycle due to steering, making possible for the balance at  $v = 0$  [TL18a]. Further, the nonlinear model from [TL18c] describes a proper mathematical model for the purpose of trajectory planning, trajectory tracking control and observer design for an autonomous bike. The model includes the nonholonomic constraints at the wheel contact and also describes the phenomena

leading to self-stability of the bicycle.

In this thesis, a multibody bicycle model is developed which would be generally valid, representing vehicle dynamics for every set of parameters such as forward velocity. Further investigating bicycle Eigenmodes from linear models as well as controllability (or ride-ability) from nonlinear models such as in [TL18a] exhibiting possibility of balance at  $v = 0m/s$ , hands-free riding into a curve, riding in a curve by actuating the steering also including the non-minimal phase behavior of the bicycle. The model should include the nonholonomic constraints to be maintained by the wheels as well as maintaining the self-stability of the bicycle in the simulation. Further, the model shall be easily extendable for adding controllers such as a CMG or designing controller and observer algorithms for trajectory tracking control.

## 3.2 Tyre modeling and models in practice

While ignoring the aerodynamic effects, most of the interaction of a vehicle with its environment comes from the tyres attached to it. The forces and moments generated by the vehicle in motion come from the interaction of tyres with the road while the vehicle is accelerating, braking or turning. The modeling of a vehicle, therefore, is strongly dependent on the tyre behavior. This is especially true for bicycles and motorcycles, as the stability of these vehicles prominently depends on the tyre behavior. The quality of the bicycle model that will be developed further in this thesis is strongly dependent on the accuracy of the tyre model implemented. In the following sections, a detailed review of the literature on tyre mechanics is given, in relation to developing a tyre model in SimMechanics environment.

Tyre models are mathematical relationships established between the tyre forces and input slip quantities that describe the behavior of a tyre and help establish the holistic dynamics of the vehicle for the purpose of simulation and testing. Most of the tyre models available today are mainly from the works of H.B.Pacejka from *TU Delft* where a model-based approach was adopted for defining tyre geometry and establishing forces and moments generated by a tyre. Tyre models can be expressed as a relationships between tyre forces and moments and the input slip quantities and deformation:

$$[F_x \ F_y \ F_z \ M_x \ M_y \ M_z]^T = f(\kappa, \alpha, \phi_t, d) \quad (3.1)$$

The tyre mechanics that are described using the brush model are fundamental models that bring out the physics of tyres in motion. Brush models have been helpful in vehicle dynamics to establish the first principles of a tyre behavior

and for deriving mathematics associated with it. However, over time it has been found that though brush models with their good description of physical and mathematical aspects still lack to produce an exact behavior at higher speeds. It has also been found that in tyre modeling, there are always certain aspects of the physical description that is not always captured with the help of the conventional theory of dynamics.

In order to get a more precise description of tyre behavior, it was found that the task at hand was more complicated with the help of theory on dynamics. Rather, empirical and semi-empirical approaches were adopted, where the tyre behavior was fit into a black-box model. One of such important tyre models is Pacejka's *Magic Formula Tyre model* which is widely used in automobile industry. Magic Formula Tyre models can be fit parametrically for a specific type of tyre and vehicle by adjusting the coefficients of the black-box model after conducting experiments.

Magic Formula Tyre models still were an approximation based on experiments and assumptions on road profiles. In order to incorporate a more dynamically advanced model, that encapsulates various low and high-frequency noise, vibrations and disturbances coming from the road and their effect on various automotive components such as timing belts, vibrations and harshness on the vehicle body etc., a more sophisticated model called *SWIFT* model was developed. Figure 3.1 shows the development of tyre models based on the required level of sophistication in the analysis: Lastly, more sophisticated models are also available that are

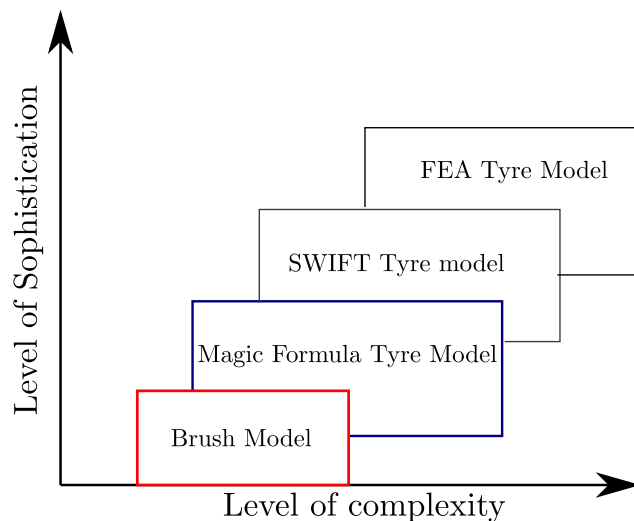


Figure 3.1: Various tyre models in practice

based on *Finite Element Approach (FEA)*. FEA considers the entire geometry of the tyre as close to being a real tyre itself also modeling the road profile and the contact patch between them. With the flexibility FEA provides, entire physical

aspects of the tyre can be included such as establishing the actual contact patch between the tyre and road interface, the non-linear behavior of the tyre material, hysteresis and its effect on rolling resistance, non-linear pressure distribution near the contact patch, micro-slips near the contact patch, temperature distribution among various others factors. FEA provides the most sophisticated numerical model available in the industry today and is the most accurate model developed so far. However, FEA has its own disadvantage, FEA discretizes a system into an extremely large number of elements and integrates their behavior numerically at boundary-conditions. Numerically this approach is quite intensive, complex FEA analysis is known to take even a span of days to complete the analysis and produce results.

As can be seen, in figure 3.1, the level of details that are required to be included in the analysis, increases the level of complexity of analysis and costs associated with them. For the analysis based on this thesis, one of the important behavior that is considered to be maintained by the simulation are for the wheels to follow the *Nonholonomic constraints*. With the model developed based on the theory laid down by the brush model, the level of sophistication was enough to establish the required behavior for this thesis. Hence, brush models are considered throughout this thesis and the dynamic behavior of tyres, tricycle and the bicycle are described accordingly.

### **Assumptions in the brush model**

In general, the brush model considers the following physical aspects while deriving the dynamic tyre model:

- Longitudinal slip ratio
- Lateral slip angle
- Pressure distribution in the contact patch
- Location of lateral forces from the center of wheel center (Pneumatic trail)
- Slip due to spinning (Camber and Turn-slip)
- Self-Aligning moment generated due to Pneumatic trail and Turn-slip
- Ply-steer and Conicity

From the slips defined in the brush model, relaxation length is added to the dynamic behavior of the model, in order to accommodate the transient behavior of tyre force and moment generation.

For deriving the tyre model in this thesis, a simplified assumption is made on

the contact of the tyre and road interface. For the sake of simplicity, the contact patch is reduced to a point such that all the forces generated are now focused at a single point. With that assumption, the self-aligning moment caused by pneumatic trail is neglected. Also, factors such as Ply-steer and Conicity that generate lateral forces and camber like forces due to the stresses developed in the steel meshing embedded inside the tyre are also neglected. Apart from these two assumptions, the rest of the physical aspects of the tyre described by the brush model as described in the above list is considered in detail and models are generated accordingly.

### 3.3 Sign convention

The most important factors that are associated with tyre mechanics are the forces and moments along with the slip angles and the camber angle that are associated with the generation of these dynamics. Figure 3.2 shows the sign conventions used to describe the dynamics of the tyres which are consistent with SimMechanics environment. In SimMecahnics environment, the spinning axis of any cylindrical

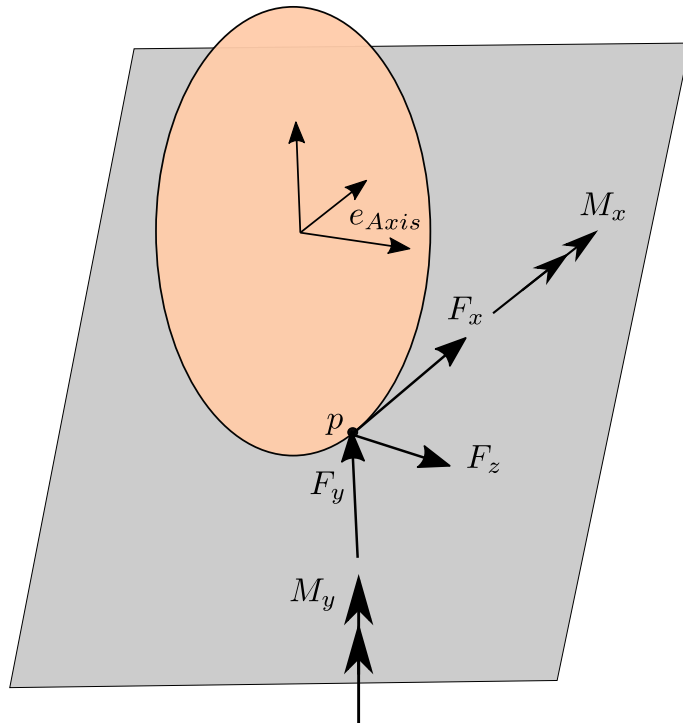


Figure 3.2: Sign convention used in SimMecahnics environment

object is always fixed to be the  $z$  axis of the body coordinate system. Developing from this, a right-handed coordinate system can be developed by choosing  $+x$

along the positive direction of the wheel propagation and  $+y$  as pointing in the upward direction. Therefore, the acceleration due to gravity  $g$  is acting along the  $-y$  direction. The  $e_{Axis}$ , indicates the axis of the wheel.

Assuming the tyre is moving along the longitudinal  $x$  direction, the forces acting at the contact point are resolved into vertical and horizontal components. The normal reaction force from the ground acting towards the center of the wheel axle is given by  $F_y$ . The horizontal forces induced by the slip angles and the camber angle are given by  $F_x$  and  $F_z$ .  $F_x$  represents the longitudinal force and  $F_z$  represents the lateral force.

$M_y$  represents the self-aligning moment, in a real tyre, either due to the non-central application of the lateral forces or stiffness of the tyre to roll about the vertical axis, a moment is generated such that it aligns the common plane of the wheel towards the propagation velocity.

### 3.4 Tyre material behaviour

Due to the compression of the material of the tyre both during motion and standstill, there is more than one radius of interest developed in the study of dynamics. Consider figure 3.3 that shows a silhouette of a tyre, developing various radii. Due

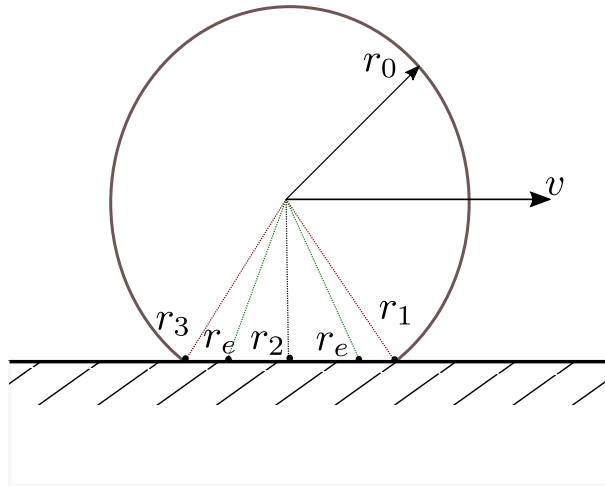


Figure 3.3: Equivalent radius of the tyre under compression

to the elastic behaviour of the tyre material, during the motion, the tyre compresses at three distinct points as shown by red, green and black radii.  $R_0$  is the undeflected tyre radius,  $r_1$  and  $r_3$  are the radius when the tyre material just enters the contact patch.  $r_e$  is the termed as equivalent radius in tyre dynamics,

it is the radius about which the actual velocity of the tyre contact point is given and is expressed as  $v = \omega r_e$ .

Realizing however that the radius at different points of contact have different radii which can be summarized as  $r_2 > r_e > r_1$ . Therefore, leading to different velocities near these radii, therefore, the velocities can be summarized as  $v_2 > v_e > v_1$ . These varying velocities cause the material of tyre under the contact point to undergo pull and push at various points, therefore developing a tendency to generate forces. Such a model of a tyre which generates forces due to compression and hysteresis is useful in describing the various forces that affect the dynamics of the tyre as a system.

## 3.5 Generation of forces and moments in a tyre

### 3.5.1 Rolling resistance

Due to the variation of the velocities near the contact patch as described in section 3.4, The variation of pressures and the forces in this region is as shown in figure 3.4

Due to the change in velocities in the contact patch, the longitudinal force changes both in magnitude and direction as shown by the green plot in figure 3.4. In an ideal case, both the top and the bottom regions of the curve should equate to zero. However, due to the hysteresis of the tyres material, these two regions are always not equal. Therefore, leading to a net force induced in the region of the contact patch whether the tyre is rolling or at standstill. This force is called the rolling resistance force and is a constant resistance acting both during acceleration and braking.

### 3.5.2 Vertical loading in a bicycle wheel

The spokes of the bicycle wheels are assembled in such a way that they are always experiencing equal and opposite tension when hung freely from the center. This is usually done to avoid the buckling of the wheel during loading as shown in the left of figure 3.5.

When the same wheel is loaded,(in contact with the ground), the reaction force  $F_n$  from the ground will balance out a part of  $F_t$  on the lower spoke. But the  $F_t$  on the upper spoke will remain same as before. The resultant of all the acting forces will be such that,  $F_{t,upper} = -F_{t,lower} - w + F_n$ . In other words, the static equilibrium of the wheel is balanced out by the upward pull of the wheel spoke and

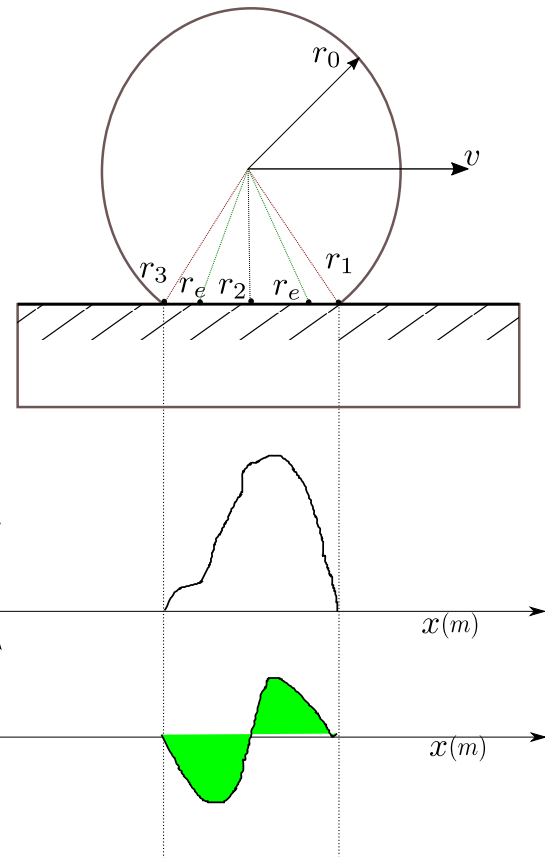


Figure 3.4: Pressure variations under the contact patch

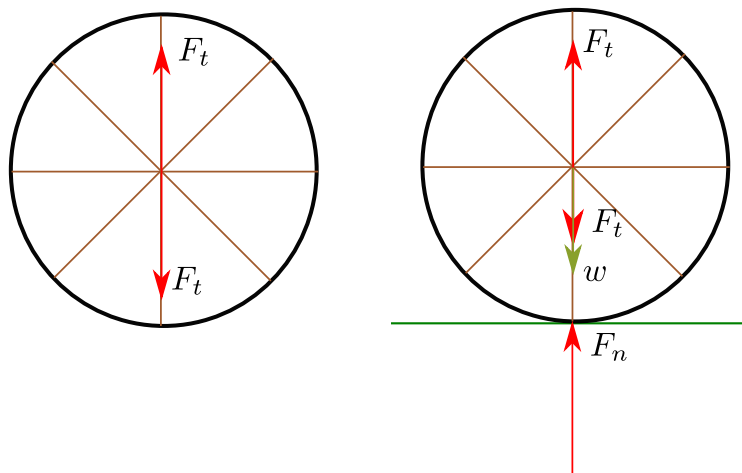


Figure 3.5: Vertical loading in a bicycle wheel

therefore, a wheel under contact with the ground hangs from the top. In wheels used in cars or trucks, such vertical hanging is generated by the air pressure on the upper sidewalls of the tyre.

### 3.5.3 Longitudinal tyre forces (Brush model)

The longitudinal forces generated in a tyre can be best studied using a brush model as described in Pacejka [Pac]. The threads that run along the length of the tyre are approximated to bristles as shown in figure 3.6. The forces generated in the tyre are due to slips that occur along the longitudinal and lateral directions. However, the slips have a different meaning in tyre mechanics than the usual use of the word slip in English literature. In English slip and sliding both means the same thing. In this thesis, sliding literally has the same meaning as in English, however, slips have technical definitions which is described later in this section.

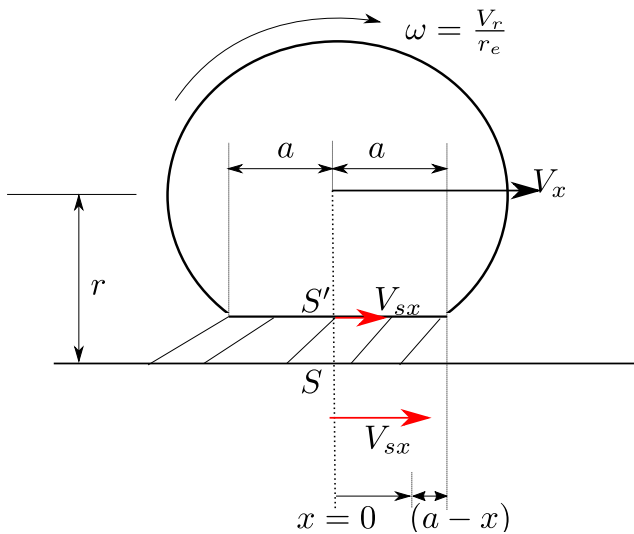


Figure 3.6: Brush model for longitudinal tyre force calculation [Pac]

In figure 3.6,  $V_x$  is the velocity of wheel's center.  $S$  is located as a point in the contact patch area, its velocity in case of pure rolling is same as the velocity  $V_r$ . However, during acceleration and braking along with the effects of sticking-sliding in the area of contact patch,  $V_s$  is not same as the free rolling velocity, such that:

$$V_{s_x} = V_x - \omega r_e \quad (3.2)$$

where,  $V_{s_x}$  is the component of  $V_s$  due to the difference in the velocities at two different points. The velocities along the different points bear the relationship  $V_r > V_x > V_{s_x}$ . Every bristle is defined with its head and tail, a head is in contact with the road and tail is fixed to the tyre carcass. Assumptions are made in defining the velocities at the two ends of the bristle.  $V_r + \omega r_e$  is defined to be the velocity along the tyre carcass and the bristle tail, the velocity along the bristle head is defined to be  $V_x$ . Therefore, the time interval for any bristle tail covering a distance  $(a - x)$  is expressed as:

$$\Delta t = \frac{a - x}{V_r} \quad (3.3)$$

During the same interval  $\Delta t$  the bristle head, covers the distance:

$$d = V_x \Delta t \quad (3.4)$$

Therefore, the above two equations show that every bristle undergoes deformation between the head and the tail, which can be expressed as:

$$u = (V_r - V_x) \Delta t \quad (3.5)$$

Substituting (3.5) with equations (3.3 and 3.4) leads to:

$$u = \frac{V_{s_x}}{V_r} (a - x) \quad (3.6)$$

Where  $V_{s_x}$  is the slip velocity at the contact point as defined by equation (3.2). Also, noting that the deformation occurs in the direction opposite to the direction of the wheels motion. Therefore, rewriting the above equation:

$$u = - \left( \frac{V_{s_x}}{V_r} (a - x) \right) \quad (3.7)$$

### Theoretical slip and Practical slip

Theoretical slip is defined as the ratio:

$$\sigma_x = - \frac{V_{s_x}}{V_r} \quad (3.8)$$

with (3.8),

$$u = (a - x) \sigma_x \quad (3.9)$$

Practical slip is defined as:

$$\kappa = - \frac{V_{s_x}}{V_x} \quad (3.10)$$

With equation (3.10) and (3.8),

$$u = (a - x) \frac{\kappa}{\kappa + 1} \quad (3.11)$$

The material of the tyre has a longitudinal stiffness  $C_{F_x}$ , therefore, the longitudinal force generated due to the deformation of the bristle is expressed as the sum of forces generated in the two regions of stick and slid of the contact patch:

$$F_x = F_{stick} + F_{sliding} \quad (3.12)$$

Lets assume a distance  $x_s$  where the sliding occurs, point  $-a$  is where is the sliding is maximum and point  $a$  is the where the sticking is maximum. The force

at the stick region will be the maximum of the force supported by friction and the force in the sliding region is formed by integrating the force generated by deformation [Pac]:

$$F_{stick} = \int_{-a}^{xs} \mu F_n dx \quad (3.13)$$

$$F_{slid} = \int_{xs}^a C_{F_x}(a - x) \sigma_x dx \quad (3.14)$$

The solution to the above equations is rather complex, however, in this thesis, the contact between the tyre and the road is taken only as a point instead of a patch. Therefore,  $a = x$  and the area of sticking disappears. The simplified equation for longitudinal force can be expressed as:

$$F_x = C_{F_x} \sigma_x \quad (3.15)$$

In terms of  $\kappa$  the slip ratio and longitudinal force can be defined as follows:

$$\kappa = -\frac{(V_x - V_r)}{V_x} \quad (3.16)$$

$$F_x = C_{F_x} \kappa \quad (3.17)$$

### 3.5.4 Lateral tyre forces (Brush model)

#### Insights from vehicle dynamics

The complexity of the dynamics of a vehicle in motion is not because of the individual complexity, but rather the complexity of their interactions with each other. Lateral dynamics is important when studying the vehicle stability in turning, accelerating and braking. Typically in a car like a vehicle, a handwheel is used to give a steering input (yaw-rate) to the front wheels. For a vehicle to take a turn, a combination of both the forward velocity vector and the yaw-rate as the inputs are required, generating a curved path. The relationship between the handwheel and the front wheel yaw-rate is linear for most of the day-to-day cases, however, this linearity departs under certain conditions. When the vehicle is under this linear region, the linear behavior can be represented as a series of connected sets of steady-state events. A steady-state condition in which all the vehicle states (speed, yaw-rate, path curvature etc.,) remain constant when the handwheel remains stationary [BH14, p.4].

This steady-state condition in turning is established by considering a fictitious force called the *centrifugal force*. In dynamic analysis, the acceleration that is considered while turning is the centripetal acceleration. The centrifugal effect

experienced by the vehicle body is due to the inertia of the body to restrict the motion, while the wheels connected to them accelerates towards the turning center. Due to such an inertia in the body, the relative motion experienced by an observer sitting inside experiences the centrifugal acceleration. In dynamics, therefore, the relationship is established between the centripetal acceleration and the yaw-rate  $\omega$  [BH14, p.6]:

$$a_N = V^2/R = \omega V = \omega^2 R \quad (3.18)$$

where,  $a_N$ ,  $V$ ,  $R$  and  $\omega$  are centripetal acceleration, body velocity in the direction of the motion, radius of curvature and yaw-rate respectively. The limit on  $a_N$  and  $\omega$  are set by the maximum friction between the tyre-road interface.

### D'Alembert's force and steady-state of cornering

While a vehicle is turning into a corner, the vehicle is constantly under the influence of the centripetal acceleration given by equation (3.18). Dynamically the system is in non-equilibrium with the dynamics of the system now depending on  $a_N$ . However, for an observer in the accelerating frame of reference (body fixed frame), feels a pull outward which is opposite to the direction of  $a_N$ . This outward pull experienced by an observer is termed as inertial force given by Newton's second law  $F_i = ma$ , where  $F_i$  is the inertial force. A free body diagram of mass  $m$  would show  $m$  to be in static equilibrium under the influence of  $F_i$  and the force associated with  $a_N$ . The inertial force is just a fictitious force which is placed in the direction opposite to  $a_N$  so as to analyze the system in equilibrium while the vehicle mass  $m$  is turning into a corner. According to D'Alembert's principle, such fictitious forces can be placed into the system so that the system can be studied at equilibrium. In vehicle dynamics this outward acting force is called *Centrifugal Force* and is important in understanding the non-holonomic constraints imposed on the wheel.

### Lateral slip angle and Centripetal force

A tyre at a given steering angle  $\delta$  generates a lateral slip angle  $\alpha$  as shown in the figure 3.7. The tyre under the influence of lateral slip angle  $\alpha$  generates a lateral force which is a necessary condition to keep the balance with centrifugal force as described in section 3.5.4. The slip angle  $\alpha$  is a deformation produced in the direction opposite to that of steering  $\delta$  as shown in figure 3.7. The tyre thread elements can be studied as a brush as described in the *Brush model*, each individual brush acts like a spring with stiffness  $C_{F_{Lat}}$ . The force produced by this deformation acts in the direction opposite to  $\alpha$  and is the necessary force to produce centripetal acceleration  $a_N$ .

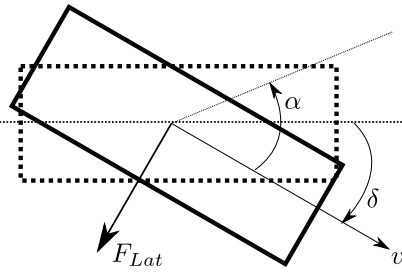


Figure 3.7: Lateral slip angle for a steered wheel

### Lateral slip definition

Lateral slip is defined as the angle between the direction of the center of the tyres propagating versus the direction to which the tyres common plane is pointing to as shown in the figure 3.8. It is due to this lateral or side slip a force is produced parallel to the wheel's axle. Lateral slip is expressed as [Pac]:

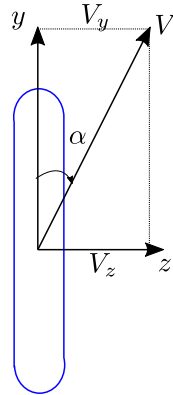


Figure 3.8: Defining lateral slip angle

$$\alpha = \tan^{-1} \left( \frac{V_z}{V_y} \right) \quad (3.19)$$

For small angles,  $\alpha$  can be approximated to:

$$\alpha \approx \frac{V_z}{V_y} \quad (3.20)$$

#### 3.5.5 Self-Aligning Moment

In pneumatic tyres, under the contact patch, the lateral force due to centripetal acceleration as described in section 3.5.4 is developed slightly behind the center

of the contact patch. This is due to the fact that in the contact patch, the lateral forces are generated between the two regions of sticking and sliding as shown in the figure 3.9(a).

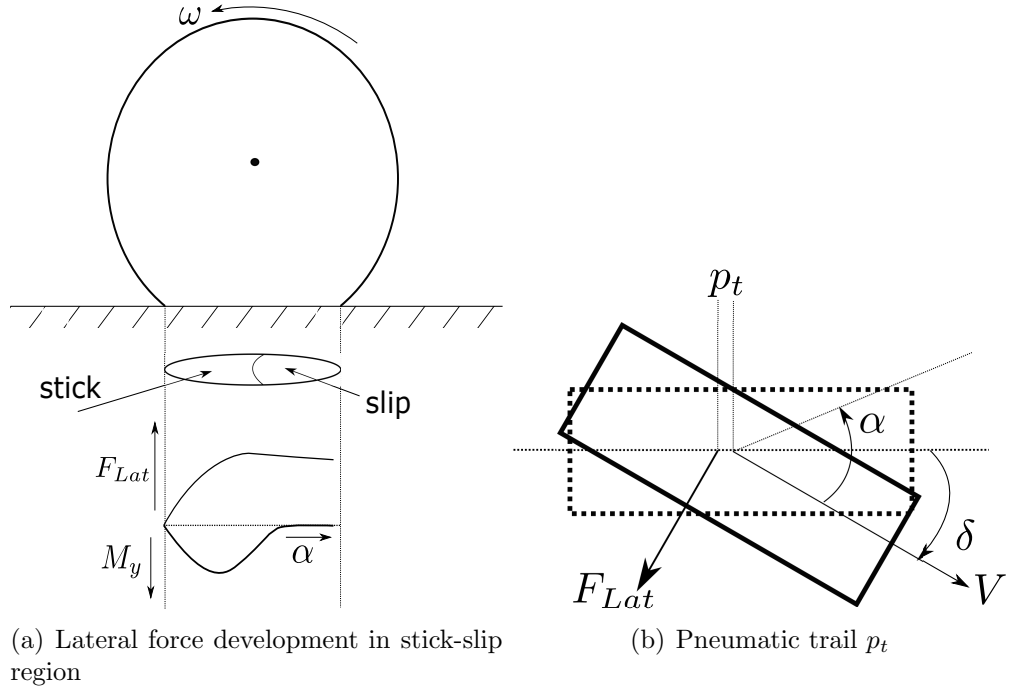


Figure 3.9: Lateral force and Self-Aligning moment

In the region of sticking, the threads of the tire are sticking completely to the road due to a maximum of frictional force acting between tyre and the road. The lateral force developed in this region is increasing linearly as shown in the figure 3.9(a). The lateral force continues to increase until the sliding region. Sliding region is characterized by sliding of the threads under the road surface due to the tangential forces near the tyre-road interface exceeding the limit of maximum frictional force given by Coulomb's law. The maximum of the lateral force appears just behind the center of the tyre by a distance  $p_t$ . This causes a moment that orients the tire towards the direction of propagation velocity. This moment is called *Self-Aligning Moment* and distance  $p_t$  is called *pneumatic trail*. According to [Pac05a], self-aligning moment is also caused by a third kind of slip called spin as explained in section 3.5.6.

### 3.5.6 Turn slip

Besides the two main slips considered in tyre dynamics, there is a third slip which is termed as spin in [Pac05a]. Turn slip is defined as the rate of change of wheel's

heading angle with respect to its propagation speed [den, p.34]. Referring to the figure 3.10, this spin velocity is defined as the component of the rotational velocity of the wheel planes spin normal to the plane of contact point [Pac05a]. The slip due to the spin is the result of two components, the wheel's camber angle and so-called *Turn slip* [Lu13].

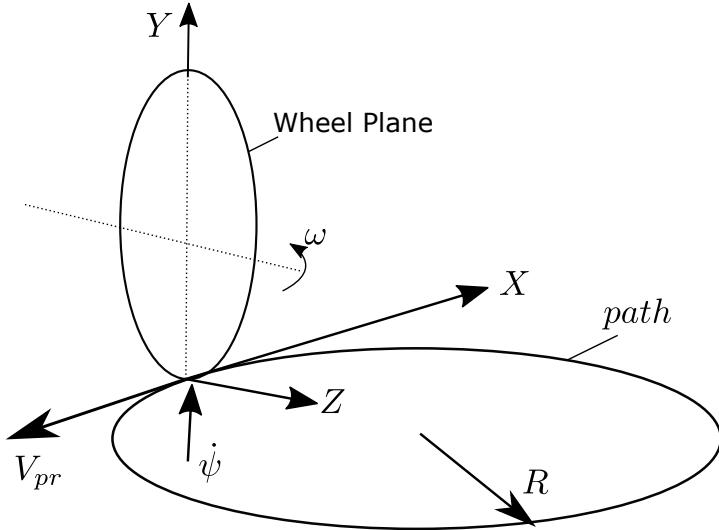


Figure 3.10: Condition of pure turn slip [Lu13]

where  $\dot{\psi}$  is the component of rotational velocity of the wheel spin around normal axis  $Y$ . The condition of pure turn slip is defined for both longitudinal slip ratio  $\kappa = 0$  and lateral slip angle  $\alpha = 0$ , the turn slip ratio  $\phi_t$  is then defined as the ratio of the wheel's yaw-rate to the propagation velocity of the contact point. " $\phi_t$  reflects variation of tyres yaw angle per unit contact patch updating length" [Lu13]. In case of pure turn slip, the turn slip ratio is equal to the path curvature  $1/R$ , therefore, expressed as:

$$\phi_t = \frac{\dot{\psi}}{V_{pr}} = \frac{1}{R} \quad (3.21)$$

The units of turn slip being  $rad/m$ . Pure turn slip acts as a moment that offers resistance around normal axis to the contact point [den, p.34]. Like lateral slip that occurs in the direction opposite to the motion causing a ground resistance from the contact point, turn slip also acts as a resistance moment and therefore equation (3.21) can be re-written as:

$$\phi_t = -\frac{\dot{\psi}}{V_{pr}} \quad (3.22)$$

### 3.5.7 Camber Thrust

Apart from the slips, a tyre also generates forces due to a camber in the road. Road cambers are given generally for clearing the rainwater. When a vehicle is traveling on a road which is cambered by an angle  $\varphi$ , it is compressed in the lateral direction. To understand this behavior, consider a tyre which cambers with no road. In such a case, the tyre would simply camber about its plane of center and the projection of the contact point on the ground forms an ellipse as shown in the figure 3.11(a). Now, with the restriction due to the road, the side wall of the tyre is pushed laterally and the projected ellipse is now compressed on the side as shown in the figure 3.11(b). For such a compression to take place, there appears to be a lateral force from the ground in the direction of compression acting on the tyres side wall as shown in the figure 3.11(b).

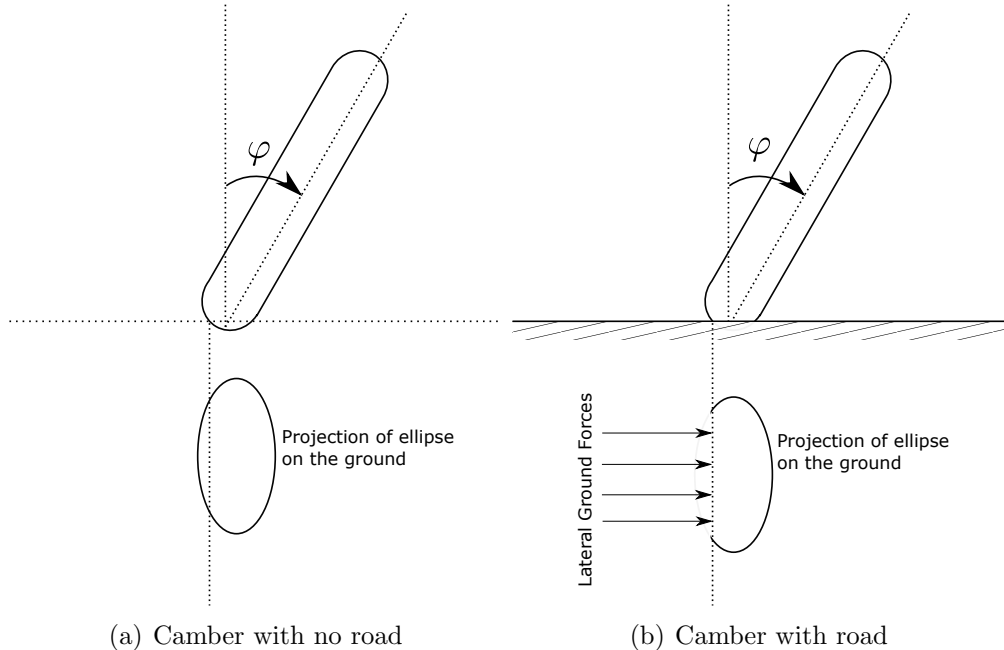


Figure 3.11: Lateral compression due to road camber

The lateral force which is acting on the tyres side wall as shown in the figure 3.11(b), produces a thrust on the tyre in the direction of camber. Such a force is called camber force. Camber angles are also given to vehicles themselves by the manufacturers, especially in trucks with higher load carrying capacities. Camber angle is however induced in a single wheel rolling on a plane either by the camber of the plane or a lateral perturbation and/or overturning moment induced in the motion. Along with lateral force due to slip, camber thrust plays a major role in the lateral stability of the vehicle against external disturbances and aids in cornering stability by generating forces required for  $a_N$ . Various factors that affect

this phenomenon include tyre pressure, material, thread stiffness, thread dimensions etc,. Physically the relationship between the lean angle and the camber force is linear and given by[Pac]:

$$F_{camber} = F_n \sin \varphi \quad (3.23)$$

## 3.6 Cornering stability in a slip induced tyre

In tyres, the lateral forces are generated by two mechanisms, camber and slip angle. Generally, lateral forces generated by slip angles are much higher compared to that generated by camber angles. The magnitude of the lateral forces induced by these two angles is influenced by the vertical loads acting on the tyres.

While a vehicle is changing its direction from a straight line to a curved path, there is a region of transition where the yaw-rate of a vehicle is accelerating. The yaw acceleration is controlled by vehicle yaw moments acting on the vehicle yaw inertia [BH14, p.8]. These yaw-moments (self-aligning torques) are induced in the vehicle by the force generating quantities in the tyres. The transition behavior can be written down in the following sequence [BH14]:

- The handwheel induces the slip angles to the front wheels.
- After the delay associated with the front tyre relaxation behavior, lateral forces are induced near the front of the vehicle by the front wheels, leading to lateral and yaw acceleration development.
- The yaw-rate of the body applies slip angles to the rear wheels.
- After the delay associated with rear tyre relaxation behavior, lateral forces are applied near the rear of the vehicle by the rear wheels. In this stage, lateral acceleration increases and the yaw-rate decreases to zero.

## 3.7 Tyre relaxation length

In an automobile tyre, there is always a delay in time between the application of slip angles and the development of lateral forces required for cornering stability. This kind of delayed response behavior, which is in fact the dynamic behavior of a tyre and is an inherent behavior in a pneumatic tyre. As defined by Pacejka [MP97, p.341], tyre relaxation length is defined as the distance required by the tyre to reach a certain percentage of its steady-state behavior for a step input of slip angle. This dynamic behavior is equivalent to the first order type mass-damper system connected in series.

The cornering stability of a vehicle is determined by its cornering force generation. In a pneumatic tire, the cornering force build-up is dependent on the tyres relaxation length for a step input of slip angle. For the prediction of the dynamics of tyres behavior, an experiment conducted by Pacejka et.al [MP97] has concluded that the tyre forces can be represented by a first-order relaxation length and expressed as[MP97, p.340]:

$$\frac{\sigma}{V} \frac{d\alpha_F}{dt} + \alpha_F = \alpha \quad (3.24)$$

where,  $\alpha_F$  serves as a new filtered output for a step input  $\alpha$ .  $\alpha_F$  is particularly the deflection angle of the leading tyre edge,  $\alpha$  is the input slip angle and  $\sigma$  is the tyre relaxation length. With the new filtered output, the lateral force along  $e_{lat}$  is expressed by:

$$F_{lat} = C_{F_\alpha} \alpha_F \quad (3.25)$$

### Speed wobble or shimmy in motorcycle tyres

Speed wobble is the phenomena that cause the steering wheels to oscillate increasingly leading to a loss of control. These oscillations are of the nature of an under-damped second order or a higher-order system with a positive feedback mechanism, thereby rendering the system increasingly unstable. This phenomenon is commonly observed both in a pneumatic tyre as well as a solid disk. But in a pneumatic tyre, wheel shimmy is controlled by two factors. The slip-induced due to turn-slip induces stiffness about the normal axis of the tire, self-orienting the wheel along the direction of propagation velocity leading to a more stable motion. Another factor is the tire relaxation length, due to which the tire behaves like a mass-spring system in series along the longitudinal and lateral directions.

## 4 Multibody modeling

In a multibody environment, modeling mechanical systems such as a tyre uses a contact model. A contact model establishes the contact forces that act between the tyre and the road interface. Using the dynamics calculated from the contact model, a force element (external force and moment block in SimMechanics) applies the calculated forces and torques generally at the center of the rigid-body.

A bicycle wheel is constructed in the multibody environment by considering a flexible disc with stiffness along its longitudinal, lateral and vertical directions and having a point contact with the ground. For modeling the contact forces, slip models as described in section 3.5 is used. The contact forces act at the contact point between the ground and the tyre. The contact point is located as a radial vector distance pointing down from the center of the tyre to the road. This radial vector changes during tyre rolling (camber) and therefore, care has to be taken during modeling to correctly define and calculate this parameter.

Important aspects to consider while establishing contact between body elements in a multibody environment:

- Determine the impact between the tyre and ground and calculate the vertical tyre forces.
- Determine longitudinal and lateral slips and calculate the longitudinal and lateral forces respectively.
- Determine the turn-slip and calculate the self-aligning moment.
- Express the calculated forces and moments in the body reference frame.

In SimMechanics though a contact forces library exists [Mil], this library is more for demonstration purpose and cannot be used directly for establishing vehicle specific tyre-ground contact. Therefore, a custom contact library is developed based on the important aspects considered above.

## 4.1 Wheel coordinate system

The location of a rigid-body in three dimensional space is generally described by two attributes: position and orientation. A rigidly attached coordinate to the body is defined as a frame, the position and orientation of this frame is then defined with respect to a reference coordinate system. Three frames are defined, an inertial frame of reference  $I$  is chosen, as shown in the figure 4.1. Frame  $B$

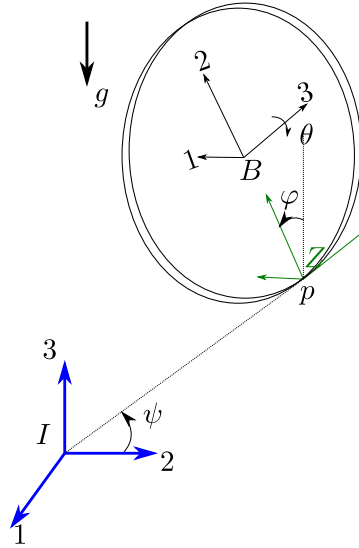


Figure 4.1: Wheel coordinate frames

defines the body-fixed coordinate frame which rotates along with the wheel when it is spinning. Frame  $Z$  defines the body-fixed coordinate frame such that it *does not* rotate with the wheel but translates along with it. Frame  $Z$  is helpful to define the moments of inertia about the principal axes as well as establish the position of the contact point.  $p$  is the contact point expressed in  $Z$ . The rotation from frame  $I$  to frame  $B$  is given by a transformation matrix:  ${}^I B R$ , measured directly through the sensor block. Where,  ${}^I B R$  is the rotation of  $B$  with reference to  $I$ .

## 4.2 Tyre model for generation of tyre forces and moments

For calculating the contact forces generated at the tyre-ground interface, a mathematical model is developed that takes certain input quantities and calculates the forces and moments as output quantities. In a tyre model that is described by

slips along longitudinal and lateral directions, input quantities that are of importance are  $\kappa$ ,  $\alpha$ ,  $\varphi$  and  $d$  which represent the longitudinal slip, lateral slip, camber angle and penetration respectively. The vector of output forces and moments acting on the tyre is expressed as  $[F_{long} \ F_{lat} \ F_n \ M_x \ M_\phi \ M_\theta]^T$ . The tyre model can now be expressed as a mathematical function that takes inputs and computes the outputs as shown in the figure 4.2.

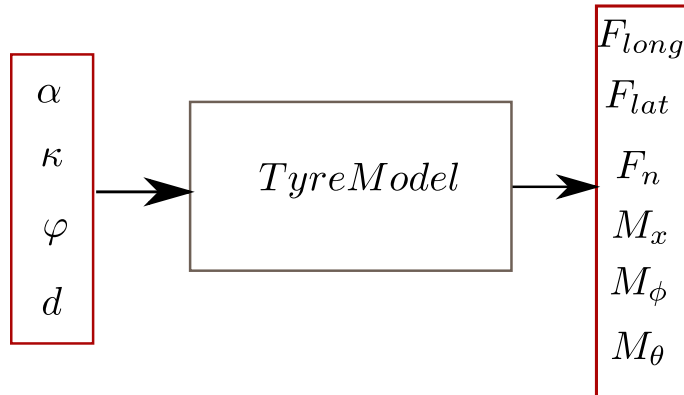


Figure 4.2: Tyre model for tyre forces and moments

## 4.3 Body element simulation in SimMechanics

In SimMechanics, a physical element such as a wheel is connected through a joint to dynamic model such a tyre model in this case. The flow of action sequence through these connections can be summarized through figure 4.3. Additionally, there is a force element such as an external force and torque block. Various kinematic parameters of the wheel is determined through a sensor placed at the center. The outputs of the sensor values are discretized in time, these sensors values serve as the inputs to the tyre model. The inputs in terms of positions and velocities are used to calculate slips. From the current sensor values, the next time integration values are calculated by the Simulink solvers. The tyre model serves as a mathematical function for this time integration. The outputs from the tyre model are in the form of signals, which are then converted into physical values using MATLAB in-built function and supplied to an force element. The force element acts as an actuator that actuates the physical signals in the wheel fixed frame  $B$ . The loop completes with the sensor sensing the kinematics of the current time interval. The simulation is terminated by specifying the end time.

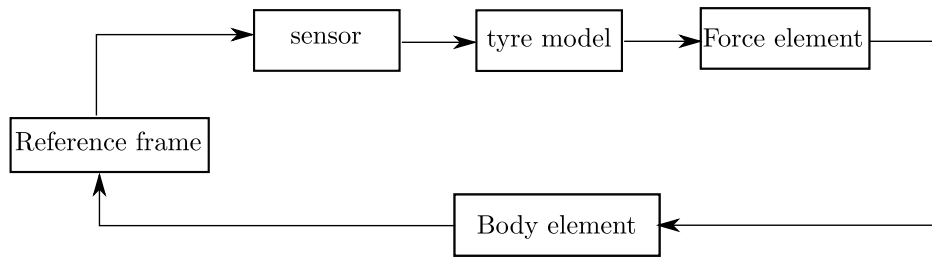


Figure 4.3: Wheel model in SimMechanics environment

## 4.4 Wheel geometry

In order to calculate the forces and moments as described in section 4.2, a geometrical wheel element has to be constructed, that defines the point of application of these forces and moments. Also in SimMechanics, the sensing and actuation are possible only about a joint that is located at the center of the body element. With the help of vector calculus, the contact point is defined and located using vectors. The forces are calculated near the contact point and moments are calculated due to these forces acting about the center of the wheel and the moment due to self-alignment. The vector calculation is similar to that given in [Pac], [DD10], where the initial orientation of the wheel axis  $e_{axis}$  is considered for determining the longitudinal, lateral and vertical unit vectors of the body element in the body-fixed frame  $B$  and finally the position of the contact point from the center of the wheel  $\mathbf{r}$ .

## 4.5 Defining plane normal

A plane normal is defined as a perpendicular to the tangent plane to that surface. For a plane that is at an inclination with a reference horizontal as shown in the figure 4.4, the plane normal can be defined as a vector of a vertical reference.

Therefore, the plane normal for a plane inclined at an angle  $\beta$  with the reference horizontal is expressed as a vector in a 3D space:

$$\mathbf{n} = \begin{bmatrix} \sin\beta \\ \cos\beta \\ 0 \end{bmatrix} \quad (4.1)$$

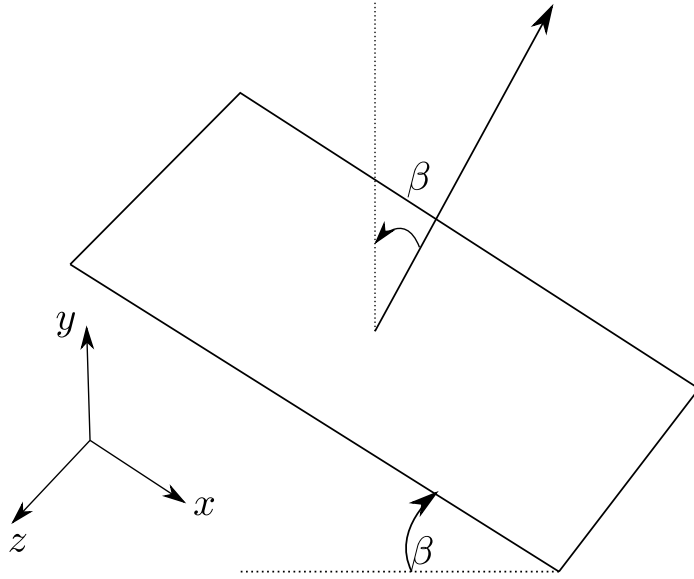


Figure 4.4: Plane normal

## 4.6 Wheel vector calculation

From an known initial position of the wheel axis  $e_{axis}^* = [0 \ 0 \ 1]^T$ , the wheel axis can be expressed in frame I as  $e_{axis} = {}^{IB}Re_{axis}^*$ . Referring to figure 4.5, the longitudinal and lateral directions of the contact point are calculated using vector calculus, for such a purpose, the ground plane normal is defined using equation (4.1) with zero inclination as a unit vector  $\hat{n} = [0 \ 1 \ 0]^T$ . Similar to the vector calculus given in [DD10], the wheel vectors are defined as cross-products:

$$\mathbf{l} = \hat{n} \times \mathbf{e}_{axis} \quad (4.2)$$

$$\mathbf{e}_{long} = \frac{\mathbf{l}}{\|\mathbf{l}\|} \quad (4.3)$$

$$\mathbf{e}_{lat} = \hat{n} \times \mathbf{e}_{long} \quad (4.4)$$

$$\mathbf{e}_r = \mathbf{e}_{long} \times \mathbf{e}_{lat} \quad (4.5)$$

$$\mathbf{r} = r\mathbf{e}_r \quad (4.6)$$

where,

- $\mathbf{l}$  is the longitudinal vector in frame  $B$ .
- $\mathbf{e}_{long}$  is the longitudinal unit vector normalized in frame  $B$ .
- $\mathbf{e}_{lat}$  is the lateral unit vector in frame  $B$ .
- $\mathbf{e}_r$  is the radial unit vector in frame  $B$ .
- $\mathbf{r}$  is the radial vector in frame  $B$  pointing from center of the wheel to the

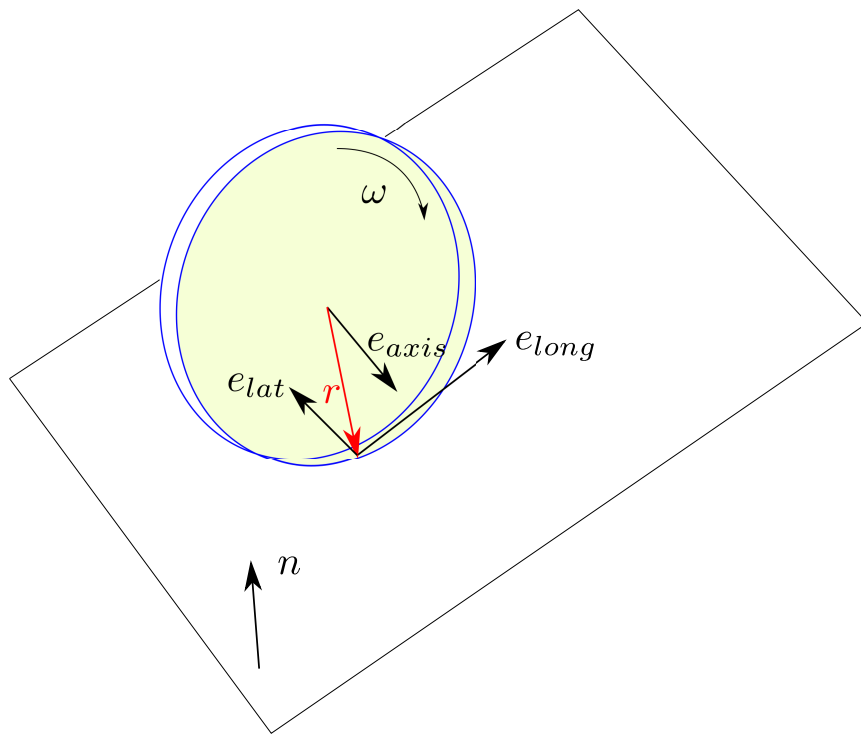


Figure 4.5: Wheel element showing vectors along the contact point

contact point.

## 4.7 Tyre model for Multibody application

For the geometry described in section 4.6, a model on the generation of the tyre forces is required. The tyre model determines the motion of the wheel under action of external forces and constraints. The tyre model developed in this section uses the theories and mathematical models described in section 3.5.

### 4.7.1 Vertical tyre force

The vertical tyre forces from the ground are calculated with respect to the deflection (or penetration) of the tyre. A holonomic constraint is placed on the distance between the center of the wheel to the road plane and any deviation is recorded as the penetration parameter  $d$ . By defining the tyre vertical stiffness, a force proportional to this deformation can be obtained using a linear force law. For the calculation of penetration, the position of the contact point from the center

of the wheel is determined as:

$$\mathbf{x}_p = \mathbf{x}_c + \mathbf{r} \quad (4.7)$$

where,  $x_c$  is the position of the center of the wheel, this position is given as the output from the sensor placed in the wheel body element. The tyre deformation is calculated as the projection of the vertical component of the contact point vector  $\mathbf{x}_p$ :

$$d = \dot{\mathbf{x}}_p \cdot \hat{n} \quad (4.8)$$

with the known penetration  $d$ , the vertical tyre force can be formulated with vertical tyre stiffness given by a spring with stiffness  $k$  and a damper with damping co-efficient  $d$  the force is expressed as:

$$\mathbf{F}_n = kd + cd \quad (4.9)$$

The calculated force is expressed in the wheel frame  $B$  as a vector:

$${}_B\mathbf{F}_n = \mathbf{F}_n \hat{n} \quad (4.10)$$

where,  ${}_B\mathbf{F}_n$ ,  $F_n$  is expressed in frame  $B$ .

### 4.7.2 Defining slips

As seen in the brush model described in section 3.5.3, the horizontal forces generated are due to the reaction forces from the contact patch. The deformation of the tyre threads occurs in the direction opposite to that of the orientation of the tyre. As described in section 3.5.3 *Brush model*, the longitudinal and lateral slips are expressed as:

$$\kappa = -\frac{(V_x - V_r)}{V} \cdot e_{long} \quad (4.11)$$

$$\alpha = -\frac{(V_x - V_r) \cdot e_{lat}}{V \cdot e_{long}} \quad (4.12)$$

where,  $V_r = \omega \times \mathbf{r}$  and  $V_x$  is the velocity of the center of wheel. The slip ratios are expressed as the functions of slip velocity  $V_s$  along longitudinal and lateral directions respectively.  $V_s$  is expressed as:

$$V_s = V_x - V_r \quad (4.13)$$

The longitudinal and lateral slips can now be re-written in the following form:

$$\kappa = -\frac{V_s \cdot e_{long}}{V_x} \quad (4.14)$$

$$\alpha = -\frac{V_s \cdot e_{lat}}{V_x} \quad (4.15)$$

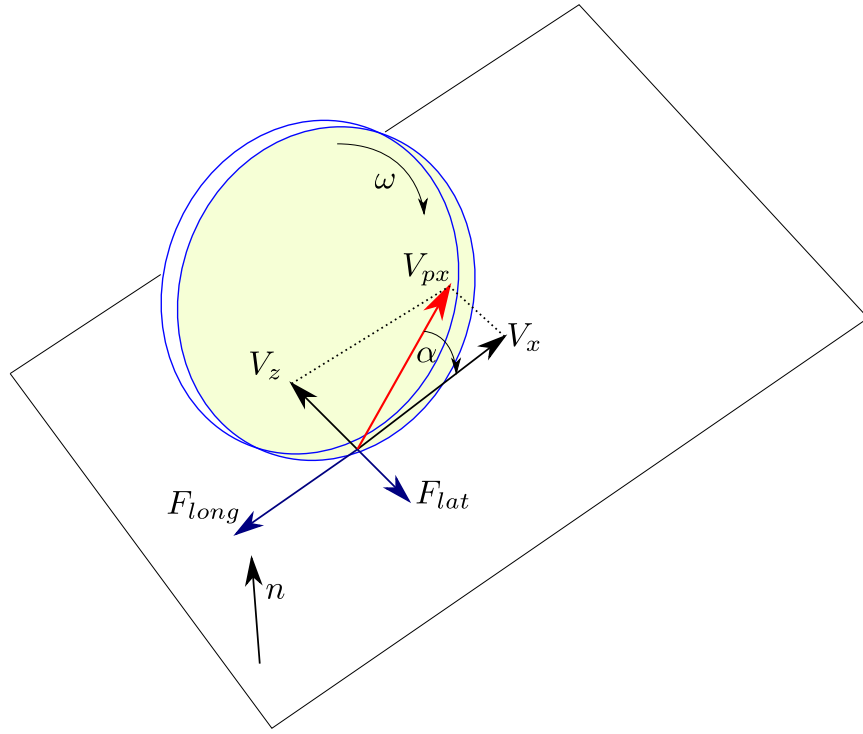


Figure 4.6: Horizontal forces at the contact point

#### 4.7.3 Longitudinal and lateral tyre forces

Considering the tyre stiffness  $C_F$ , a reaction force is generated due to a slips  $\kappa$  and  $\alpha$ . Due to the stiffness of the tyre material some force is required to deform the tyre material and this force is modeled as a spring force. Since slips are in the direction opposite to the propagation velocity  $V$ , the horizontal forces are generated in the direction opposite as shown in the figure 4.6. With longitudinal and lateral tyre stiffness  $C_{F_x}$  and  $C_{F_z}$  respectively, the forces are expressed as:

$$F_x = C_{F_\kappa} \kappa \quad (4.16)$$

$$F_z = C_{F_\alpha} \alpha \quad (4.17)$$

Since  $\kappa$  and  $\alpha$  are functions of  $V_x$ , at the first simulation step,  $V_x = 0$ , this causes numerical problems. Therefore, a correction factor  $\epsilon$  is added which avoids the division with zero.  $\kappa$  and  $\alpha$  are re-written as:

$$\kappa = -\frac{V_s \cdot e_{long}}{V_x + \epsilon} \quad (4.18)$$

$$\alpha = -\frac{V_s \cdot e_{lat}}{V_x + \epsilon} \quad (4.19)$$

#### 4.7.4 Propagation speed

Even though the slips are defined in theory as the functions of  $V_x$ , applying such a relationship leads to enormous propagating numerical errors in case of pure spinning of the wheel like a spinning top. In which case the speed at the center of the wheel is momentarily zero unlike the speed near the contact point where it is still rolling as described in [DD10, p.3]. Therefore, the slips are normalized as the functions of velocity of the wheel near the contact point also called the propagation speed of the wheel  $V_p$ .

In order to calculate the propagation speed, vector relationships are used to determine the position of the contact point from the reference frame:

$$\mathbf{x}_c = \mathbf{x}_0 + \mathbf{r} \quad (4.20)$$

The contact point velocity can be derived by differentiating equation (4.20):

$$\dot{\mathbf{x}}_c = \mathbf{V}_p = \dot{\mathbf{x}}_0 + \dot{\mathbf{r}} \quad (4.21)$$

propagation velocity along the longitudinal direction:

$$V_{px} = \mathbf{V}_p \cdot e_{long} \quad (4.22)$$

Both the derivatives  $\dot{\mathbf{x}}_0$  and  $\dot{\mathbf{r}}$  are obtained form Simulink blocks. With the propagation velocity now defined, the slips can be rewritten in the form:

$$\kappa = -\frac{V_s \cdot e_{long}}{V_{px}} \quad (4.23)$$

$$\alpha = -\frac{V_s \cdot e_{lat}}{V_{px}} \quad (4.24)$$

## 4.8 Modeling tyre relaxation behavior

Finally, the calculated tyre forces are modeled as a first order response to the slips as described in section 3.7. This dynamic behaviour which is also called as relaxation length ( $\sigma$ ) in the tyre accounts to the distance the wheel travels before it reaches 63% of the steady-state value in the force build-up [Pac, p.22]. This kind of dynamic behavior acts like a mass-spring system in series that gives the stiffness to the wheel longitudinal and lateral axis as described in section 2.1.

### 4.8.1 Longitudinal slip with tyre relaxation

A pneumatic tyre generates longitudinal forces with the input slip ratio  $\kappa$  which is given by a first order relaxation [MP97, p.340]:

$$\frac{\sigma}{V_{px}} \kappa \dot{F} + \kappa_F = \kappa \quad (4.25)$$

where,

- $\kappa$  is the input slip ratio.
- $\sigma$  is the tyre relaxation length found from experimental results as described in [MP97, p.342].
- $V_{px}$  is the propagation velocity of the wheel.
- $\kappa_F$  is the response to  $\kappa$ .

also,

$$\begin{aligned} \kappa &= \frac{V_{s_1}}{V_{px}} \\ V_{s_1} &= V_s \cdot e_{long} \end{aligned}$$

therefore, simplification leads to:

$$\dot{\kappa}_F = \frac{V_{s_1} - V_{px}\kappa_F}{\sigma} \quad (4.26)$$

The above equation is solved numerically in Simulink for  $\kappa_F$ . The longitudinal force is expressed by a spring force with longitudinal stiffness  $C_{F_\kappa}$  proportional to  $\kappa_F$  as described in [MP97, p.340]:

$$F_{long} = C_{F_\kappa} \kappa_F \quad (4.27)$$

### 4.8.2 Lateral slip with tyre relaxation

Similar to the relaxation for  $\kappa$ , the lateral slip  $\alpha$  is also expressed with relaxation length  $\sigma$  given by[MP97, p.340]:

$$\frac{\sigma}{V} \dot{\alpha}_F + \alpha_F = \alpha \quad (4.28)$$

with,

$$\begin{aligned} \alpha &= \frac{V_{s_2}}{V_{px}} \\ V_{s_2} &= V_s \cdot e_{lat} \end{aligned}$$

where,  $\alpha$  is the input slip angle and  $\alpha_F$  is deflection angle near the leading edge of the contact area. Simplifying above equation leads to:

$$\dot{\alpha}_F = \frac{V_{s_2} - V_{px}\alpha_F}{\sigma} \quad (4.29)$$

The above equation is solved numerically in Simulink for  $\alpha_F$ . The lateral force is given by:

$$F_{Lat} = C_{F_\alpha} \alpha_F \quad (4.30)$$

### 4.8.3 Turn Slip with tyre relaxation

Apart from the two main slips considered in most of the automotive tyre applications, there is also a third slip due to spin [Pac05b]. Spin velocity here is defined as the component of  $\omega$  that is acting normal to the contact point. Pure turn-slip is defined as the ratio of rate of change of heading direction  $\dot{\psi}$  with respect to the propagation velocity  $V_{px}$ . As described in section 3.5.6, the slip due to spinning of the wheel is described by the equation:

$$\phi_t = \frac{\dot{\psi}}{V_{px}} \quad (4.31)$$

Further, turn-slip is an input similar to lateral slip angle  $\alpha$  that defines the dynamic generation of self-aligning moment, the dynamic behavior of the tyre given by the relaxation length  $\sigma$  has to be included into the system.

Consider the equation that describes the first order response of the tyre for slips with relaxation  $\sigma$  as given by [MP97], re-writing the equation for turn-slip ratio ( $\phi_t$ ):

$$\frac{\sigma}{V_{px}} \dot{\psi}_F + \psi_F = \phi_t \quad (4.32)$$

where,  $\psi_F$ , is the response of the system to slip input  $\phi_t$ .  $\dot{\psi}$  is the rate of change of heading angle about the normal axis  $\hat{n}$ , expressed as  $\dot{\psi} = \omega \cdot \hat{n}$ . Simplifying above equation leads to:

$$\dot{\psi}_F = \frac{\omega \cdot \hat{n} - V_{px}\psi_F}{\sigma} \quad (4.33)$$

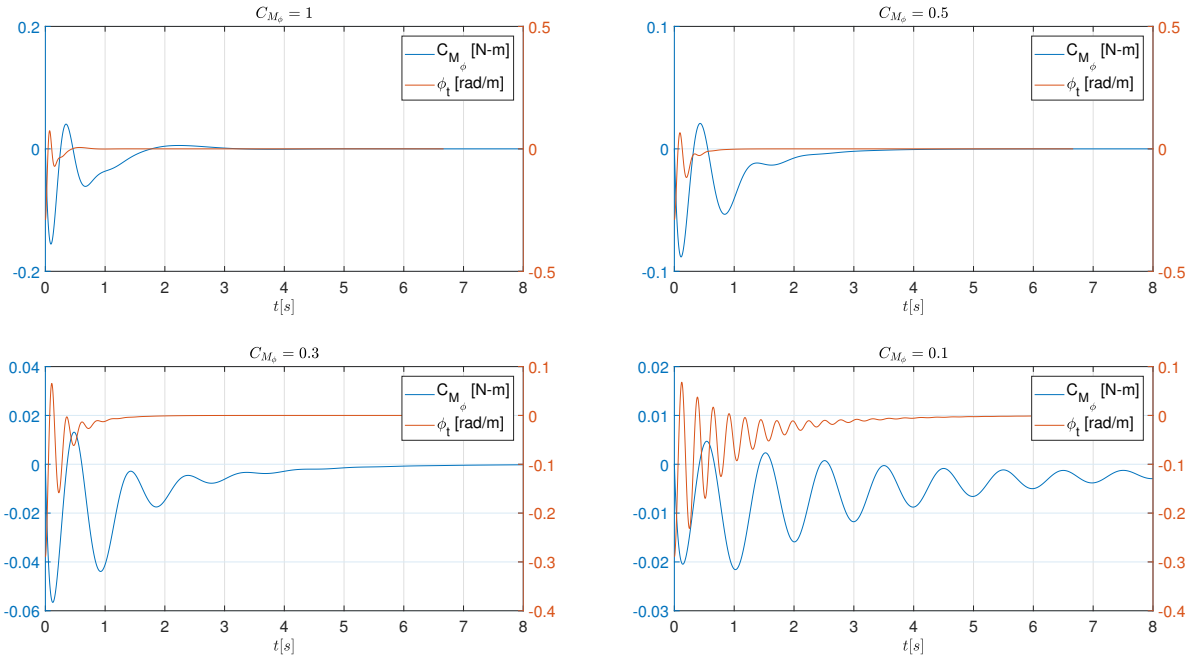
The above equation is solved numerically for response  $\psi_F$  in Simulink for  $\psi_F$ . Now, equation (4.33) is written in the same form as equations (4.26 and 4.29). Due to turn-slip, a stiffness is imparted about the vertical rotation axis by the thread elements on the tyre. A self-aligning stiffness factor  $C_{M_\phi}$  relates turn-slip with the moment generated as:

$$M_\phi = C_{M_\phi}\psi_F \quad (4.34)$$

Experiments conducted by [Lu13] have shown that  $C_{M_\phi}$  depends non-linearly on various aspects of the tyre thread elements such as the thread form factor, tyre carcass flexibility, friction in the stick-slip region among various others. Also, the self-aligning moment generated by the tyre varies depending on the turn-slip ratio  $\phi_t$ . In [Lu13], a mathematical model has been described which takes into account all these factors and results are generated for a car tyre. The resulting forces and moments generated by  $\phi_t$  are determined experimentally and a graph is plotted to show a relationship between  $\phi_t$  and self-aligning moment  $M_y$  (which also contains self-alignment due to the pneumatic trail). In this thesis, however, the factor  $C_{M_\phi}$  is chosen to be a constant value for all turn-slip ratios  $\phi_t$  for the sake of simplicity and also as the stick-slip region is completely ignored in the brush model to a point contact. A factor of  $C_{M_\phi} = 1$  would lead to a maximum stiffness and  $C_{M_\phi} = 0$  would lead to stiffness being zero and the wheel behaving similarly to a solid disc rolling on a knife-edge contact. The effect of  $C_{M_\phi}$  is such that it orients the wheel in the direction of the propagation velocity  $V_p$ .

In general, the stiffness parameters for a tyre are determined experimentally as it is dependent on the tyre stick-slip properties and the flexibility of the tyre carcass. Also, in the literature, most of the experiments conducted are available only for car or truck tyres. Therefore, in this thesis, self-aligning stiffness is chosen rather intuitively after conducting various simulations such that the observed behavior fits into the behavior similar to a bicycle's tyre. Figure 4.7 shows plots of  $C_{M_\phi}$  with  $\phi_t$  for a wheel at initial velocity  $v_0 = 1.5m/s$  and initial camber angle  $\gamma_0 = 5^\circ$  under various stiffness factor values. The trajectories of the wheel under these various  $C_{M_\phi}$  factors are visualized as shown in figure 4.8, in order to appreciate the difference with a solid disc, a plot of wheel's trajectory is shown in comparison in figure 4.9 for  $C_{M_\phi} = 0$ .

It can be seen in figure 4.7, the lag between  $\phi_t$  and  $C_{M_\phi}$  which is evident of a first order system response. Also the self-alignment is at its maximum for  $C_{M_\phi} = 1.0$  gradually reducing down as  $C_{M_\phi}$  is decreased. The trajectories shown in figure

Figure 4.7: Plots showing the variation of  $C_{M_\phi}$  with  $\phi_t$ 

4.8 show the effect of self-alignment which is at its maximum again at  $C_{M_\phi} = 1.0$  where the trajectory is almost straight instantly soon after the initial orientation is aligned with the propagation velocity  $V_{px}$ . As  $C_{M_\phi}$  is decreased, the trajectory starts curving increasingly towards the starting point (*SP* and *EP* indicate the star and the end of the trajectory).

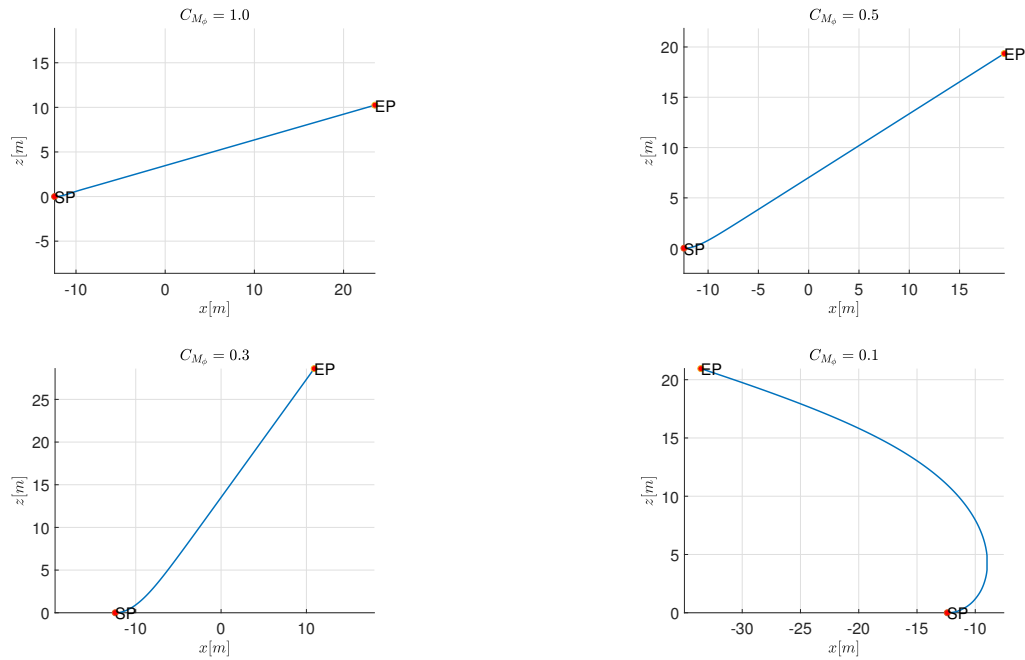


Figure 4.8: Plot showing the deviations in wheel trajectories for various stiffness  $C_{M_\phi}$

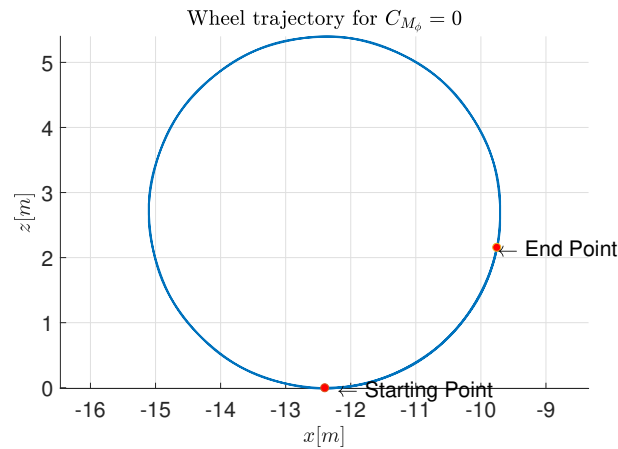


Figure 4.9: Wheel trajectory for  $C_{M_\phi} = 0$

#### 4.8.4 Camber thrust

There is no relaxation length associated with the camber thrust and therefore, the model for camber thrust remains as described by equation (3.23) in section 3.5.7.

## 4.9 Integrating tyre model in the simulator

At this point both the physical definition of a wheel and a tyre model for modeling a bicycle wheel are established. With the results from the vector calculation from section 4.6 and the tyre models from sections (4.7 and 4.8), a multibody model of a single wheel model are built in the simulator.

### Defining Vertical Force

From the vertical tyre force as given by equation (4.9), the force vector is defined to act normally from the ground and expressed in the reference frame  $I$  as:

$${}_I\mathbf{F}_n = F_n \hat{n} \quad (4.35)$$

### Defining Longitudinal Force

From longitudinal tyre force including relaxation length and normalized with the propagation speed  $V_{px}$  as described by equation (4.27), force is expressed in vector form as:

$${}_I\mathbf{F}_{long} = F_{long} \mathbf{e}_{long} \quad (4.36)$$

### Defining Lateral Force

From lateral tyre force including relaxation length and normalized with the propagation speed  $V_{px}$  as described by equation (4.30), force vector is expressed in the vector form as:

$${}_I\mathbf{F}_{lat} = F_{lat} \mathbf{e}_{lat} \quad (4.37)$$

### Defining Camber Force

From camber force generated by tyre as described by equation (3.23), the force vector acting along the lateral wheel direction is expressed as:

$${}_I\mathbf{F}_{camber} = F_{camber} \mathbf{e}_{lat} \quad (4.38)$$

### Defining Self-Aligning moment

Finally, from turn-slip moment including relaxation length as described by equation (4.34), the self-aligning moment along the normal direction to the contact

point is expressed as:

$${}_I \mathbf{M}_\phi = M_\phi \hat{n} \quad (4.39)$$

### Force and moment vector

The force and moment vectors are expressed as:

$${}_I \mathbf{F} = {}_I \mathbf{F}_n + {}_I \mathbf{F}_{long} + {}_I \mathbf{F}_{lat} + {}_I \mathbf{F}_{camber} \quad (4.40)$$

$${}_I \mathbf{M} = \mathbf{r} \times {}_I \mathbf{F} + {}_I \mathbf{M}_\phi \quad (4.41)$$

The application of forces and moments through the force elements are applied in the body fixed frame  $B$ :

$${}_B \mathbf{F} = {}^{BI} \mathbf{R} {}_I \mathbf{F} \quad (4.42)$$

$${}_B \mathbf{M}_\phi = {}^{BI} \mathbf{R} {}_I \mathbf{M} \quad (4.43)$$

## 4.10 Construction of physical models in SimMechanics

### 4.10.1 Construction of a single wheel model

In SimMechanics, the wheels physical geometry is defined through a CAD model attached to a six DOF joint. The follower axis of the six DOF joint are the body fixed axes of the wheel. Tyre model for generation of tyre forces and moments are modeled in Simulink. At the beginning and the end of the Simulink blocks a physical sensor and a physical force element is placed respectively. Using the feedback from the sensors, the tyre model calculates the slips and the forces and moments associated with them. The calculated dynamics are actuated to the wheel at every time step by the force element. The simulation process can be summarized through figure 4.10. The detailed tyre model library along is shown in the appendix A.

Figures (4.11(a) and 4.11(b)) show the SimMechanics model of a single wheel modeled to the parameters described in tables (4.1 and 4.2).

### Degrees of freedom

For a rigid body in 3D space, there are six degrees of freedom. Among these six degrees of freedom, the constraints are applied on the motion as *holonomic*:

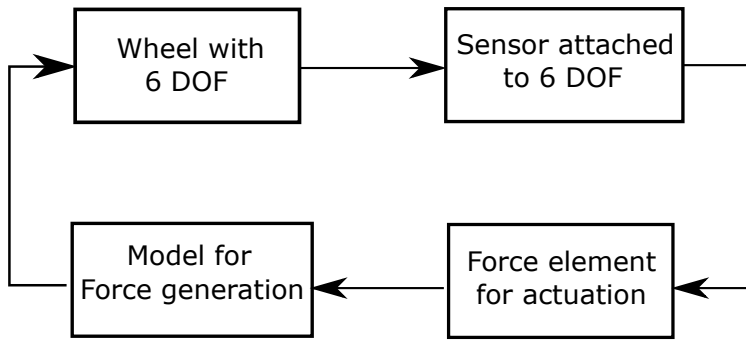
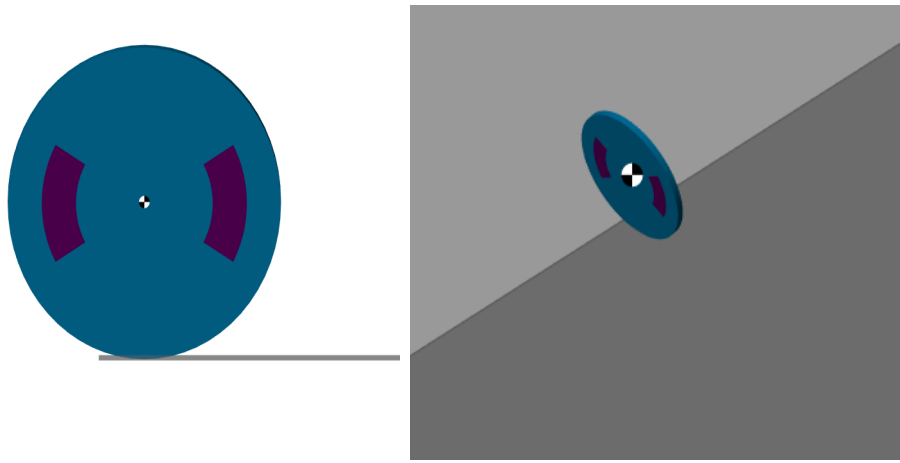


Figure 4.10: Simulation Data flow in SimMechanics



(a) Front view of the tire model

(b) Isometric view of the tire model

Figure 4.11: Figures showing the single wheel model built in SimMechanics

on the position of the wheel center from the ground and two *non-holonomic*: on the velocities of the contact point along longitudinal and lateral directions. Therefore, the total number of accessible configuration space for the wheel are:  $6 - 3 = 3$ .

#### 4.10.2 Construction of a Tricycle model

An intermediate vehicle model (a tricycle model) is constructed in SimMechanics mainly for the intermediate validation of tyre model behavior for various tyre parameters, vehicle steering conditions and velocities as well as establishing the nonholonomic constraints by observing the centrifugal forces acting on the vehicle. The tricycle model simulation flow is similar to the flow described in figure 4.10 for a single wheel model, except in this case the rigid body modeling in SimMechanics involves additional steps for assembling the parts and ensuring the sensor and

actuator data match the respective tyre models. A six degree of freedom joint is placed at the center of the tricycle frame, wheels, rear axle, front wheel and its steering column are built around it. The wheels are build again with the same parameters given in tables (4.1 and 4.2). Figure shows the SimMecahnics representation of the tricycle model and figure 4.12(b) shows the tricycle model with a pendulum. The detailed model of tricycle built in SimMechanics and its user manual is described in appendix B.

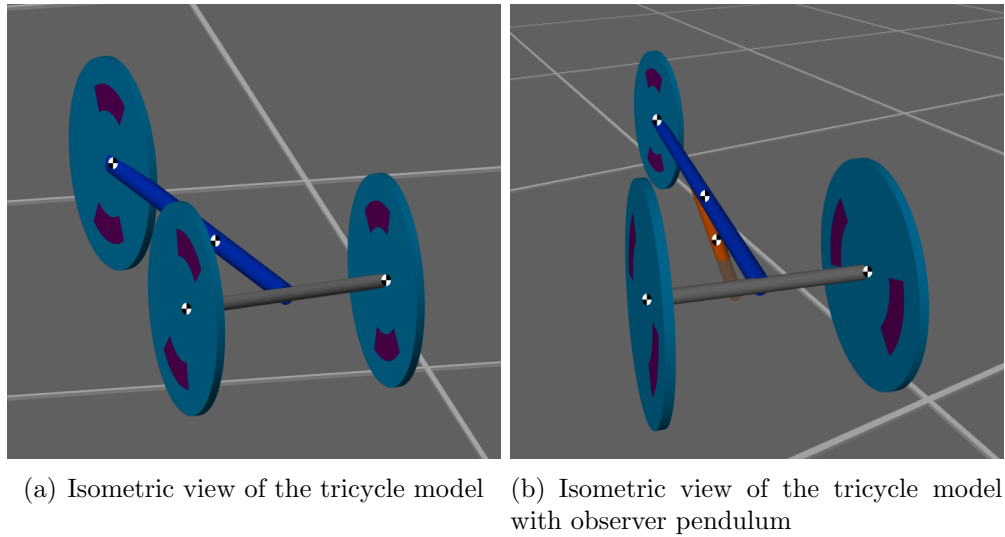


Figure 4.12: Figures showing the tricycle model built in SimMechanics

An pendulum is built in the accelerating frame of reference of the tricycle frame for sensing the centrifugal forces that enforce the nonholonomic constraints. The results of the simulation are described later in section 5.2

### Degrees of freedom

In order to determine the accessible configuration space of the tricycle, a systematic technique is employed as follows. For a rigid body in 3D space, the position and orientation can be described by three translational and three rotational degrees of freedom, therefore, leading to six degrees of freedom for each body-element. For a five body model as shown in figure 4.12(a), it is in total ( $5 \times 6 = 30$ ) degrees of freedom. From here, following constraints are applied, *holonomic*: four revolute joints at every wheel and a steering axis ( $-4 \times 5 = -20$ ), three holonomic constraints on the positions of the wheel centers from the ground ( $-3$ ). Therefore, leading to a system described by an accessible configuration space of ( $30 - 23 = 7$ ). These 7 accessible configuration space can be parameterized by the following: the position of the tricycle frame ( $x_p, y_p$ ), three angles

of each wheel ( $\theta_R, \theta_L, \theta_F$ ), yaw-rate of the frame  $\dot{\psi}$  and the steering angle  $\delta$ . In summary the configuration space is given by the tuple:  $(x_p, y_p, \dot{\psi}, \delta, \theta_R, \theta_L, \theta_F)$ .

From the six *non-holonomic* constraints that are applied on the velocities of the three wheels (1 lateral and 1 longitudinal at every wheel), the configuration space remains unaffected. The nonholonomic constraints affect the way in which the frame accesses the 7 dimensional configuration space.

### 4.10.3 Construction of a Bicycle model in SimMechanics

The design of the bicycle is modeled exactly like the four body model as described in [MPRS07, p.6]. This model is build using a rear wheel (*RW*), a front wheel (*FW*), a rear frame (*B*) and a front frame (*H*) as shown in the figure 4.13(b). Unlike rigid disc used in the [MPRS07, p.6], the SimMecahnics model is build using the tyre model as described in section 4.7. Revolute joints assemble the rear frames and the front frames with the rear and the front wheels respectively which basically forms the rear and front axles of the bicycle. All the 25 design parameters given in [MPRS07, p.9] are included into the model, also making room for allowing other design parameters apart from these for future simulations. The design also ensures the trail  $c$  for the front wheel the location of the center of mass of the front frame just ahead of the steering axis as shown in figure 4.13(a).

In SimMechanics all rigid bodies modeled are considered to be perfectly rigid, that is, the total strain energy stored in the material is *zero*. A measure of strain energy gives the total measure of the material straining (displacement) under elastic conditions. Therefore, the lesser the strain energy, the higher the stiffness of the material is. In SimMecahnics rigid bodies are considered to have an infinite stiffness and therefore no structural compliance. Further, the joints are considered to be made of perfect bearings having 100% accuracy and no damping or friction. Therefore, the SimMechanics bicycle model does not consider the structural compliance. Further assumption is made that the rider is fixed relative to the rear frame of the bicycle as shown in figure 4.13(a). The moment of inertia of both the wheels is assumed to be at the center. The brush model also does not consider the structural compliance and hysteresis of the tyre material.

Similar to [MPRS07, p.9] the rear and the front wheel diameters are chosen differently, so as to be able to investigate the possibility of effects of angular momentum on either wheels separately. Apart from the parameters that are given in [MPRS07, p.9] also given here in table 4.1 for reference, SimMechanics bicycle model requires a tyre model parameters which are given in table 4.2.

With all the design parameters setup, the SimMechanics model is developed as shown in the figures (4.13(a) and 4.13(b)), the model is build to match the exact

Parameter	Symbol	Value
Wheel base	m	$1.02m$
Trail	c	$0.08m$
Steer axis tilt	$\lambda$	18 deg
Gravity	g	$9.81m/s^2$
<b>Rear Wheel</b>		
Radius	$r_{RW}$	$0.3m$
Mass	$m_{RW}$	$2kg$
Mass moments of Inertia	$(I_{R_{xx}}, I_{R_{yy}})$	$(0.0603, 0.12)kg - m^2$
<b>Front Wheel</b>		
Radius	$r_{FW}$	$0.35m$
Mass	$m_{FW}$	$3kg$
Mass moments of Inertia	$(I_{R_{xx}}, I_{R_{yy}})$	$(0.1405, 0.28)kg - m^2$
<b>Rear Frame B</b>		
Center of mass	$(x_B, y_B)$	$(0.3, 0.9)m$
Mass	$(m_B)$	$85kg$
Mass moments of Inertia	$\begin{bmatrix} I_{B_{xx}} & 0 & I_{B_{xz}} \\ 0 & I_{B_{yy}} & 0 \\ I_{B_{xz}} & 0 & I_{B_{zz}} \end{bmatrix}$	$\begin{bmatrix} 9.2 & 0 & 2.4 \\ 0 & 11 & 0 \\ 2.4 & 0 & 2.8 \end{bmatrix} kg - m^2$
<b>Front Frame H</b>		
Center of mass	$(x_H, y_H)$	$(0.9, 0.7)m$
Mass	$(m_H)$	$4kg$
Mass moments of Inertia	$\begin{bmatrix} I_{H_{xx}} & 0 & I_{H_{xz}} \\ 0 & I_{H_{yy}} & 0 \\ I_{H_{xz}} & 0 & I_{H_{zz}} \end{bmatrix}$	$\begin{bmatrix} 0.05892 & 0 & -0.00756 \\ 0 & 0.06 & 0 \\ -0.00756 & 0 & 0.00708 \end{bmatrix} kg - m^2$

Table 4.1: Benchmark Parameters for bicycle model in SimMechanics

parameters as in [MPRS07, p.9].

### Degrees of freedom of the bicycle

Following similar techniques described in [MPRS07, p.8] on the arguments concerning degrees of freedom, the following analysis can be made. For the bike of four rigid bodies connected as links in a 3D space, the total  $DOF = 6 \times 4 = 24$ .

Parameters	Value
Longitudinal Stiffness	$1 \times 10^4 N$
Lateral Stiffness	$1 \times 10^4 N$
Vertical Stiffness	$1 \times 10^5 N/m$
Damping	$1 \times 10^2 N - s/m$
Relaxation Length	$0.12m$

Table 4.2: Tyre Parameters for bicycle model in SimMechanics

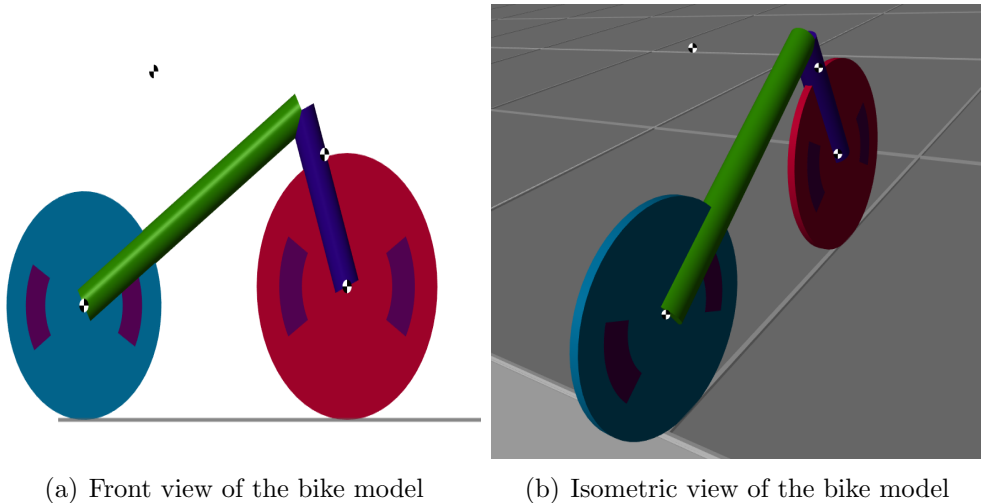


Figure 4.13: Figures showing the bicycle model built in SimMechanics

Among these, the following constraints apply to the model: two non-holonomic constraints for each of the two wheels, two holonomic constraints for the position of the contact point from the ground. Other holonomic constraints are applied on the three revolute joints at the rear frame, front frame and the steering head. Among all these constraints only the five constraints from joints and two holonomic constraints on position affect the accessible configuration space. Therefore reducing the degrees of freedom to  $24 - (3 \times 5) - 2 = 7$ . The two non-holonomic constraints on velocities of rear and front wheels do not change the accessible configuration space but change the way the position and orientation of the bicycle would be reached in the configuration space due to these constraints.

These 7 dimensional configuration space can be parameterized similar to the technique described in the [MPRS07, p.8]. The position of the bicycle is measured with reference to the rear wheel contact point  $(x_p, y_p)$ . The orientation of the rear frame is given by the sequence of rotations measured through a global sensor attached to the rear wheel. These rotations are given by 6 degrees of freedom joint attached to the wheel center and measure the rotation through a

quaternion [Mat18]. The three angles measured are given by their rates: rolling rate  $\dot{\phi}$ , yaw-rate  $\dot{\psi}$  and pitching rate  $\dot{\theta}$  of the rear wheel. The steering angle  $\delta$  is measured as the angular position of the steering frame about the steering axis. Finally the rotation of the rear and the front wheel are measured:  $(\theta_{RW}, \theta_{FW})$ . From all these parameters, the configuration space can be summed up as  $(x_p, y_p, \psi, \phi, \delta, \theta_{RW}, \theta_{FW})$ .

Generally, for a 7 dimensional configuration space, there are 7 velocity degrees of freedom. However, in the case of 4 non-holonomic constraints applied to the rear and front wheel velocities, the accessible configuration is now reduced to 3 degrees of velocity freedom given by the yaw-rate  $\dot{\psi}$ , lean-rate  $\dot{\phi}$  and the pitching-rate  $\dot{\theta}_{RW}$  of the rear wheel.

### Published model in the web

The detailed model of various bicycles with different design parameters and tyre parameters built in SimMechanics is described later in appendix C. The bicycle built using a standard bicycle design, which was also used in *Investigation 3* for comparing the results with [MPRS07] and [BDBK15] was published in the public domain. The model files can be found under the following link [TA18a] and a short video description of all the models including a single wheel and a tricycle is available in the *YouTube* channel of *EIT, TU Kaiserslautern* [TA18b].

# 5 Multibody Simulation Results

## 5.1 Single wheel model

Simulation of a single wheel model is compared with the results from a mathematical model of a solid disk that is constrained to follow nonholonomic constraints on velocity as described by:

$$\dot{x} = v \cos \psi \quad (5.1)$$

$$\dot{y} = v \sin \psi \quad (5.2)$$

where  $\psi$  is the orientation or the heading angle of the wheel in the direction of the propagation velocity  $V_{px}$ . From the observations after running the two simulations, an intuitive study can be made and the results from mathematical models can be compared. Consider a bicycle parametric model as described in [MPRS07, p.9]. The parameters are given here again in table 5.1 for reference:

Some simulations were conducted previously in section 4.8.3 where the behavior of self-aligning moment  $M_\phi$  of a single wheel was established with a relationship to the turn-slip ratio  $\phi_t$ . Further, in this section the behavior of the physical model is compared with that of the mathematical model previously developed at the *Institute of Control Systems, TU Kaiserslautern*. In these simulations, a comparative study can be established between the trajectories of the mathematical model and physical model and the deviations observed. The simulations were conducted for various initial speeds  $v_0$  and initial camber angle  $\varphi_0 = 5^\circ$  for a time span of  $t = 50s$ .

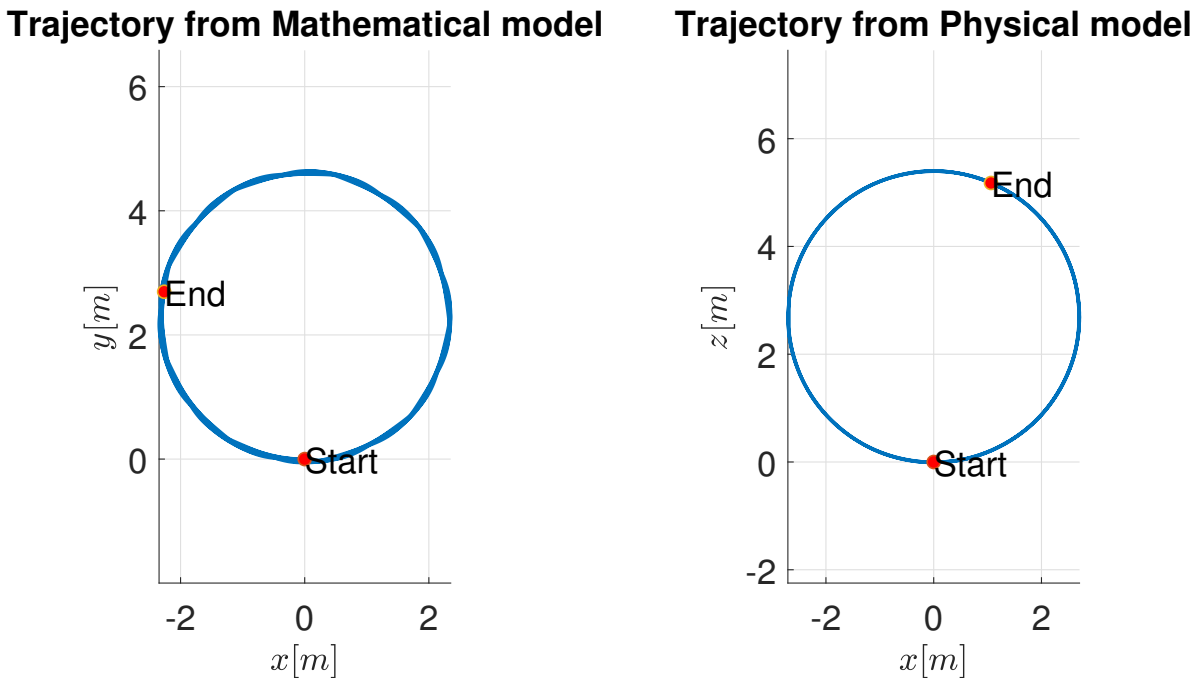
For the purpose of simulation, following tyre parameters as given in table 5.2 are considered:

Parameter	Symbol	Value
radius	$r_R$	$0.3\ m$
mass	$m_R$	$2\ kg$
Mass moment of Inertia	$(I_{xx}, I_{yy})$	$(0.0603, 0.12)\ kg - m^2$

Table 5.1: Wheel parameters for a single wheel simulation

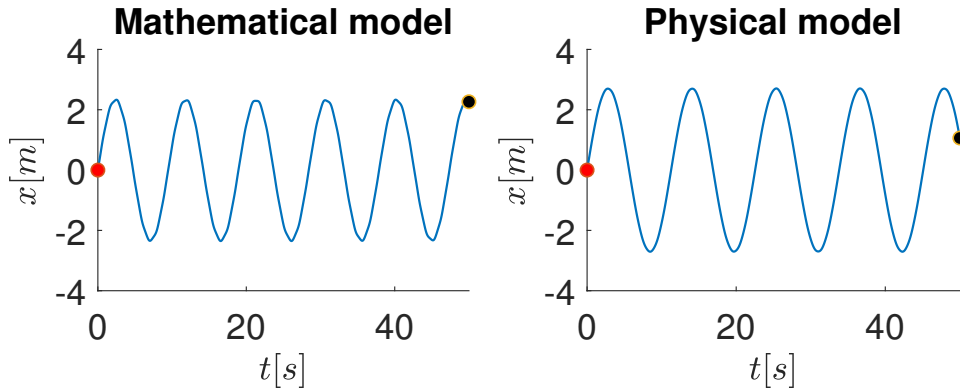
Parameter	Symbol
Longitudinal tyre stiffness	$2 \times 10^4 \text{ N/m}$
Lateral tyre stiffness	$2 \times 10^4 \text{ N/m}$
Vertical tyre stiffness	$5 \times 10^4 \text{ N/m}$
Vertical damping	$1 \times 10^2 \text{ N} - \text{s/m}$
Relaxation length	0.12 m

Table 5.2: Tyre parameters considered for a single wheel simulation

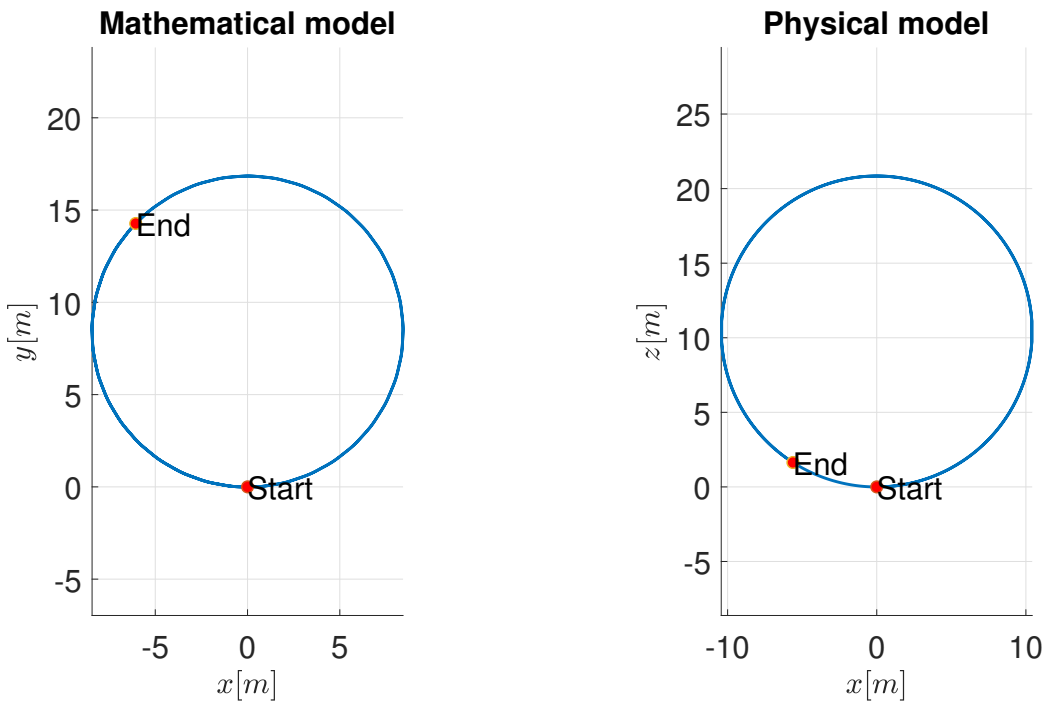
Figure 5.1: Comparison of wheel trajectories at  $v_0 = 1.5\text{m/s}$ 

As can be seen in figure 5.1, at lower initial velocities (ranging up to  $v_0 = 2.0\text{m/s}$ ), there is a good agreement between the mathematical and the physical models both in terms of behavior and parameters. A plot of a number of running cycles in the given simulation time of  $t = 50\text{s}$ , shows that the mathematical model produces approximately a quarter of a cycle more than the physical model (red and black dots indicate start and end) as shown in figure 5.2. This fact can be appreciated by the tyre model which considers slips along longitudinal and lateral directions.

Generally, in a no-slip disc, the lateral forces generated by a disc are such that the contact point of the disc does not slip while cornering. In the case of tyre model with slips, the wheel would slip laterally compared to a no-slip solid disc. Such results can be seen from the simulation run at higher initial velocities. Figure 5.3

Figure 5.2: Comparing cycles at  $v_0 = 1.5 \text{ m/s}$ 

show the plots generated for the initial conditions  $v_0 = 2.5 \text{ m/s}$  for mathematical and physical models.

Figure 5.3: Comparing wheel trajectories at  $v_0 = 2.5 \text{ m/s}$ 

The deviation in the trajectory is now more pronounced as the initial velocity is increased to  $v_0 = 5 \text{ m/s}$  under the same camber angle  $\varphi_0 = 5^\circ$ . Figure 5.4 shows the plots generated for this case.

Further simulations are done for friction at the joint (wheel bearings) that would eventually damp the motion and bring the wheel to halt. A damping coefficient

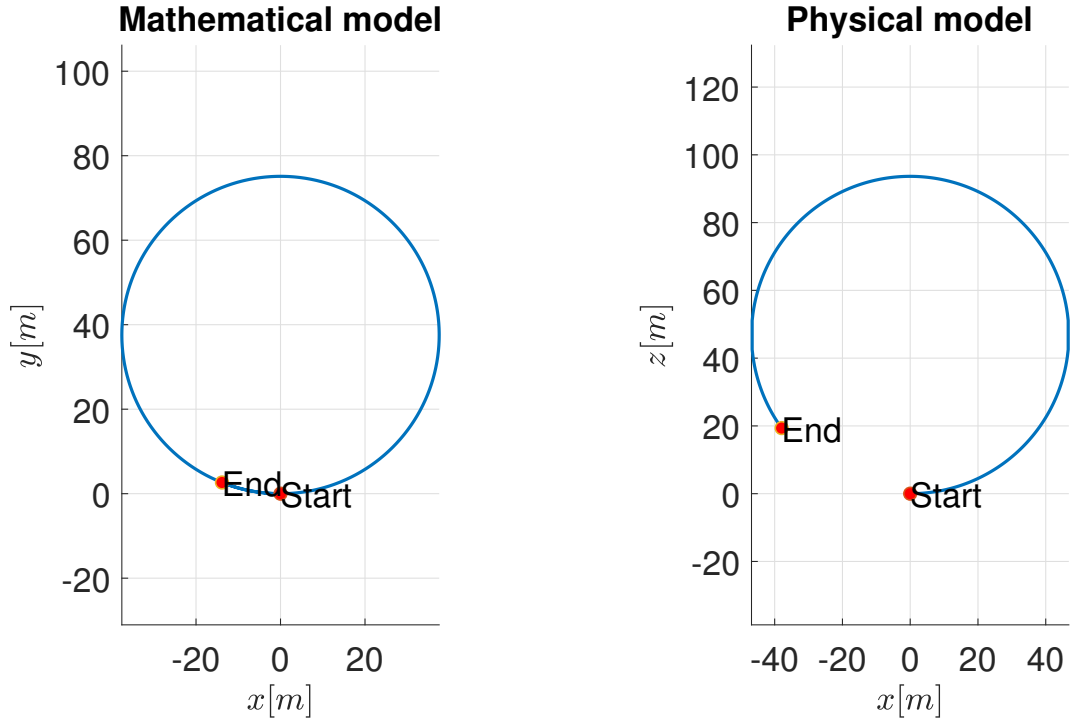
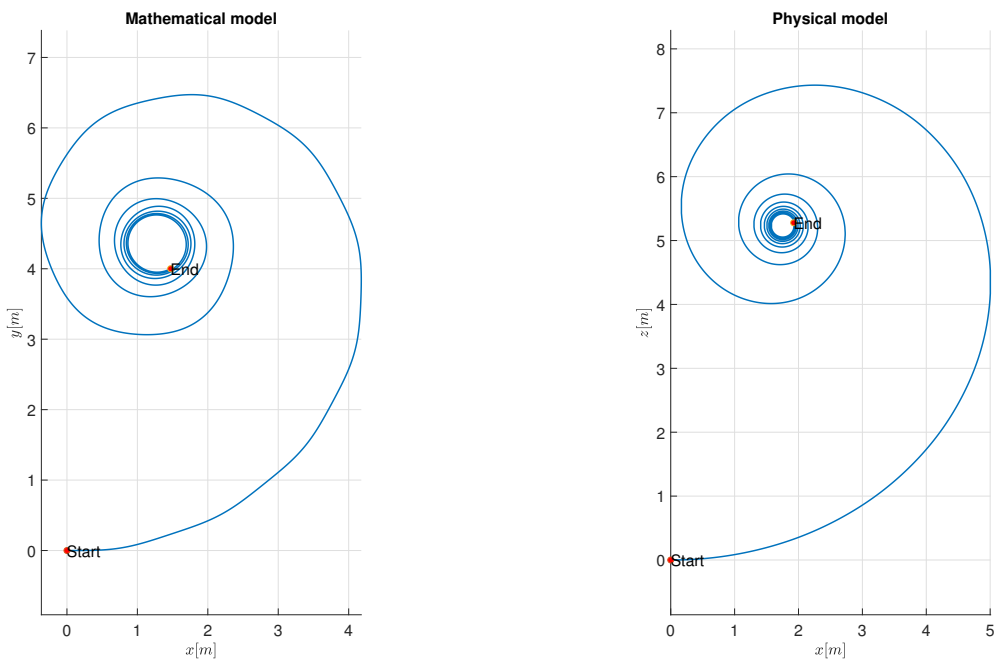
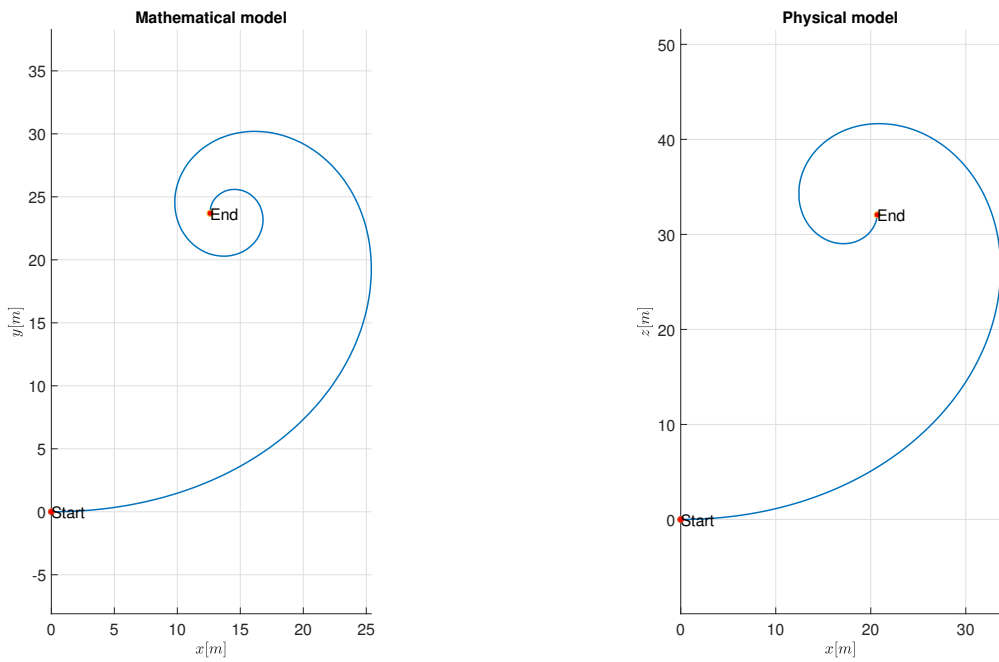


Figure 5.4: Comparing wheel trajectories at  $v_0 = 5.0\text{m/s}$

of  $1 \times 10^{-2} N - m(\text{rad/s})$  is given at the spherical primitive of the 6 DOF joint in SimMechanics to simulate the behavior of friction in joints. Unlike in mathematical model, 6 DOF in SimMechanics does not provide with the flexibility of choosing a particular axis of rotation, damping is provided equally on all the axes of the follower frame as a torque required to maintain a constant joint primitive angular velocity between the base and follower frames [Mat18]. Figures (5.5 and 5.6), show the comparison of damping between mathematical and physical model for initial velocities  $v_0 = 2.0\text{m/s}$  and  $v_0 = 5.0\text{m/s}$  for initial lean angle  $\varphi_0 = 5^\circ$  respectively. The simulation were run for a total time  $t = 30\text{s}$ .

Figure 5.5: Comparing wheel trajectories with friction at  $v_0 = 2.0\text{m}/\text{s}$ Figure 5.6: Comparing wheel trajectories with friction at  $v_0 = 5.0\text{m}/\text{s}$

## 5.2 Tricycle model

In addition to the behavioral analysis done with the solid disc, the forces that are generated by the tyre model for vehicles can be studied through an intermediate tricycle model. In order to investigate the nonholonomic constraints enforced by the lateral tyre forces, a pendulum is attached to the frame of tricycle. The accelerating frame of tricycle experiences a centrifugal force and the sensor attached with the pendulum would help to measure this force. The nonholonomic constraints are maintained by vehicles like a tricycle and a bicycle by generating centripetal forces in the tyres that maintain the constraints as described in section 3.5.4. For a tricycle as shown in figure 5.7. with the same tyre model as described in section 5.1 (additionally a  $C_{M_\phi} = 0.3$ ) a simulation is conducted at an initial speed  $v_0 = 8m/s$  and an input steering torque was given as shown in figure 5.8 to produce trajectory as shown in figure 5.9.

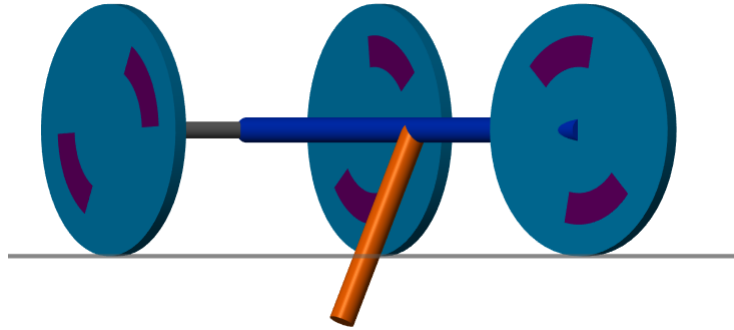


Figure 5.7: Construction of SimMechanics tricycle model with a pendulum attached

A sensor attached to the pendulum measures the torques that are applied to the pendulum due to the turning of the tricycle. Figure 5.10 shows the plot of the torque measured by the sensor, it can be seen that the torque is zero until time  $t = 4s$  when the tricycle is traveling along a straight line. As the tricycle turns due to the applied steering torque, a torque is measured by the pendulum's sensor as shown in the figure 5.10. This torque is analogous to the D'Alemberts force felt by an observer sitting inside a vehicle taking a corner as described in sections (3.5.4 and 3.5.4). However, the vehicle itself generates centripetal acceleration to turn into a corner due to the lateral tyre forces generated by the tyre. Therefore, with the results from figure 5.10, it can be seen that there are only the centrifugal forces that are present during cornering that keeps the vehicle stable such as complying to the nonholonomic constraints.

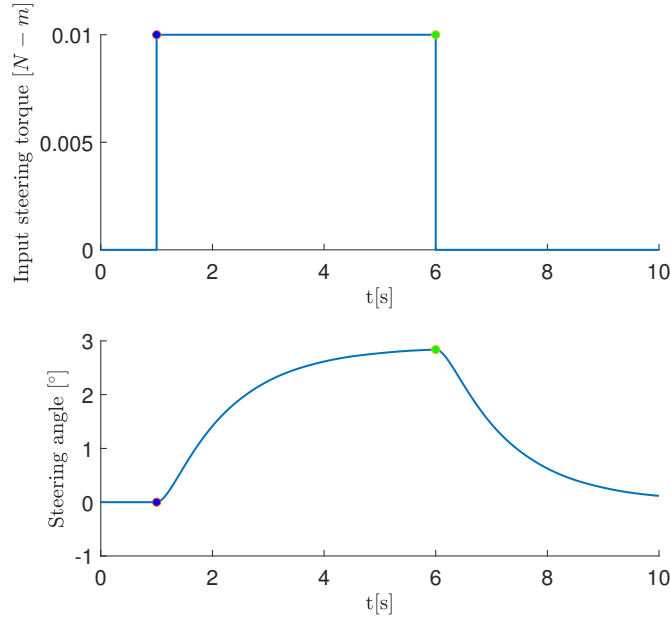
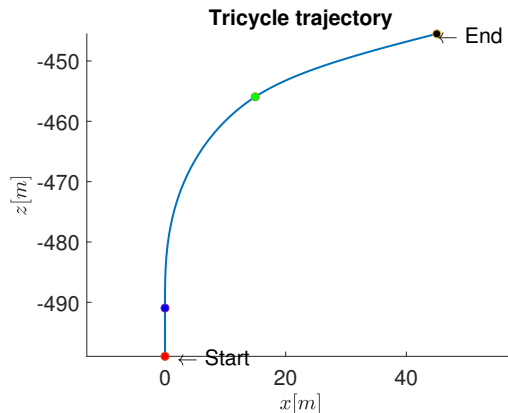


Figure 5.8: Input steering torque and output steering angle

Figure 5.9: Trajectory of a tricycle for tyre with  $M_{\phi}$ 

Another set of investigations are conducted for a wheel with no-self aligning stiffness with the tyre parameters as given in table 5.2. It can be seen in figure 5.11, that the trajectory in case of a tyre with no self-aligning stiffness is to go around circles, which is converse to behavior in figure 5.9 where the wheel aligns itself in the direction of the propagation velocity  $V_{px}$ .

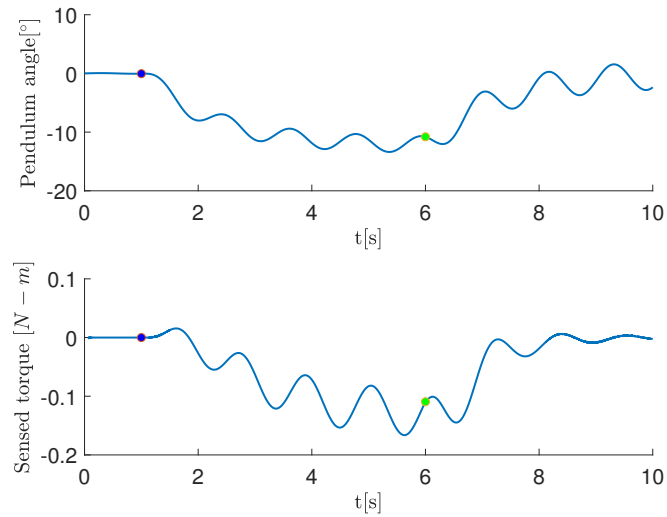


Figure 5.10: Pendulum angle and measured torque for tricycle with  $M_{\phi}$

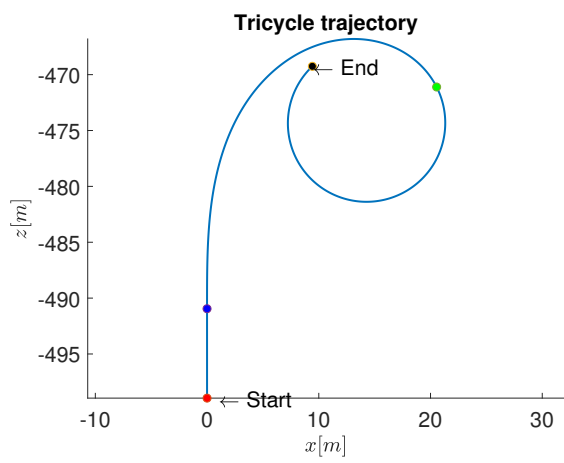


Figure 5.11: Trajectory of a tricycle for tyre with no  $M_{\phi}$

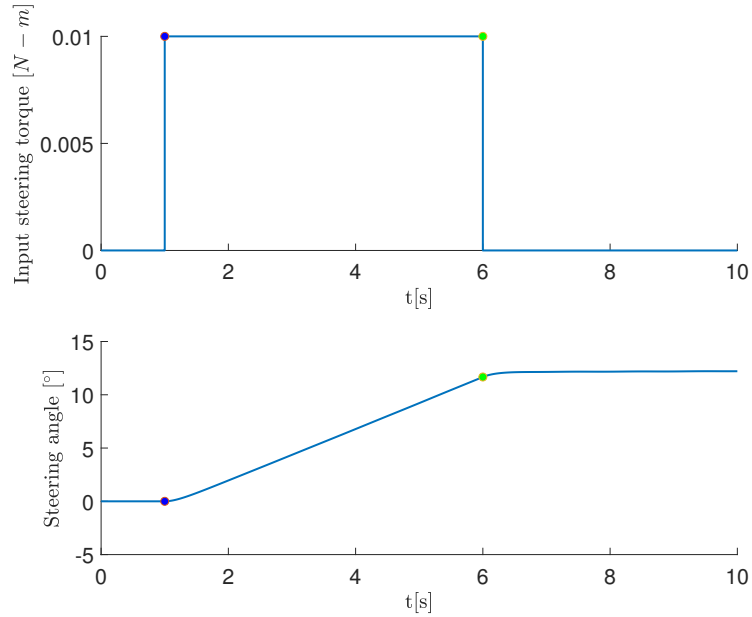


Figure 5.12: Input steering torque and output steering angle for tyre with no  $M_\phi$

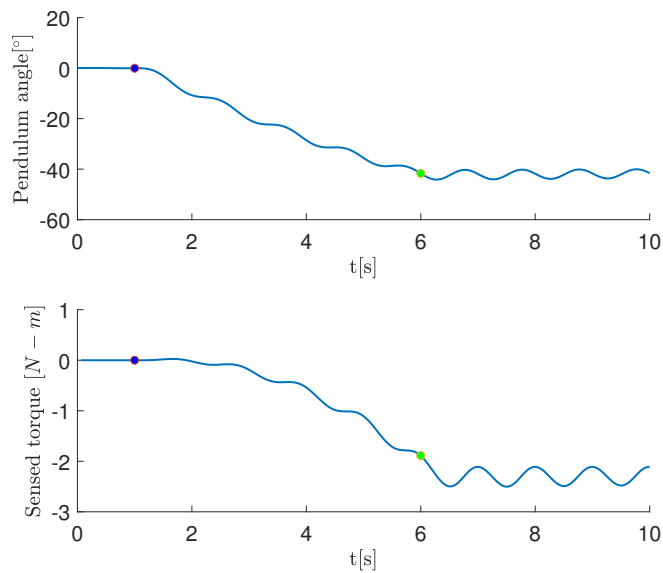


Figure 5.13: Pendulum angle and measured torque of tricycle for tyre with no  $M_\phi$

### 5.3 Bicycle validation from linear benchmark model

The *Linear Benchmark model* provides systematic analysis of the bicycle motion through establishing four distinct Eigenmodes, corresponding to different Eigenvalues. From each of these Eigenvalues, the following conclusions in table 5.3 have been summarized from [MPRS07, p.15]:

Velocity range	Eigenvalues	Eigenmodes	Corresponding motion
$0 < v < v_d$	two positive and two negative pairs	inverted pendulum like	unstable like an inverted pendulum
$v_d < v < v_w$	complex pair, coalesced from two positive pairs	wave mode	bicycle leans and steers from side to side, at certain speeds weave motion becomes stable and the lean rate becomes zero
$v_w < v < v_c$	complex pair, one of the negative pair crosses the positive axis	capsize mode	beginning of mild instability, leading to progressive leaning and falling over
$0 < v < v_w$	large real negative	castering mode	caster wheel like trajectory pursuit

Table 5.3: Eigen modes of the bicycle

The weave mode is characterized by the oscillations in both the lean and the steer rates with steering rate having a phase lag relative to leaning [MPRS07, p.15]. The frequency of the weave increases with increasing speeds indicated by increasing magnitude of the imaginary parts of the complex conjugate pairs, leading to a constant wavelength between the successive oscillations [den, p.61]. For certain bicycle configurations and at certain velocities, the wave motion damps out completely making the motion of the bicycle asymptotically stable as described in section 2.2.2. It should also be noted that there is no actual damping in the system, in fact the energies from the lean and the steering oscillation are transferred

to forward speed and the energy of the whole system is conserved.

Unlike the benchmark model, the SimMechanics model differs from the types of wheels chosen and it would not be possible to make exact parametric validation. Also since Eigenvalue analysis is not possible for non-linear systems like a bicycle, analysis on the modes of bicycles motion is made based on developing scenarios and relating the various modes to the Eigenmodes described in table 5.3. The self-stable mode of the bicycle where the weave motion of the bicycle damps to zero is also established by the simulator. Most of the scenarios described are taken from [TL18b, p.11,12,13,14]. In order to describe various modes of the bicycle motion adequately, following parameters are chosen: steering angle  $\delta$  and steering rate  $\dot{\delta}$ , leaning angle  $\varphi$  and leaning rate  $\dot{\varphi}$  and finally the forward velocity of the bicycle  $v$ . The simulations conducted are based on the bicycle design parameters as described in section 4.10.3.

## 5.4 Investigations for testing SimMechanics models

As described in section 5.3, for validating the bicycle model, scenarios are defined in order to test for four distinct Eigenmodes of bicycle motion as described in the linear benchmark model and given in table 5.3. For sufficiently measuring the behavior of the bicycle following parameters are chosen  $[\varphi \ \delta \ \psi \ \xi]$  which are the bicycles lean angle, steering angle, the orientation angle of the rear frame and the forward velocity respectively. Also as described in section 5.1, the bicycles tyre model deviates from the model of a solid disc on one important factor, that is the self-aligning moment generated by the turn-slip , which in the case of a solid disc is lacking. In order to appreciate this deviation more clearly and also to establish the various modes of bicycle motion with the model built in SimMechanics, series of investigations are conducted.

In *Investigation 1*, the bicycle is first simulated with no self-aligning stiffness and the results are compared directly with the results from the benchmark model. In *Investigation 2*, tyre model with self-aligning stiffness is included and the deviations in the weave velocity and capsize velocity from *Investigation 1* are studied. In *Investigation 3* (Blue bike), a different bicycle design parameters are considered and all the bicycle modes from *Investigation 1* are established. Further, in *Investigation 3* (Red bike), a bicycle model is used which is built at the *Institute of Control Systems, TU Kaiserslautern* and simulations are conducted to investigate Eigenmodes from linear bicycle model as well as scenarios from nonlinear model and adding a CMG. From Investigations 3 (both for blue and red bikes), the flexibility of the SimMechanics bicycle model can be re-enforced

to test with various bicycle design parameters. Finally, in *Investigation 4* various scenarios are defined in order to simulate the scenarios from a nonlinear bicycle model [TL18a]. Also, the investigations are summarized in the following table 5.4 for easy referencing.

Title	Simulation parameters	Investigating
Investigation 1	Tyres with no-self aligning stiffness	Comparison with the benchmark bicycle model
Investigation 2	Tyres with self aligning stiffness	Comparison of the deviations form the benchmark model with the bicycle with tyre models as described in [BDBK15]
Investigation 3	Different bicycle design ( <b>Blue bike</b> )	Investigations on a standard bicycle design
	Different bicycle design ( <b>Red bike</b> )	Investigations on autonomous bicycle developed at [Tur18]
Investigation 4	Using feedback to actuate steering and lean	Investigate controllability (or ride-ability) scenarios from nonlinear bicycle model

Table 5.4: Summary of various investigations to be carried out with SimMechanics models

### 5.4.1 Investigation 1: With no self-aligning tyres

#### Scenario 1: Weave mode

At zero velocities, the bicycle would fall over behaving like an inverted pendulum. At higher initial velocities, the bicycle tends to oscillate into a wave motion before falling over. The oscillatory motion of the steering towards the undesired lean is called the weave mode of the bicycle. In this mode, the steering can be seen having a phase lag with the lean as shown in the figure 5.14. The weave motion

cab be seen by running the simulation at  $v_0 = 4.3m/s$  with a lateral perturbation on the rear frame ( $T_\varphi$ ) at time  $t = 4s$  as shown in figure 5.4.1. At further higher

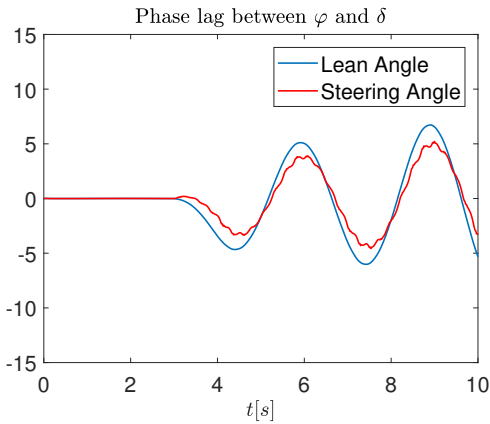


Figure 5.14: Phase lag between  $\varphi$  and  $\delta$

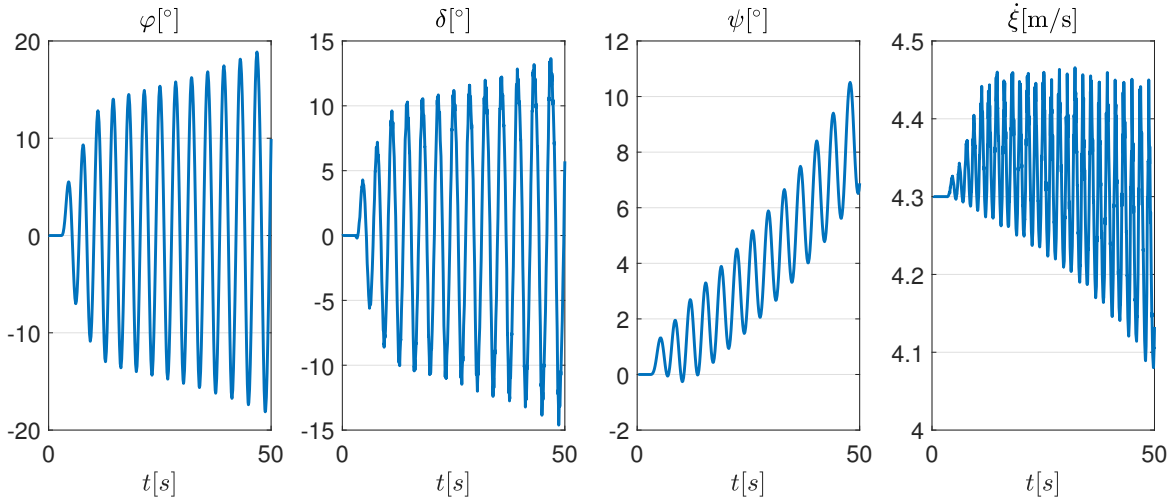


Figure 5.15: Investigation 1: Weave mode at  $v = 4.3m/s$

initial velocities, the bicycle tends to stabilize this weave motion, damping the wave-like motion of steering as shown in figure 5.16. The highest velocity at which weave oscillations of the bicycle becomes stable is called the weave velocity  $v_w$ , beyond  $v_w$  the bicycle would be self-stable damping out the oscillations. The inception of this stable weave mode appears at slightly higher velocities as can be seen in figure 5.16.

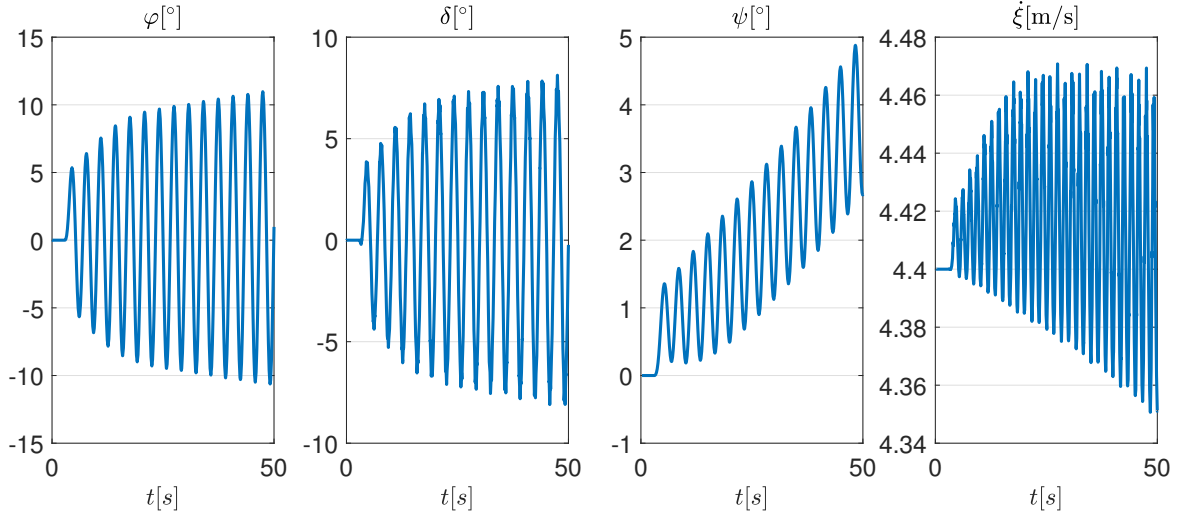


Figure 5.16: Investigation 1: Stabilization of weave motion at  $v_w = 4.4\text{m/s}$

### Scenario 2: Self-stable motion

At slightly higher velocities than the weave velocity  $v_w$ , the wave like motion of the steering damps out correcting the undesired lean of the bicycle as shown in figure 5.17. The simulations were run at initial velocity  $v_0 = 4.5\text{m/s}$  with a lateral perturbation  $T_\varphi$  at time  $t = 4\text{s}$ . This fact of achieving self-stability can also be appreciated by considering the asymptotic stability behavior of non-linear systems as described in section 2.6. As shown in figure 5.17, the bicycle is

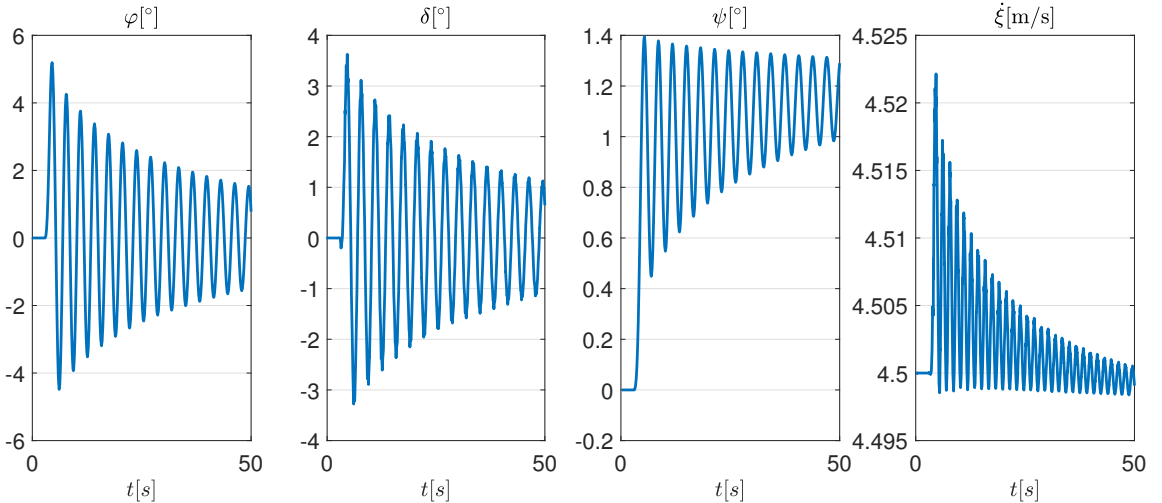


Figure 5.17: Investigation 1: Self-stable mode at  $v_0 = 4.5\text{m/s}$

self-stable at velocities starting from  $v_0 = 4.5\text{m/s}$ , this value is also in the speed

range for self-stability given in [MPRS07, p.15]. Running the simulations at much higher initial velocities leads to damping more quickly as shown in figure 5.18.

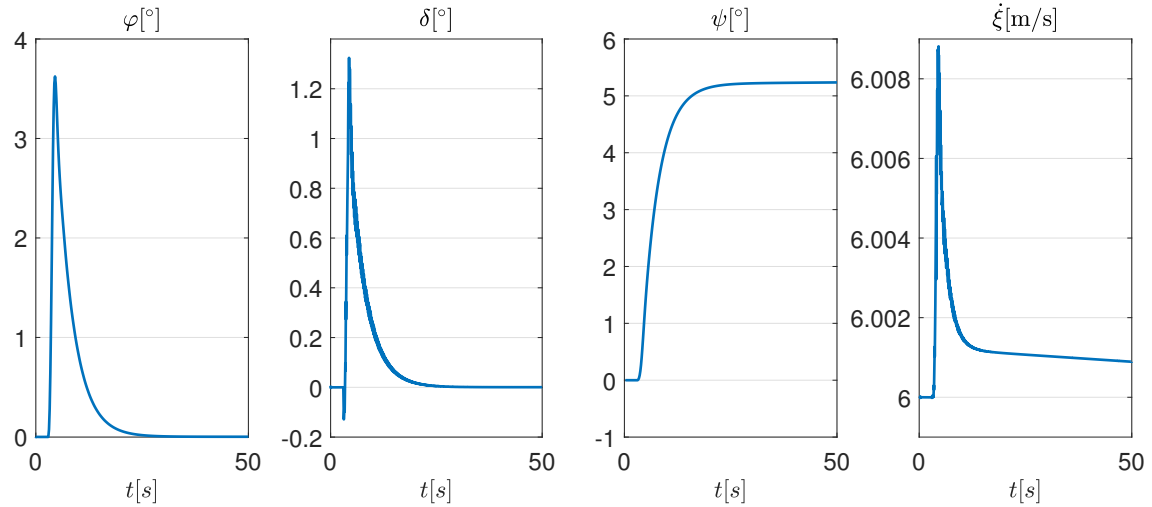


Figure 5.18: Investigation 1: Self-stability at higher velocities

For the bicycle considered by the design parameters as described in section 4.10.3 and tyre parameters as given in 5.2, the range for self-stability lies in the same range as described in [MPRS07, p.15] in case of tyres with no self-aligning stiffness.

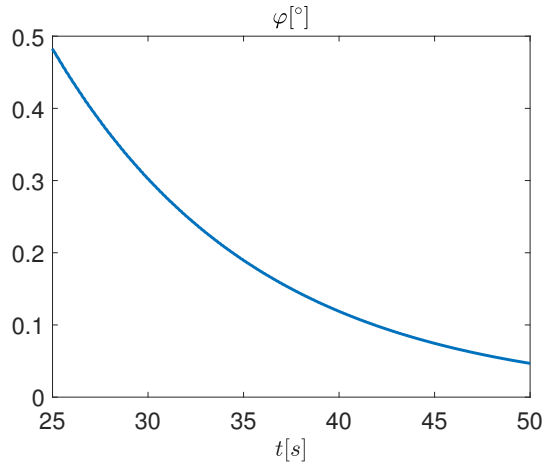


Figure 5.19: Investigation 1: Capsize velocity at  $v_0 = 6.5m/s$

### Scenario 3: Capsize speed

Capsize velocity  $v_c$  is the highest velocity where the capsizing mode of the bicycle is stable, above this velocity  $v_c$  the bicycle is unstable again. Therefore, the self - stability of a bicycle can be identified between the weave velocity  $v_W$  and capsizing velocity  $v_c$ . In order to appreciate this behavior, the bicycle is now run at higher initial velocities than  $v_c > v_w$ . The capsizing speed in the linearized model shows its inception at speeds higher than  $6m/s$ . In the SimMechanics model, investigations were conducted from initial velocities between  $v_0 = 6.1m/s$  to  $v_0 = 6.5m/s$  with a lateral perturbation at  $t = 4s$ , the lean angle started to deviate from zero though at a rather slow rate, indicating a slow falling over of the bike. Figure 5.19, shows a behavior where the bike is run at the velocity  $v_0 = 6.5m/s$ . However, appreciable behavior of capsizing mode was only noticeable at velocities such as  $v_0 = 6.7m/s$ . In order to appreciate this behavior more quickly, the simulation was run at higher initial velocities  $v = 7.5m/s$  and the response is plotted as shown in figure 5.20. The trajectory of the bicycle in this mode is shown in figure 5.21. At the end of this simulation (indicated by end point), the simulation was terminated when the bicycle falls over to the ground.

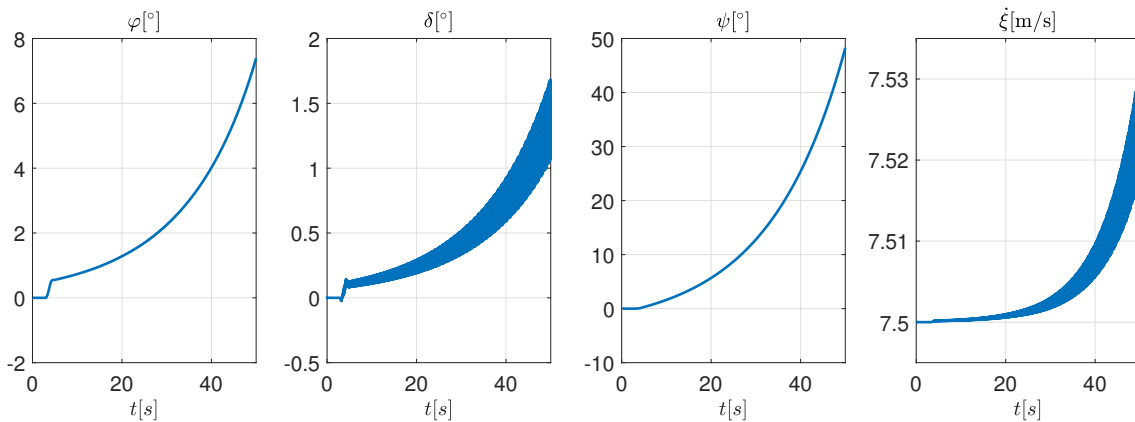


Figure 5.20: Investigation 1: Capsize mode at higher velocities

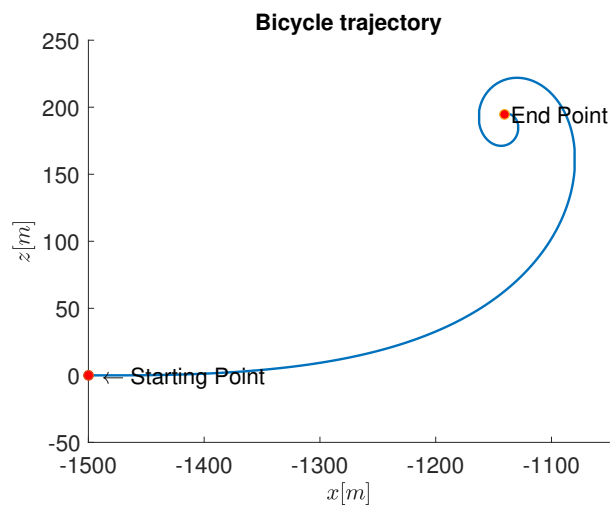


Figure 5.21: Investigation 1: Bicycle trajectory at higher capsizing velocities

### Scenario 4: Non-minimal phase behavior

It is well known phenomenon among motorcyclists, that in order to take an effective corner, the rider first turns slightly into the opposite direction. This phenomenon is called counter-steering. In order to appreciate this behavior a perturbation to the steering handle is given as an impulse torque  $T_\delta$  at time  $t = 4\text{s}$ . As shown in figure 5.22, a positive  $T_\delta$  corresponds to steering to be turned to right. A slightly turned steering bends the bicycle in the opposite direction and helps to corner more effectively. The results of  $T_\delta$  is to turn the bicycle towards left as shown in figure 5.23.

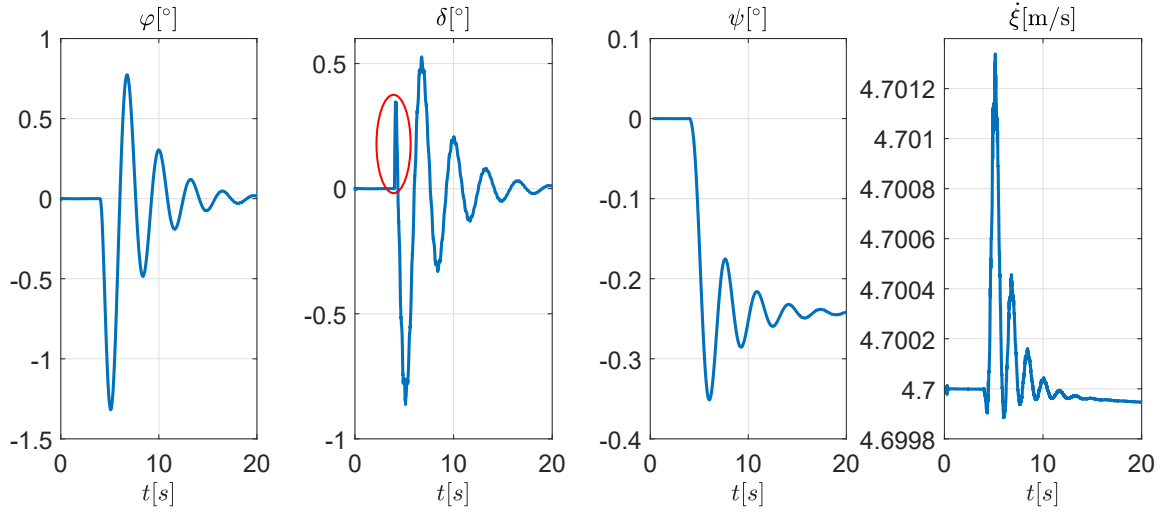


Figure 5.22: Investigation 1: Non-minimal phase behavior

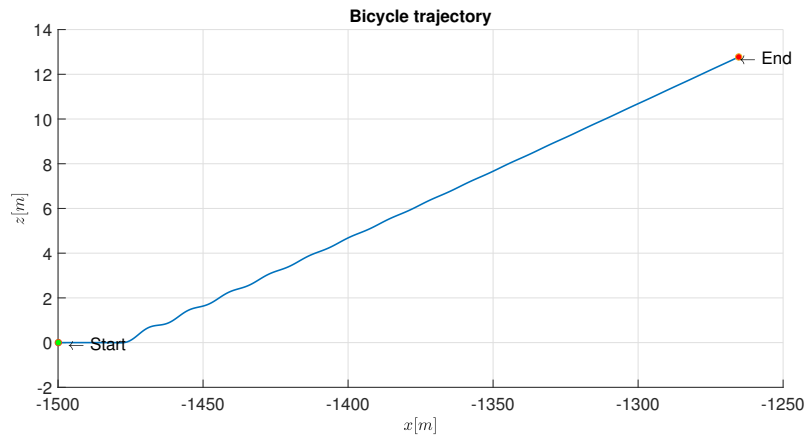


Figure 5.23: Investigation 1: Trajectory of non-minimal phase behavior

### 5.4.2 Investigation 2: With self-aligning tyres

In their paper [BDBK15], Bulsink et. al, have conducted various simulations with realistic tyre models and rider models and compared their results with the results from the benchmark model. In summary to their paper, by varying tyre parameters starting from the idealized no slip model considered in the benchmark model, noticeable deviations were observed in weave speeds  $v_w$  and capsize speed  $v_c$  of the bicycle. Infact, by implementing the *Magic Formula Tire Model*, the weave speed was observed to be stabilize at  $v_w = 9.5m/s$  and the capsize speed was always stable [BDBK15, p.6].

In the SimMechanics model, apart from the slips considered in the model, the tyre model also differs from the idealized no slip disc model from [MPRS07] on the basis that the tyre model also has a self-aligning stiffness  $C_{M_\phi}$  that a solid disc lacks. Now by including self-aligning moment generated due to turn-slip, results are generated and compared with the deviations from the results from section 5.4.1.

#### Bicycle modes

In these simulations the tyre with self-aligning stiffness is consider with  $C_{M_\phi} = 0.3(N - m)/(rad/m)$ . Consider figure 5.24, by running the simulation at initial velocity  $v_0 = 4.4m/s$ , the bicycle is now unstable as predicted. The bicycle consequently falls over at time  $t = 45s$ , following a trajectory as shown in the figure 5.25.

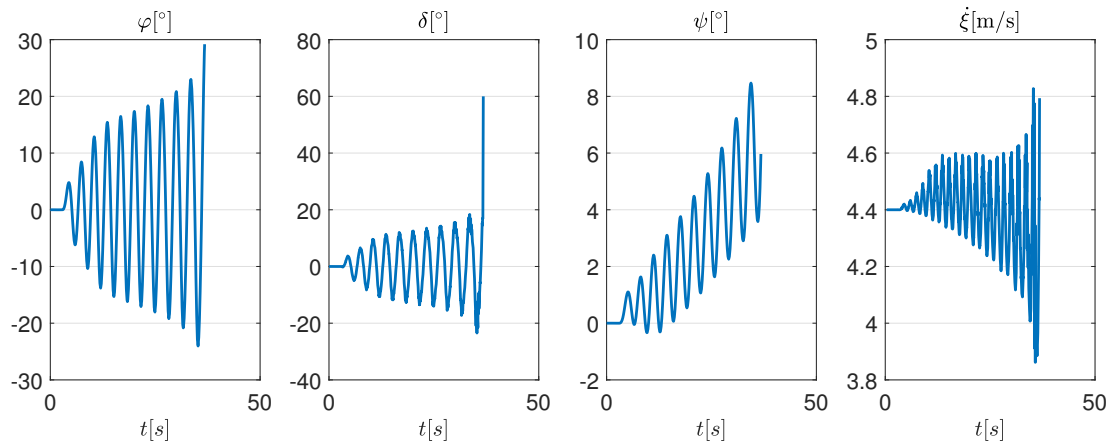


Figure 5.24: Investigation 2: Weave mode instability at  $v_0 = 4.4m/s$

The weave mode stabilizes at  $v_0 = 4.6m/s$  as shown in figure 5.24.

The capsize mode was evident from  $v_0 = 9.5m/s$  on-wards as shown in figure 5.27 beyond which the bicycle is no more self-stable for any lateral perturbations, the trajectory can be seen in figure 5.28. Therefore, this bicycle is self-stable at

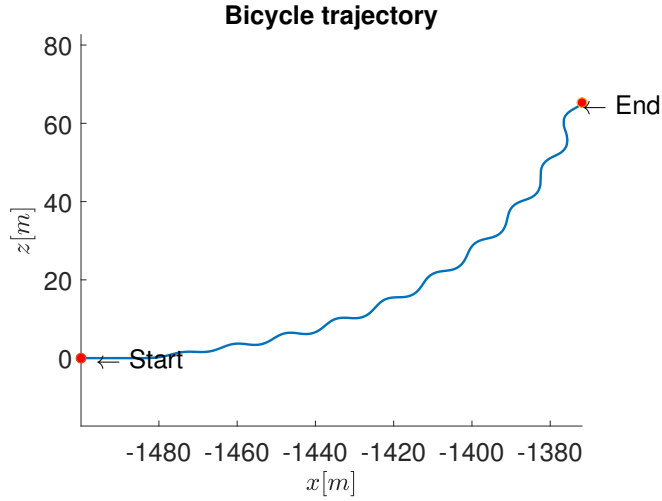


Figure 5.25: Investigation 2: Trajectory at weave velocity  $v_0 = 4.4m/s$

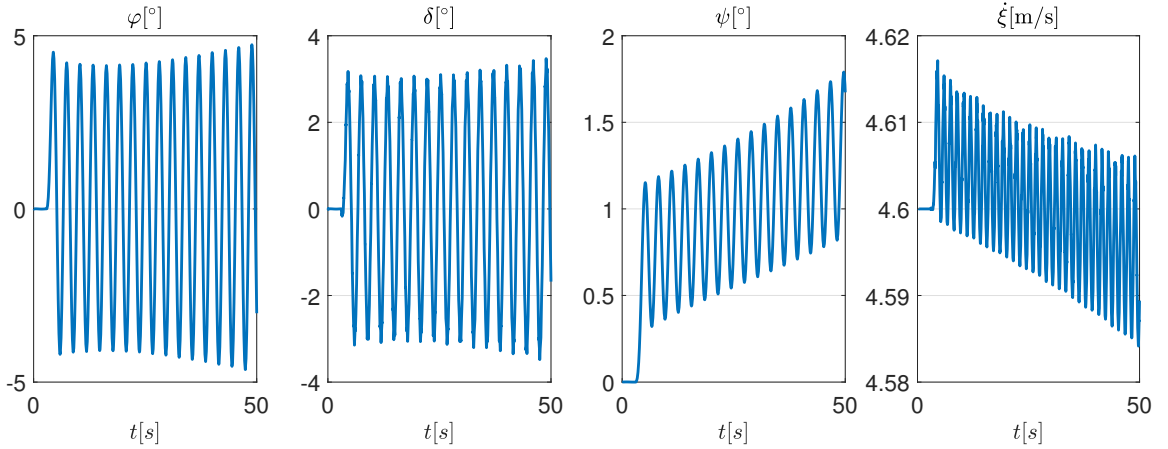
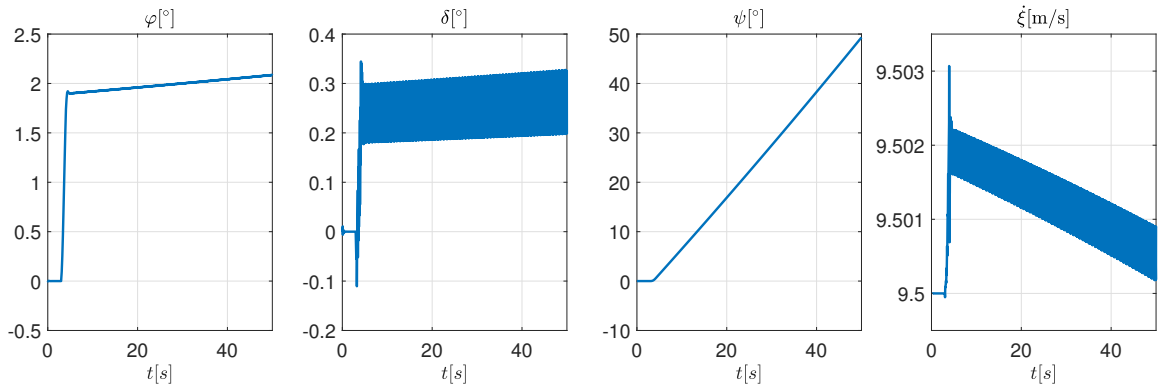
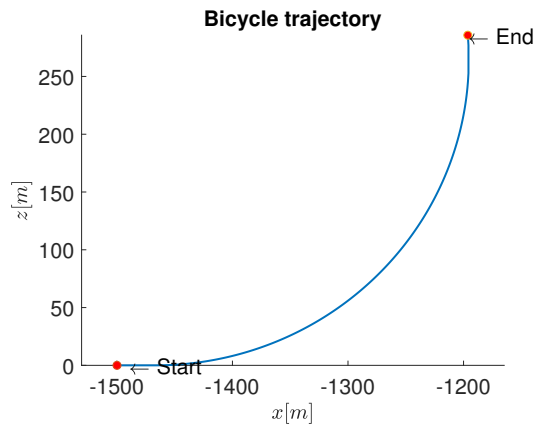
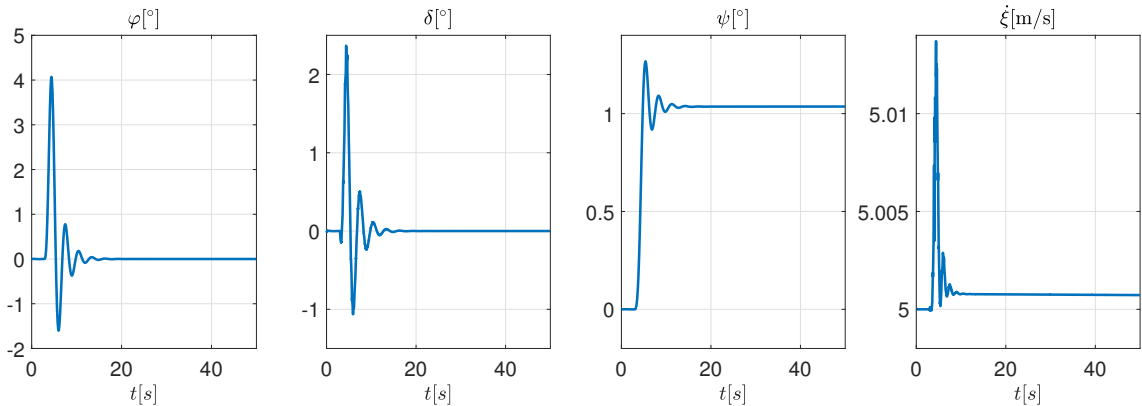


Figure 5.26: Investigation 2: Weave velocity at  $v_0 = 4.6m/s$

speeds between weave speed  $v_w = 4.6m/s$  and capsize speed  $v_c = 9.5m/s$ . Figure 5.29 shows a self-stable behavior in this region at  $v_0 = 5.0m/s$ .

From investigation 2, it can be seen that by using the tyre self-aligning stiffness properties, the weave velocity  $v_w$  and the capsize velocity  $v_c$  are increased compared to *Investigation 1*. Also, with the increase in the tyre stiffness properties, further increases the weave velocity  $v_w$  of the bicycle. An example simulation is run for tyres with slightly stiffer properties with  $C_{M_\phi} = 0.35(N-m)/(rad/m)$  and  $C_{F_\alpha} = C_{F_\alpha} = 2 \times 10^4 N/m$  compared to the previous  $C_{M_\phi} = 0.3(N-m)/(rad/m)$  and  $C_{F_\alpha} = C_{F_\alpha} = 2 \times 10^3 N/m$ . It can be seen from figure 5.30, that the weave velocity  $v_w$  has also slightly increased ( $v_w = 4.72m/s$ ) as predicted.

Figure 5.27: Investigation 2: Capsize mode at  $v_0 = 9.5 \text{ m/s}$ Figure 5.28: Investigation 2: Capsize mode trajectory at  $v_0 = 9.5 \text{ m/s}$ Figure 5.29: Investigation 2: Self-stability at  $v_0 = 5.0 \text{ m/s}$

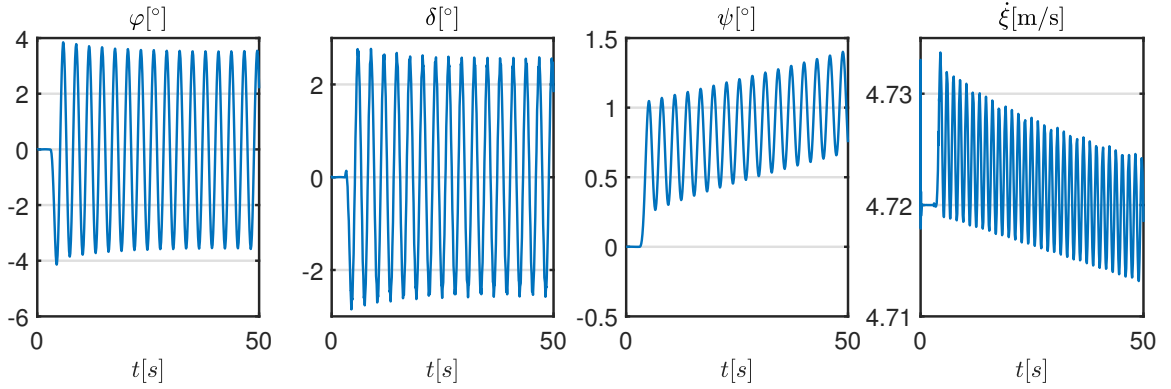


Figure 5.30: Investigation 2: Increase in weave velocity with stiffer tyres

### 5.4.3 Investigation 3: Testing with different bicycle parameters

The SimMechanics simulator is now tested with bicycle of different designs. In one design a standard bicycle model is used from open source modeling file exchange *Grab CAD* [BH14]. The parameters of the bicycle are given in table 5.5. The construction of bike in SimMechanics environment is as shown in the figure 5.31. With the same tyre parameters as for the bicycle model in section 5.4.2 are used. Simulations were run for a total time span of  $t = 50s$  for each scenario and the results were generated as follows. The weave velocity  $v_w$  was found to be at  $v = 5.9m/s$  as shown in figure 5.32.

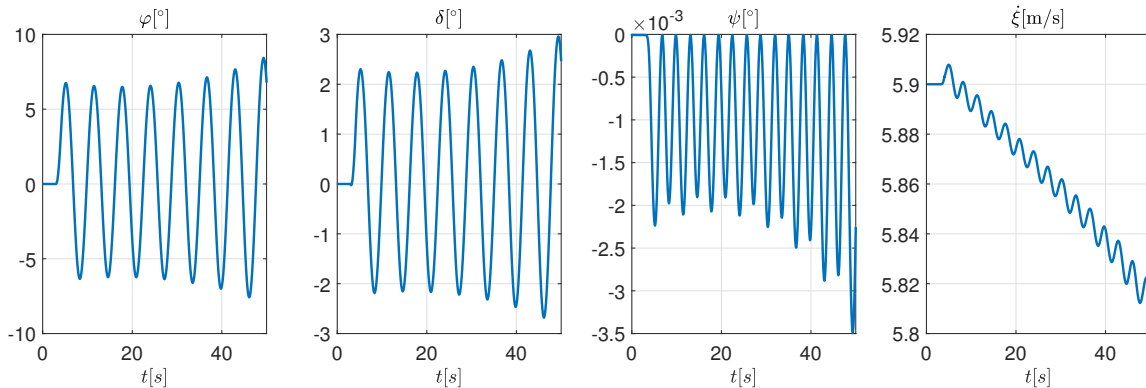


Figure 5.31: Construction of blue bike in SimMechanics

However, it was found that in case of higher velocities the capsize mode was always stable. As shown in figure 5.33, even at higher initial velocities  $v_0 = 20m/s$ , the bicycle is still stable. This stable capsize mode is also described in the [BDBK15, p.6], where a tyre model was built using *Magic Formula Tire Model*. In [BDBK15, p.6], the weave velocity was found at  $v_w = 9.5m/s$  and the capsize velocity was

Parameters	Symbol	Value
Wheel base	$w$	$1.034m$
trail	$c$	$0.09m$
front angle	$\lambda$	$18^\circ$
<b>Rear and Front wheels</b>		
radius	$r$	$0.32m$
mass	$m_w$	$2kg$
Moment of Inertia	$[I_{xx}, I_{yy}, I_{zz}]$	$[0.0512, 0.0512, 0.1024]kg \cdot m^2$
<b>Rear frame</b>		
mass	$m_B$	$20kg$
Moment of Inertia	$[I_{xx}, I_{yy}, I_{zz}]$	$[9.2, 2.8, 11]kg \cdot m^2$
Center of mass	$(x_B, z_B)$	$(0.35, 0.7)m$
<b>Front frame</b>		
mass	$m_H$	$10kg$
Moment of Inertia	$[I_{xx}, I_{yy}, I_{zz}]$	$[0.05892, 0.00708, 0.06]kg \cdot m^2$
Center of mass	$(x_H, z_H)$	$(0.95, 0.7)m$

Table 5.5: Design parameters of blue bike

Figure 5.32: Blue bike: Weave velocity stabilization at  $v_w = 5.9m/s$ 

found to be always stable. The authors have also concluded that the stabilization behavior of tyre forces and torques in the capsized mode was even larger than the destabilization by a rider model attached to the bicycle.

Another test that makes this conclusion from [BDBK15, p.6] more tangible is

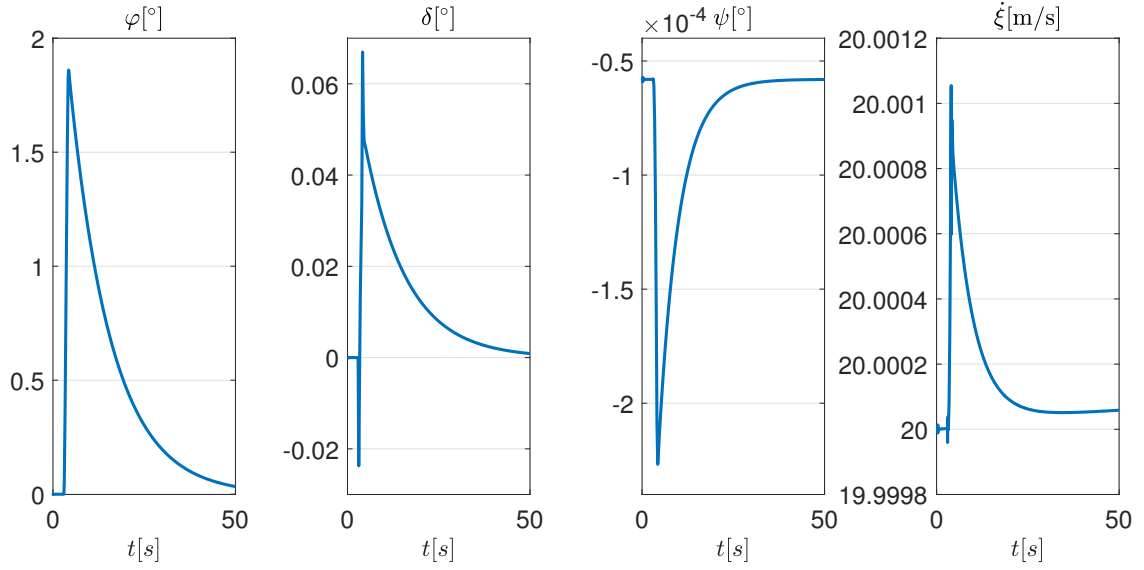


Figure 5.33: Blue bike: Stable capsize mode at higher velocities

when the self-aligning stiffness for the tyre model is set to zero. By doing so, the stabilizing moments from the tyres are no more active, just like in the case of a solid disc with a knife-edge contact. As shown in figure 5.34, the bike is already unstable when run at  $v_0 = 11.5\text{m/s}$  in the case of wheel with no self-aligning stiffness.

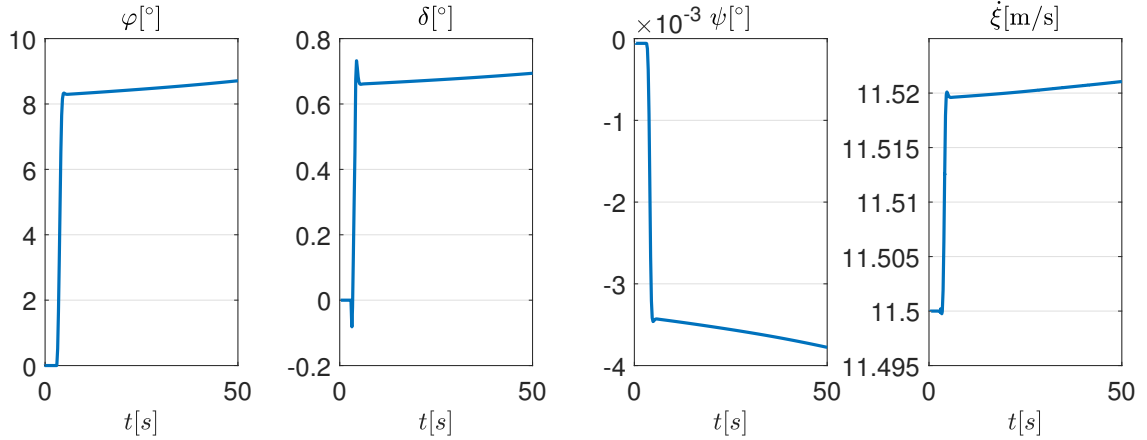


Figure 5.34: Blue bike: Capsize velocity  $v_w = 11.5\text{m/s}$  for tyre with  $M_\phi = 0$

Another set of investigations are conducted with a different bicycle design (*Red Bike*). Which is based on the autonomous bicycle developed at *Institute of Control Systems, TU Kaiserslautern*, more information on this bicycle project can be found at [Tur18]. The bicycle design parameters considered for construction in SimMechanics are given in table 5.6. The tyre parameters are given in table 5.7.

Parameters	Symbol	Value
Wheel base	$w$	$1.250m$
trail	$c$	$0.08m$
front angle	$\lambda$	$18.8^\circ$
<b>Rear and Front wheels</b>		
radius	$r$	$0.1930m$
mass	$m_w$	$1kg$
Moment of Inertia	$[I_{xx}, I_{yy}, I_{zz}]$	$[0.0093, 0.0093, 0.0186]kg \cdot m^2$
<b>Rear frame</b>		
mass	$m_B$	$15kg$
Moment of Inertia	$[I_{xx}, I_{yy}, I_{zz}]$	$[9.2, 2.8, 11]kg \cdot m^2$
Center of mass	$(x_B, z_B)$	$(0.3, 0, 0.28)m$
<b>Front frame</b>		
mass	$m_B$	$5kg$
Moment of Inertia	$[I_{xx}, I_{yy}, I_{zz}]$	$[0.05892, 0.00708, 0.06]kg \cdot m^2$
Center of mass	$(x_B, z_B)$	$(1.19, 0, 0.5)m$

Table 5.6: Design parameters of red bike

Figure 5.35, shows the construction of the bicycle in SimMechanics. The simulations were conducted for time  $t = 30s$  for each scenario. The bicycles stable weave velocity  $v_w$  was found while running the simulation at initial velocity  $v_0 = 2.4m/s$  as shown in figure 5.36, below this speed, the bicycle is unstable and above this speed the bicycle reaches its self-stability. The capsize speed was found to be stable while running at a maximum initial speed of  $v_0 = 3.8m/s$  as shown in figure 5.37. Beyond this speed the bicycle is again unstable. Therefore, the self-stable speed range of the bicycle is given between  $v_w = 2.4m/s$  and capsize speed  $v_c = 3.8m/s$ . Figure 5.38, shows the self-stable behavior of the bicycle while running the simulation at  $v_0 = 2.5m/s$ .

Parameters	Symbol	Value
Longitudinal Stiffness	$C_{F_\kappa}$	$2 \times 10^4$
Lateral Stiffness	$C_{F_\alpha}$	$2 \times 10^4$
Vertical Stiffness	$k$	$1 \times 10^6$
Vertical Damping	$b$	$1 \times 10^2$
Tire relaxation length	$\sigma$	$0.12m$
Self-Aligning Stiffness	$C_{M_\phi} = 0.3$	$0.3N - m/(rad/m)$

Table 5.7: Tyre parameters for the red bike

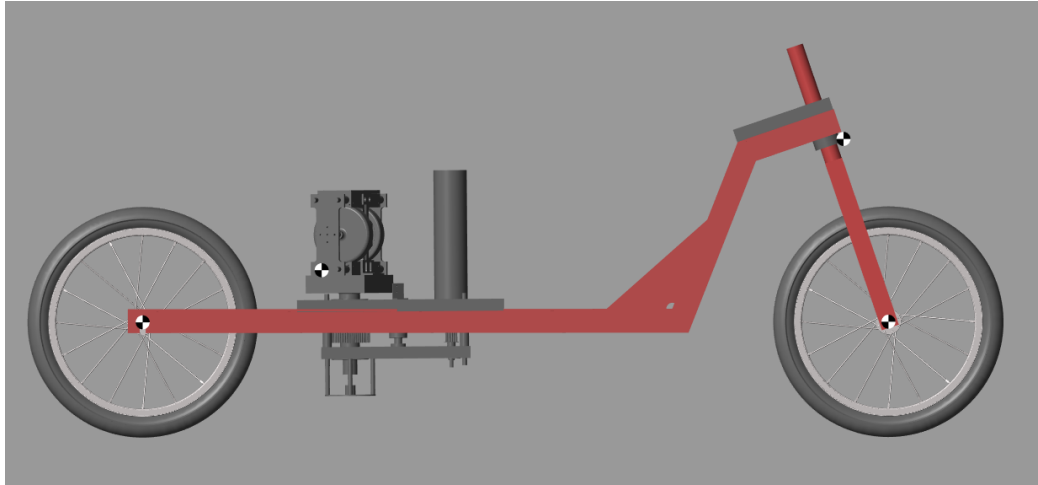
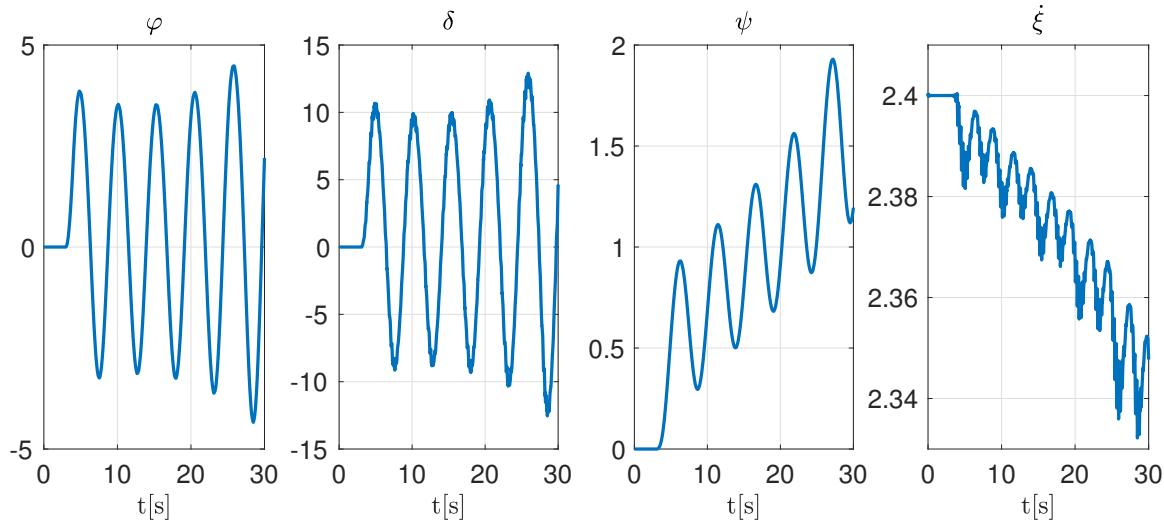
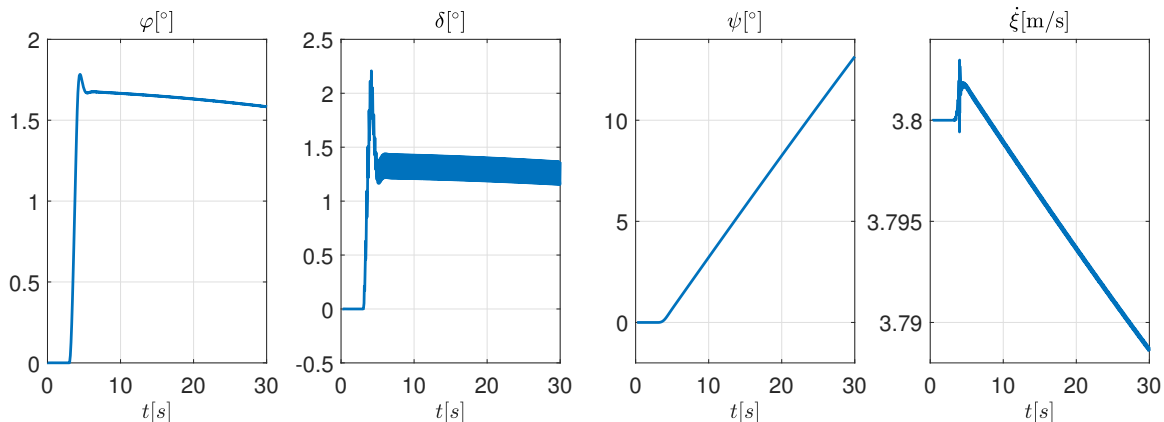
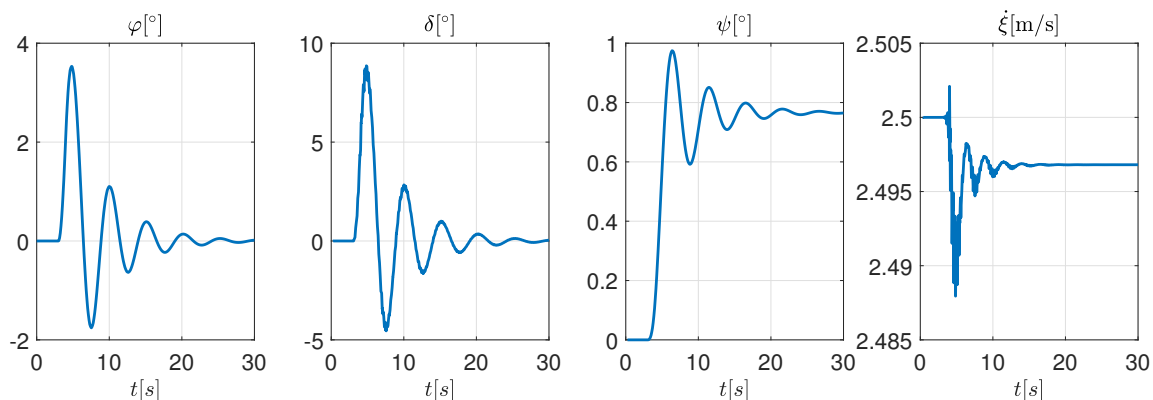


Figure 5.35: Construction of the red bike in SimMechanics

The non-minimal phase behavior is also investigated at  $v_0 = 2.5m/s$  by giving an impulse torque on steering at time  $t = 4s$ . The response of the bicycle trajectory and the output parameters can be seen in figures (5.39 and 5.40) respectively.

Figure 5.36: Red bike: Stabilization of weave mode of at  $v_w = 2.4 \text{m/s}$ Figure 5.37: Red bike: Stable capsize velocity of  $v_c = 3.8 \text{m/s}$ Figure 5.38: Red bike: Self-Stability at  $v = 2.5 \text{m/s}$

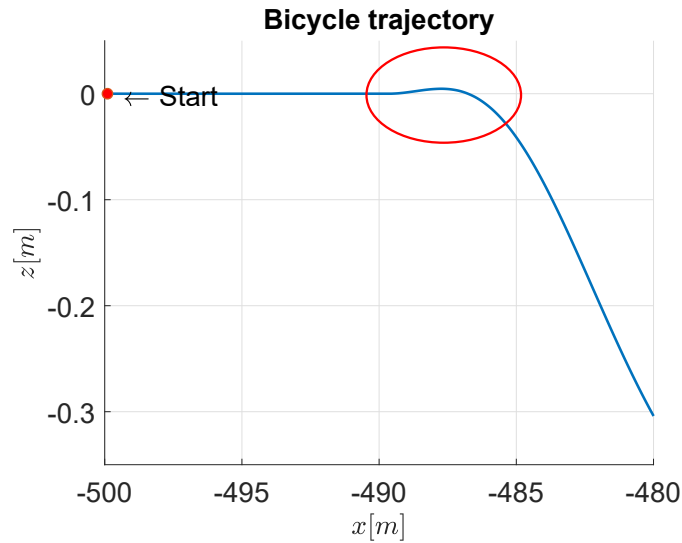


Figure 5.39: Red bike: Trajectory of non-minimal phase behavior at  $v_0 = 2.5m/s$

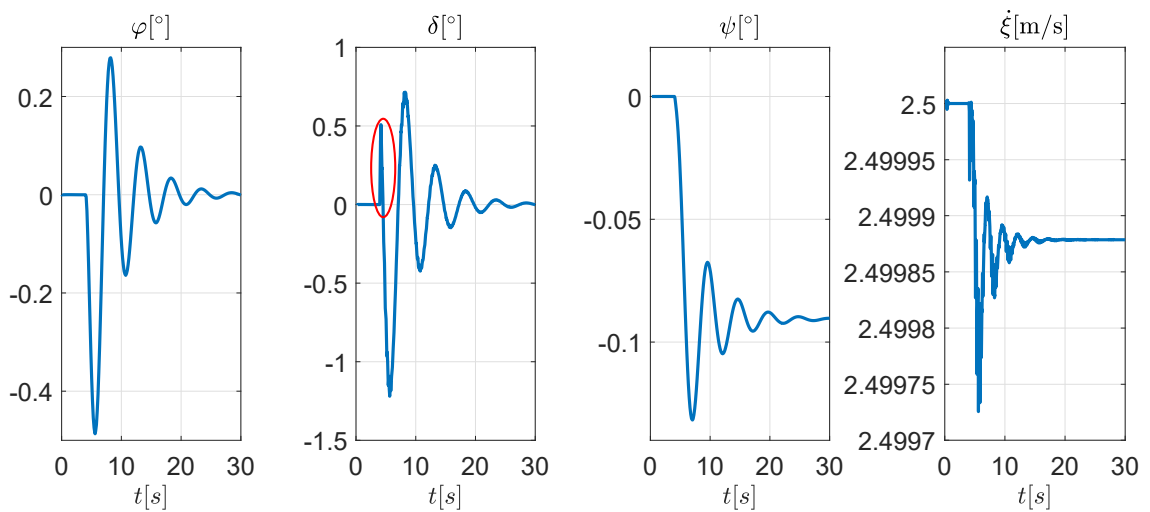


Figure 5.40: Red bike: Non-minimal phase behavior at  $v_0 = 2.5m/s$

Further, the red bike model can be easily extended to add a CMG that applies control on the undesired lean directly by applying torque on the lean of the rear frame. One such possibility is shown in figure 5.41 similar to the design from [Lam, p.11]. The design configuration includes a flywheel which is rotating at a constant angular velocity and is attached to a gimbal assembly. The rate of precession of the gimbal frame changes the direction of the angular momentum of the flywheel, thereby generating torque in the direction perpendicular to the angular velocity of the flywheel as described in [Lam]. The generated torque acts directly on the undesired lean angle of the rear frame, thereby controlling the bicycle from falling over. This model extension of the red bike to include a CMG shows the ease with which the SimMechanics models can be extended to implement control designs. Such a model extension provides great flexibility in extending the models easily and the red bike simulator is the first simulator that is known to provide such a large range of possibilities for investigating different scenarios.

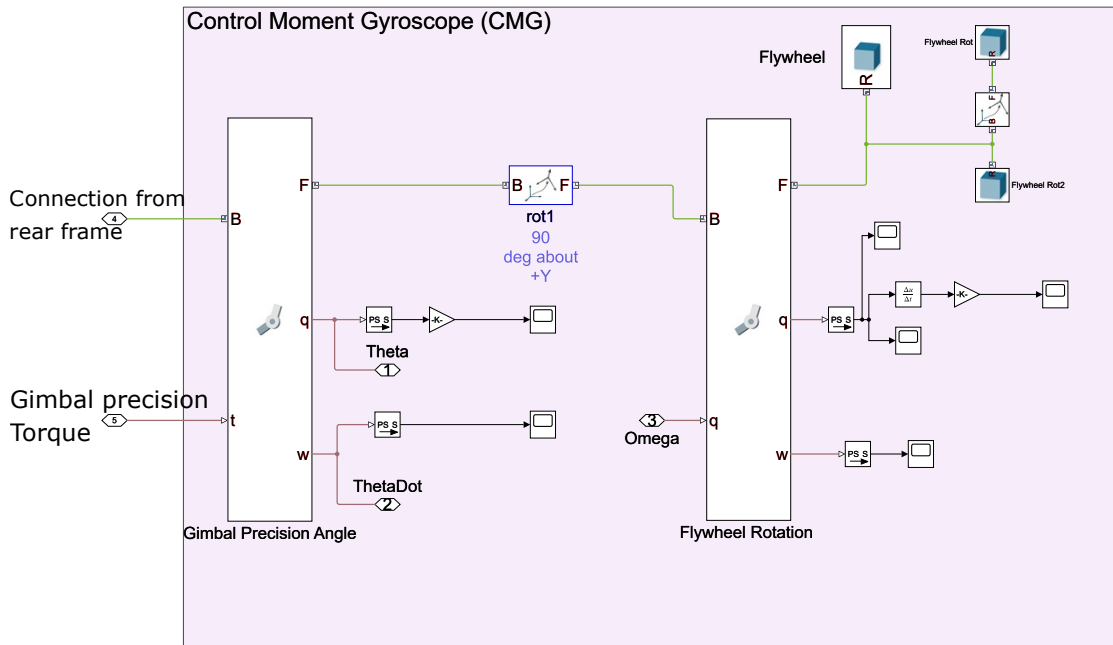


Figure 5.41: CMG model in SimMechanics for Red bike

#### 5.4.4 Investigation 4: Scenarios using feedback

With the same bicycle design parameters and tyre parameters used for *Investigation 2*, further three scenarios are simulated by actuating the steering and lean of the bicycle through a simple feedback as described in [TL18b, p.11,13,14]. The following scenarios illustrate the controllability (or ride-ability) of the bicycle by actuating a torque on lean ( $T_\varphi$ ) and the steering ( $T_\delta$ ).

**Scenario 1 - Constant  $\varphi^*$  by  $T_\delta$**  : To ride the bicycle in a curve, a controller is designed to maintain a constant leaning angle. Using the feedback from the leaning angle, leaning rate and steering rate, actuation is applied to the steering  $T_\delta$  through a simple feedback by setting  $\varphi^* = 8^\circ$ .  $T_\delta$  from the feedback can be expressed as:

$$T_\delta = -8\varphi - 8\dot{\varphi} - 25\ddot{\varphi} \quad (5.3)$$

Figure 5.42 shows the trajectory of the bike as the lean angle is controlled to  $\varphi = 8^\circ$  and figure 5.43 shows the measured output from sensors. Therefore, by controlling the lean angle at constant value  $\varphi^* = 8^\circ$ , the bicycle was able to ride in a curve. The simulation ran for total time of  $t = 30s$ , for the bicycle to complete one full curve as shown in the figure 5.42.

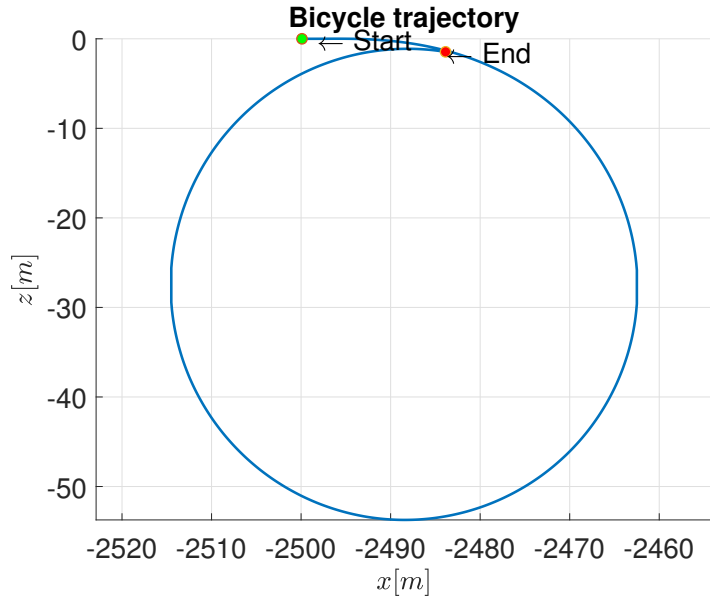
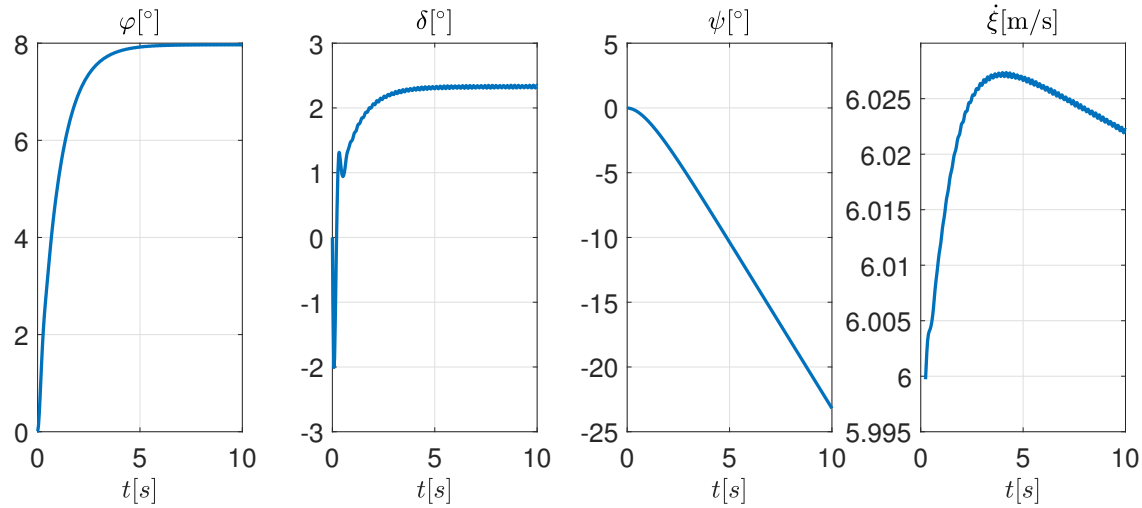


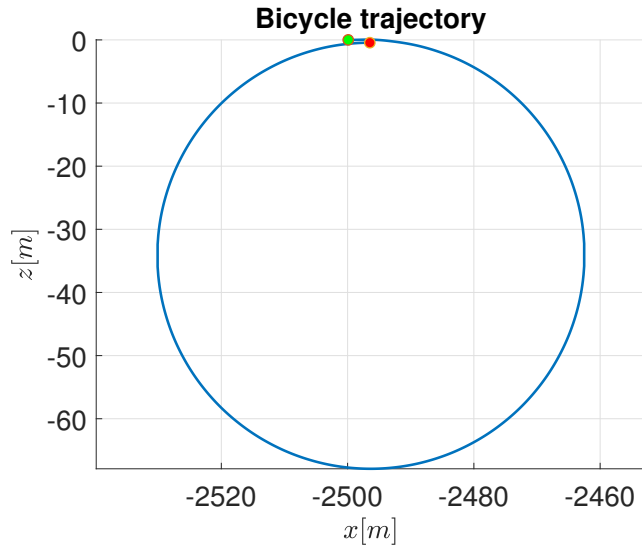
Figure 5.42: Scenario 1: Bicycle trajectory with  $T_\delta$  as input

**Scenario 2 - Constant  $\varphi^*$  by  $T_\varphi$** : A controller can also be designed by actuating an input to the lean ( $T_\varphi$ ) through a simple feedback:

$$T_\varphi = -100\varphi - 75\dot{\varphi} \quad (5.4)$$

Figure 5.43: Scenario 1: Feedback using  $T_\delta$ 

This scenario also demonstrates hands free riding by a rider just by moving the body in order to control the lean angle. Figure 5.44 shows the trajectory of the bicycle while lean angle is controlled by  $T_\varphi$  and figure 5.45 shows the outputs from the sensors. The bicycle was able to ride in a curve by controlling the lean angle through  $T_\varphi$ . The simulation ran for a total time of  $t = 37s$ , for the bicycle to complete one full curve as shown in figure 5.44 (the green and the red dots indicate the start and the end of the simulation respectively).

Figure 5.44: Scenario 2: Trajectory of bike while controlling  $\varphi$  by applying  $T_\varphi$ 

**Scenario 3 - Balance by steer at  $v = 0$ :** Generally a bicycle falls over when the center of mass is shifted away from the wheels ground contact points. This fact is

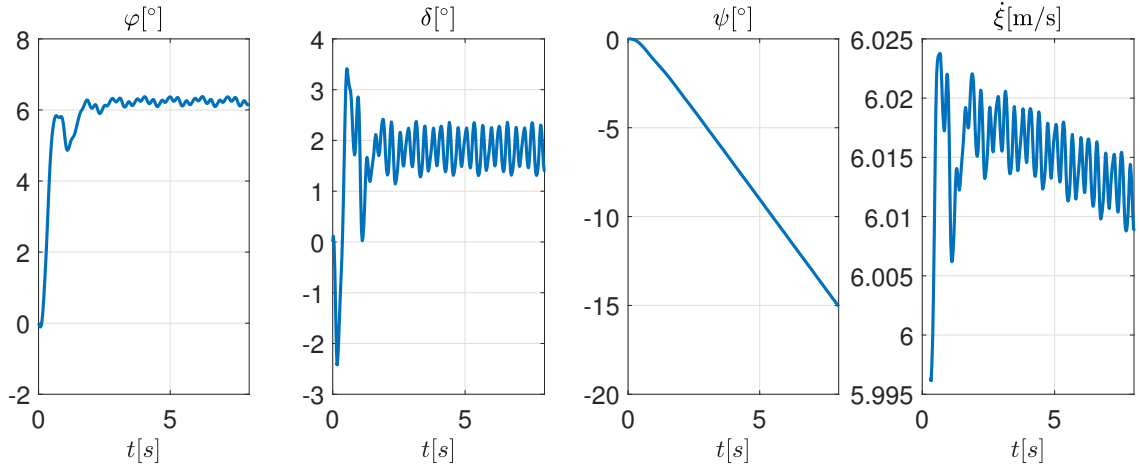


Figure 5.45: Scenario 2: Feedback using  $T_\varphi$

also true conversely, such that, if the ground contact points are moved back and they lie exactly under the center of mass, the undesired lean angle goes to zero. Such a balance can be established using again a simple feedback by applying a torque on steering  $T_\delta$ . The feedback is expressed as:

$$T_\delta = -450\delta - 800\dot{\delta} - 250\varphi - 50\dot{\varphi} \quad (5.5)$$

Figure 5.46 shows the response of the bicycles lean and steering angles with the feedback  $T_\delta$ . It can be seen that a perfect balance of the bicycle was not achieved. This scenario, however, demonstrates that the bicycle can be balanced by shifting its ground contact points under the center of mass and that this balance can be achieved by controlling the steering.

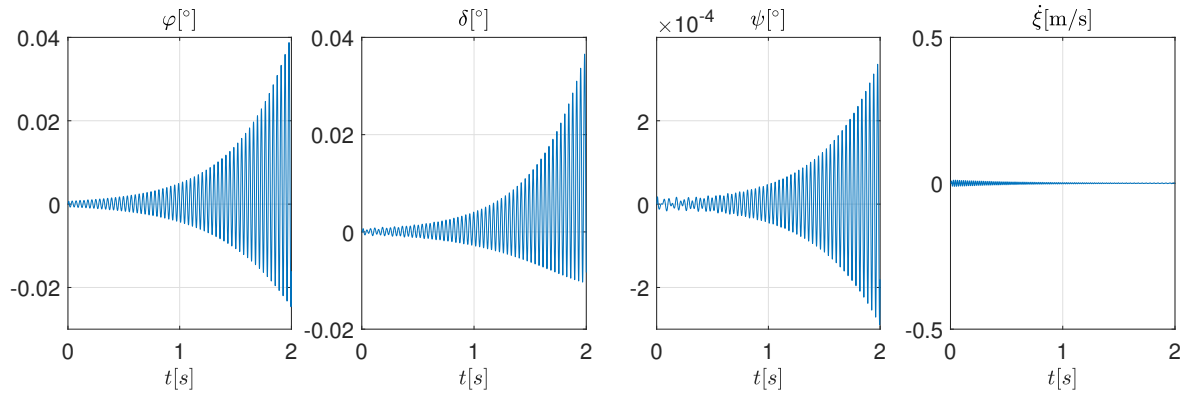


Figure 5.46: Scenario 3: Balance of bike at  $v = 0\text{m/s}$  by applying  $T_\delta$

# 6 Experimental Investigation

Based on the simulations conducted in the SimMechanics model, it can be seen that a bicycle goes through stages of weave modes up until it reaches a stable weave velocity  $v_w$ , the bicycle would be self-stable for the velocities beyond  $v_w$ . Another limit on the self-stability of the bicycle was found near capsize velocity  $v_c$ , the highest speed for which the bicycle would be self-stable. A self-stable mode for any small lateral perturbations can, therefore, be found between the velocities  $v_w$  and  $v_c$ . In order to investigate this behavior in real bicycles, Ruina and his students had conducted experimental tests on a real bicycle, first by accelerating a bicycle up to the point where it reaches its stability and then applying a lateral perturbation to verify its self - stability. The tests were published online under the following links: [Rui18b] and [Rui18a].

Similar to the tests conducted by Ruina, a similar approach is undertaken for conducting an experimental investigation on a real bicycle, which would cover the essential behavior of the bicycles motion. The aim of the experimental investigation is to measure the weave oscillations of bicycles lean and steering through sensor data up until it reaches its self-stability and also to measure the phase shift between the steering and undesired lean angle, which re-enforces the self-stability of bicycle at higher speeds than  $v_w$  as was described earlier through simulations in SimMechanics models.

## 6.1 Challenges in measuring the experimental data

Due to the use of a non-real time operating system *Robot Operating System (ROS)*, through repeated experimental measurements, it was observed that the sensor data for measuring lean angles always showed a pause in the recording which when used for generating plots showed inconsistencies. This, therefore, rendered the possibility of investigating exact bicycle motion parameters and therefore, the analysis of the bicycles motion.

However, the sensor data from the steering angle and forward velocity were mostly consistent with their recordings and helped in generating plots and therefore,

analyze the bicycles motion to a fair extent.

## 6.2 Experimental setup

Measurements for the following experimental investigations were taken from three sensors: for measuring the steering angles, measurements were recorded from a rotary sensor which is attached to the handle of the bicycle as shown in figure 6.1. The lean angle is measured from an Inertial measurement unit sensor (IMU) which is attached to the rear frame of the bicycle as shown in figure 6.2. Finally, the forward velocity of the bicycle was measured from a wheel encoder which is arched to the rear wheel of the bicycle.



Figure 6.1: Rotary sensor attached to the front steering handle [Fra17, p.40]



Figure 6.2: IMU lean sensor attached to the rear frame of the bicycle [Fra17, p.20]

The entire bicycle setup with sensors and measurement unit is as shown in the figure 6.3. The sensor data is collected and stored by the *Robot Operating System (ROS)* which runs on a *Raspberry Pi*.



Figure 6.3: Bicycle showing sensors and measurement unit [Fra17, p.4]

The system for measuring and recording the sensor data was developed previously at the *Institute of Control Systems, TU Kaiserslautern*. The procedure for conducting experimental measurement is as described in [JRLT17, p.62]. The measurement data is then used to generate a Matlab file that can directly be used for generating plots.

The experiments were carried out in the campus of *TU Kaiserslautern*, Experiments for investigations 1 and 2 were carried out at the parking lot of the **EIT Building** as shown in the figure 6.4. Experiments for investigation 3 were carried out at the running track of **Uni-sport, TU Kaiserslautern** as shown in the figure 6.5. The arrows in the tracks indicate the run where the experiments were conducted.

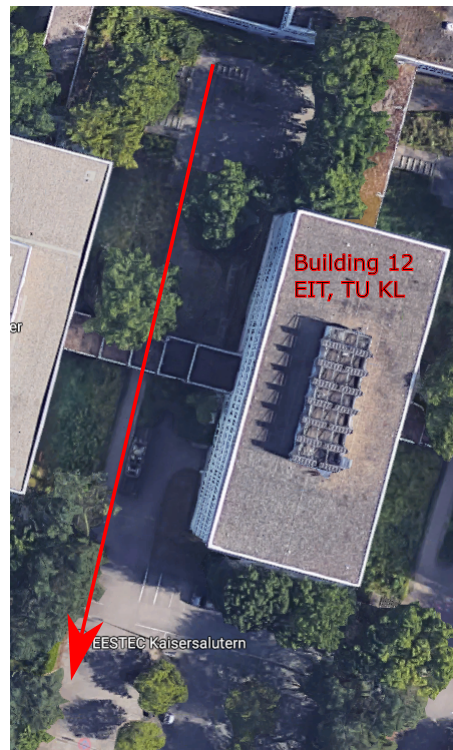


Figure 6.4: Track where tests for investigations 1 and 2 were conducted



Figure 6.5: Track where tests for investigations 3 were conducted

## 6.3 Experimental tests on a real bicycle

### 6.3.1 Investigation 1

In this test scenario, the bicycle was pushed initially to attain a certain speed, keeping up the speed approximately a constant through timely longitudinal push. The aim was to record the sensor data at a constant speed and generate the results from the sensor data for studying the bicycles behavior. The result of the entire test scenario is as shown in figure 6.6.

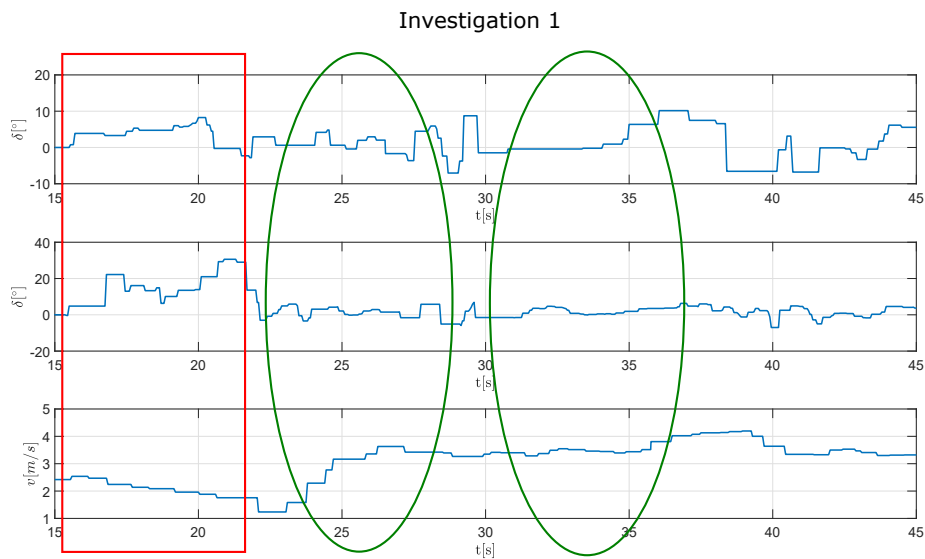


Figure 6.6: Experimental Investigation 1: Full range of experimental data

Figure 6.6 is divided into three distinct regions. In the region highlighted by the red box, it can be seen that due to low velocities both the lean and the steering angles are unstable. Further, as the bicycle accelerates, the steering and lean angles can be seen oscillating into a weave like motion as shown in the first green ellipse. As the bicycle accelerates further to higher speeds up to  $v = 4.0\text{m/s}$ , the weave motion tends to damp out, indicating the onset of self-stability shown by both the green ellipses.

The behavior of the bicycles steering motion damping out the weave motions at the higher speeds can be seen more clearly from figure 6.7. An effort was made to push the bicycle only longitudinally in the direction of the propagating velocity. The wave-like weave motion seen in the steering is purely from the self-stabilizing actions of the steering fork towards the undesired lean.

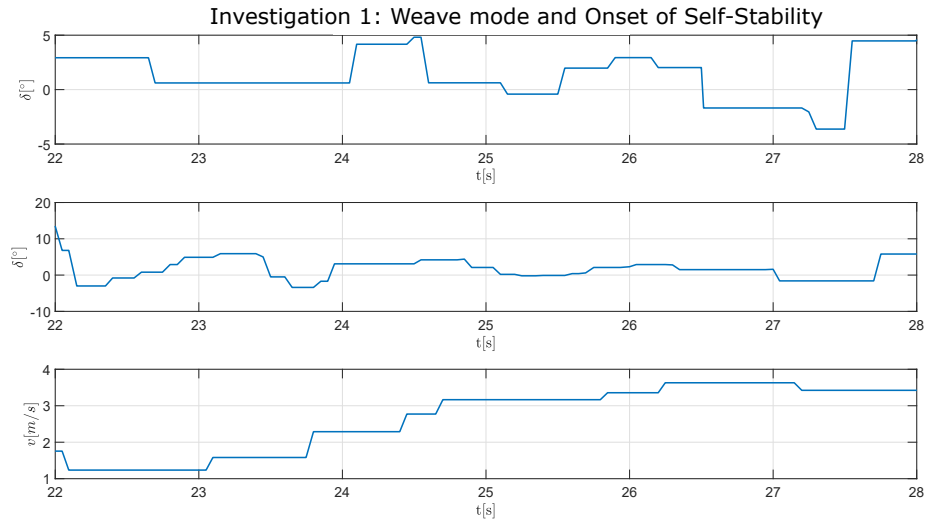


Figure 6.7: Experimental Investigation 1: Plots indicating the onset of bicycles self-stability

### 6.3.2 Investigation 2

Investigation 2 was conducted similarly to investigation 1 and the results form the sensor measurements are generated as shown in figure 6.8.

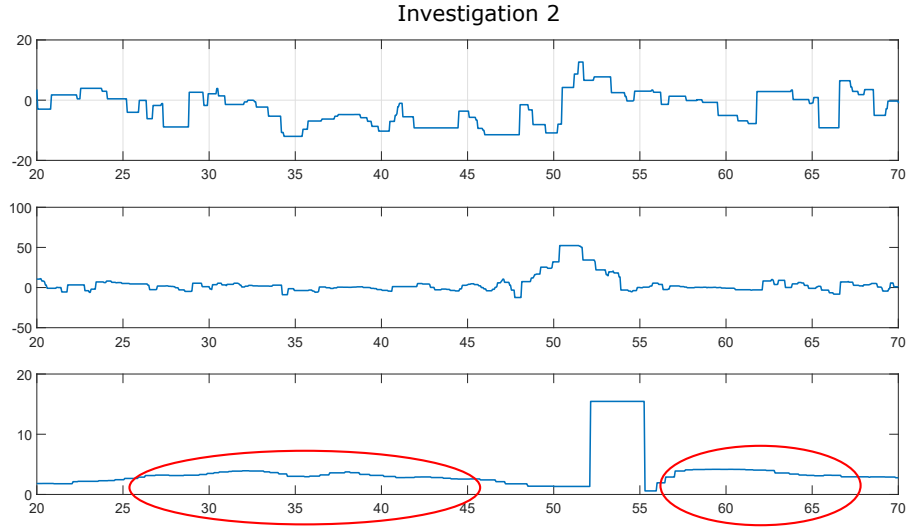


Figure 6.8: Experimental Investigation 2: Full range of experimental data

As seen in figure 6.8, there is one redundant data between time  $t = 52s$  to  $t = 55s$ . Eliminating this data gives two useful regions from (highlighted by red ellipses) the plot as shown in figures (6.9 and 6.10). Further from figure 6.9, it can be seen that as the bicycle is being accelerated and at speed  $v = 4m/s$ , the weave motion of the steering is damping out more quickly, as indicated by the green ellipse. Again, this region inside the green ellipse is indicating the onset of the self-stability of the bicycle. The region highlighted by the red box is when the bicycle is at lower velocities than in the green ellipse. It can be seen, that in this region the oscillations of the steering are more pronounced.

Further, in figure 6.10 it can be seen again that as the bicycle is accelerated to speeds  $v = 4m/s$ , the steering oscillations are damping out more quickly, indicating the onset of self-stability.

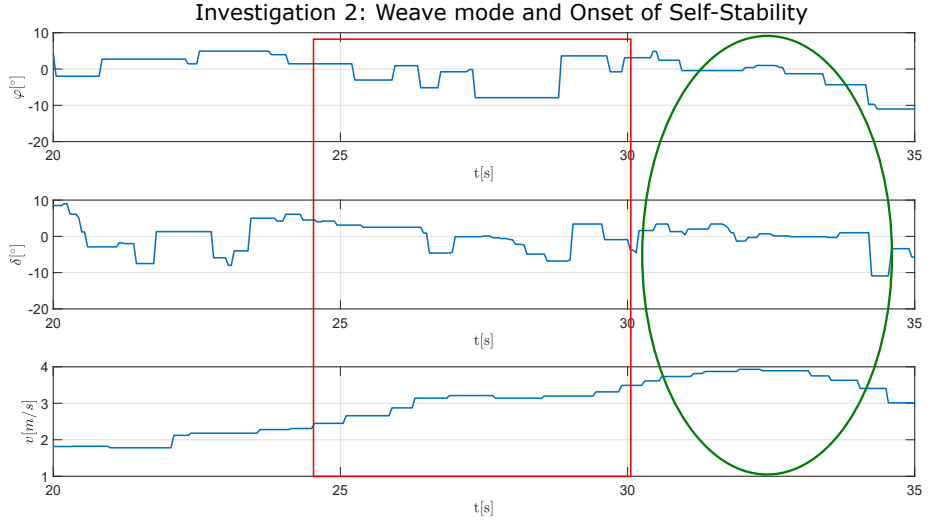


Figure 6.9: Experimental Investigation 2: Onset of self-stability is highlighted with green ellipse

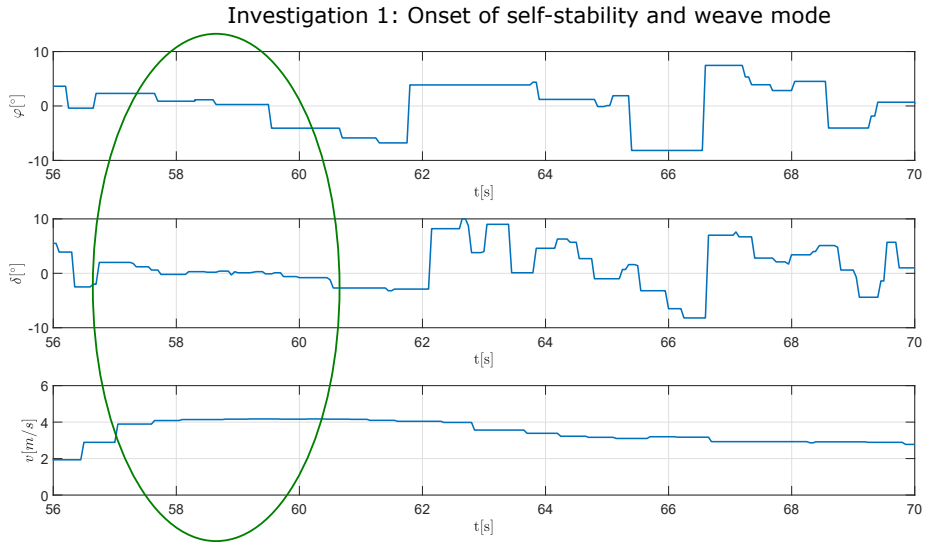


Figure 6.10: Experimental Investigation 2: Plots indicating the onset of bicycles self-stability

From the same measurement data, a plot is generated between the lean angle  $\varphi$  and the steering angle  $\delta$  as shown in figure 6.11. As previously, the bicycle was pushed only by its rear frame, leaving the steering free. Therefore, any perturbation is only possible for the lean of the bicycle and the steering oscillations comes from the self-stability action of the bicycle's steering fork. It can be seen from figure 6.11, that a perturbation on lean causes the steering fork to also turn

in the same direction, having a lag with the lean angle. This turning of the steering fork in the direction of the lean shifts the ground contact points under the center of mass of the bicycle. At certain speeds, these steering oscillations would eventually damp out self-stabilizing the bicycle.

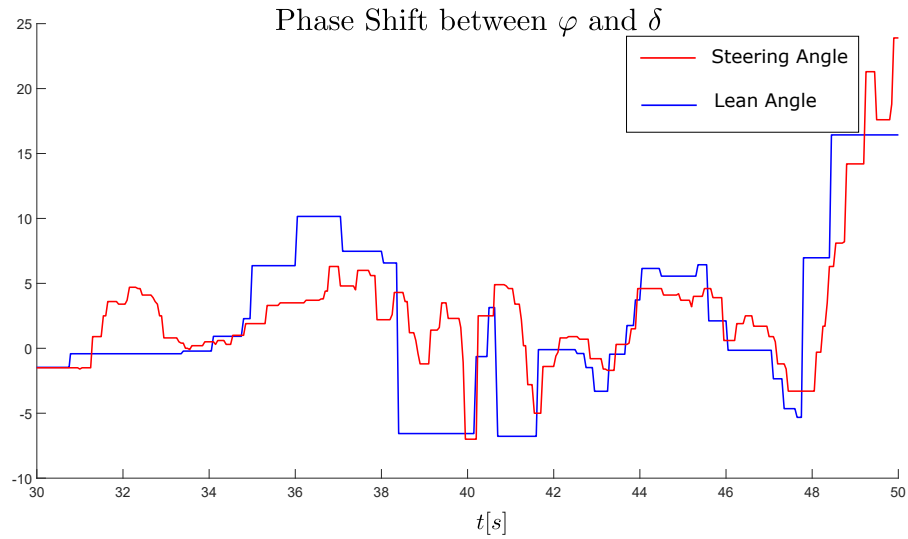


Figure 6.11: Experimental Investigation 2: Phase lag between  $\delta$  and  $\varphi$

### 6.3.3 Investigation 3

Investigation 3 was carried out on a different testing track. The test was conducted at the running track shown in figure 6.5. The full range of measured data is shown in figure 6.12. As marked by the two red ellipses, in the region of velocity increasing towards  $v = 4m/s$ , it can be seen again that the wave like weave oscillations of the steering damps out more quickly in these regions. Following with the results from *Investigations 1 and 2*, also in this case, the steering motion is stable as the velocity of the bicycle approaches  $v = 4m/s$ . Re-emphasizing the onset of self-stability as the bicycle runs at higher speeds.

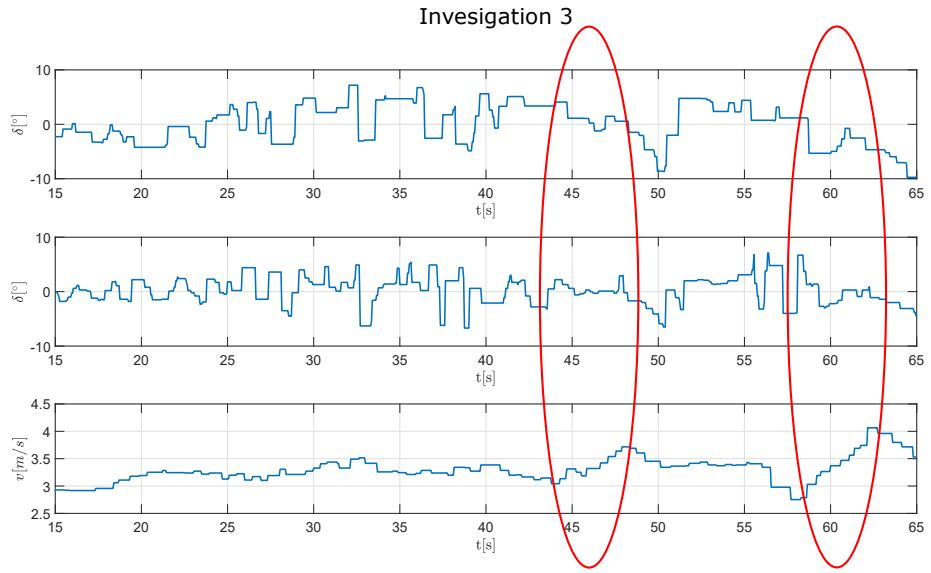


Figure 6.12: Experimental Investigation 2: Full range of experimental data

Figure 6.13, shows the region of the first ellipse more clearly. It can be seen that in this region the weave oscillation of the steering damps more quickly compared to the rest of the regions outside the two red ellipses, where is velocity is lower.

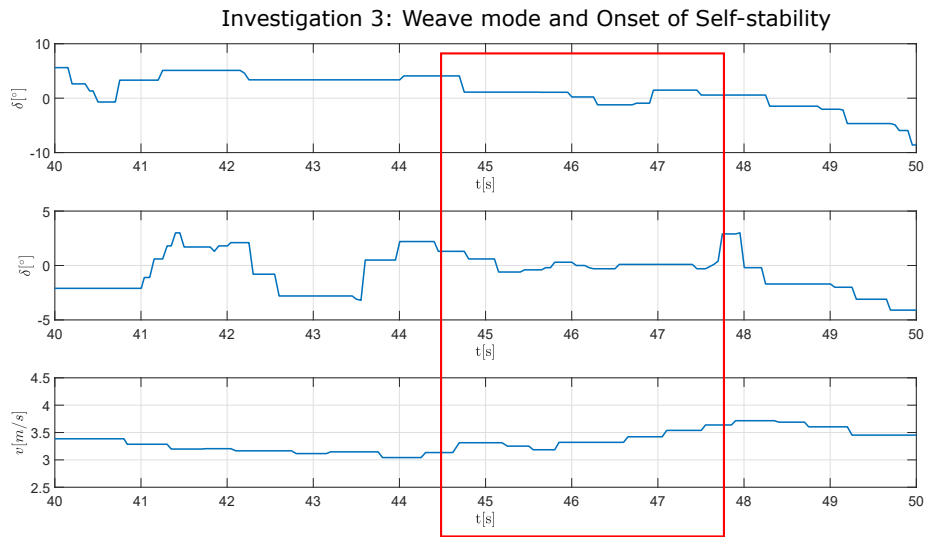


Figure 6.13: Experimental Investigation 2: Red box highlights onset of self-stability

## 6.4 Summarizing the observations from experimental investigations

Through the sensor data from the three experimental investigations it can be seen that three distinct regions of bicycles motion could be realized:

- A region of instability in lean and steering angles at low velocities. In case of measurement data from *Investigation 1*, this region was seen under the velocities  $3\text{m/s}$ .
- A region of weave mode, where the steering of the bicycle oscillates into a weave like wave-motion.
- A region of self-stability, at higher speeds (as the bicycle accelerates to speed  $v = 4\text{m/s}$ ) the steering oscillations damps out more quickly, indicating the onset of bicycles self-stability.



# 7 Conclusion and Outlook

In this thesis, three models were tested with the existing mathematical models, a single wheel model, a tricycle model and a bicycle model which was further tested with various design parameters, tyre parameters and inputs from feedback. From the simulations conducted with the SimMechanics single wheel model, the following conclusion can be made:

- At low velocities up to  $v = 2.0m/s$ , and at zero self-aligning stiffness, the behavior of SimMechanics model is close to that of the mathematical model.
- At higher velocities greater than  $v = 2.3m/s$ , noticeable deviations can be seen in the SimMechanics model compared to the no-slip mathematical model.
- The deviations in the trajectories are accounted by the slips the SimMechanics model considers while generating forces.
- The tyre model with self-aligning stiffness tends to re-align its orientation towards its heading direction. In the case of a solid disc, this behavior is lacking.

Further, the SimMechanics tyre model was used to construct a tricycle model. The main purpose of the tricycle model was to be able to construct an interim vehicle model and investigate the behavior of the tyre model built previously. With the tricycle model, the following conclusions can be made:

- By attaching a pendulum in the accelerating frame of the tricycle and by actuating the steering, a torque was measured by the sensors attached to the pendulum.
- Such a measured torque can be accounted for the existence of centrifugal forces while the vehicle is turning into a corner. The existence of centrifugal forces in-turn verifies the action of the lateral forces generated by the tyre for the steering input. These lateral forces provide the necessary centripetal acceleration that is required for the vehicle to turn into a corner. In other words, the lateral forces maintain the nonholonomic constraints.
- By switching tyre models with and without self-alignment, deviations can be observed in the trajectories of the vehicle. With self-alignment, the tyre

re-aligns the orientation of the vehicle in the direction of the propagation velocity, whereas in the case of no self-alignment, the vehicle would continue going around in circles.

Finally, a series of investigations were carried out with bicycle models built in SimMechanics. These investigations were aimed at determining if the SimMechanics model represents the bicycle dynamics for various simulation parameters and that the model represents a general bicycle model that can be used for testing different scenarios. For this purpose, four different investigations were described:

- In investigation 1, the model was constructed according to the design parameters described in *Linear Benchmark Model*. With this model, the distinct Eigenmodes of the bicycle's motion described by the linear model was validated. The bicycle model exhibited self-stability range between the stable weave velocity at  $v_w = 4.4m/s$  and the capsize velocity at  $v_c = 6.3m/s$ . The self-stability range showed a good agreement with the linear model, although there are slight deviations at this point which can be appreciated by considering that the SimMechanics models use tyres with slips.
- In Investigation 2, the tyres with self-aligning stiffness was used. In this case, it was observed that the tyre parameters such as self-aligning stiffness increases the weave velocity  $v_w$  and the capsize velocity  $v_c$  of the bicycle. The similar deviation was also noted in [BDBK15]. It was also seen that by increasing the tyre stiffness properties, the weave velocity increases further.
- In Investigation 3, the SimMechanics model was tested with two different design parameters (Blue and red bikes). The models were tested for various Eigenmodes from linear bicycle model. Further, the red bike was extended by adding a CMG for lean control. This investigation re-enforced the flexibility and the extendibility of the SimMechanics models.
- In investigations 1 and 3 (for red bike), the non-minimal phase behavior was also established, similar to nonlinear bicycle model [TL18c].
- Further, in investigation 4, scenarios were described using feedback to actuate the lean and steering angles to establish the controllability (ride-ability) of the SimMechanics models. Similar to scenarios described in Turnwald [TL18a].
- From the various simulations, it can be seen that the SimMechanics model shows good agreement in the results, both from linear model (concerning the Eigenmodes) and the nonlinear model (concerning the controllability).
- Experimental investigations conducted with real bicycle also showed the distinct modes of bicycle dynamics, such as, instability at low speeds, weave mode and onset of self-stability at higher speeds as well as the phase lag

in steering for the undesired lean angle. This re-enforces the validity of the SimMechanics bicycle models with the real bicycle.

- Finally, from all the simulations and investigations, it can be concluded that the SimMechanics model behaves more like a general model, which can be used to test various scenarios as well as being flexible to easily add control designs.
- The bicycle simulator with the *Blue Bike model* was published in the *GitHub* public domain [TA18a].

## 7.1 Future work

Finally, some ideas that are open to extend this thesis in the future:

- No-slip tyre models can be developed and added into the simulator, this would make the simulator complete with both the slip and the no-slip tyre models.
- The simulator can be further added with the observer and controller algorithms.
- More detailed study can be further performed on the tyre modeling and extended to industry standard *Magic Formula Tyre Models* or *FEA* tyre models, which are lacking as a standard in the field of bicycle development.
- The simulator can be further extended with rider model, similar to the rider model implemented in *MS Adams* in [BDBK15].



# A Appendix: Single Wheel Simulator

This appendix provides a reference manual on all the models built in SimMechanics. A single wheel model was built first using the tyre model described in section 4.9. The single wheel model is represented in SimMechanics using a CAD model of a disc which is attached with a six DOF joint as shown in figure A.1. The joint represents the six degrees of freedom of the body element in 3D space on which three constraints are applied. A holonomic constraint is applied to the position of the wheel center from the contact point using the vector definition of radial vector  $\mathbf{r}$  as described in section 4.6 and the two nonholonomic constraints are applied by the lateral tyre forces generated by the tyre model as described in sections (3.5 and 4.7). All these constraints are applied using the tyre model library which generates tyre forces and moments using slips and tyre penetration as inputs.

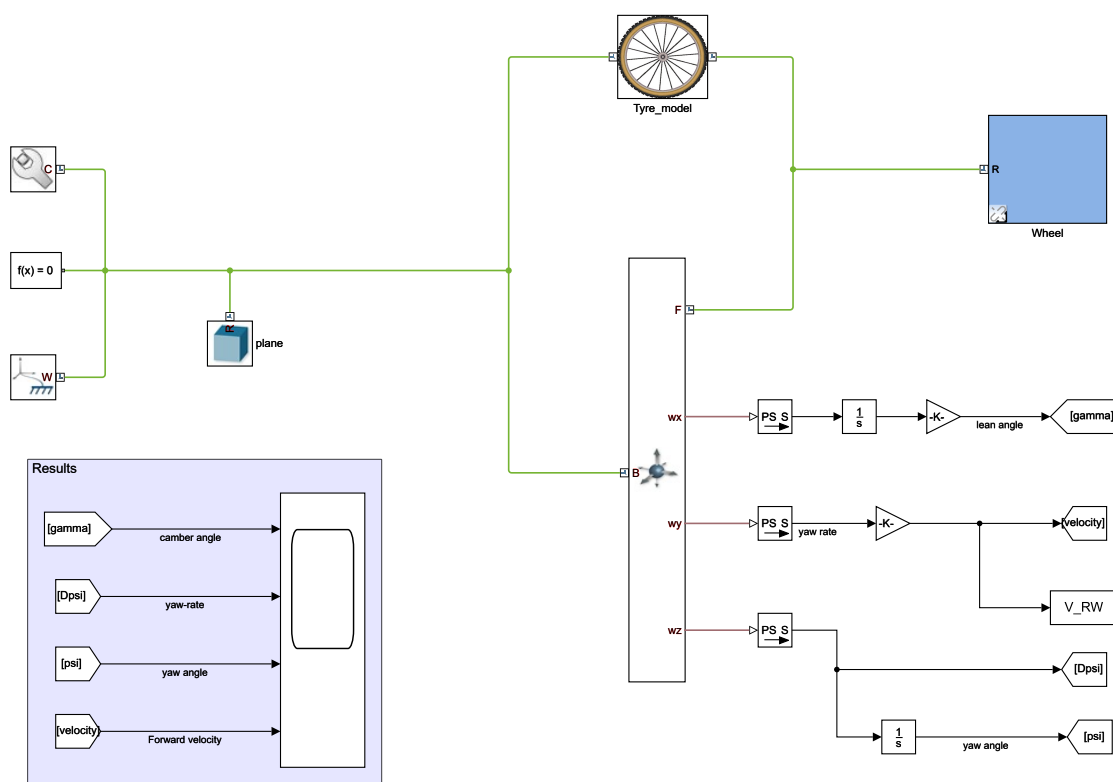


Figure A.1: Single Wheel: Model overview

## A.1 Tyre model library

The tyre model contains a sensor which measures the displacement and velocities from the physical body element and converts it to Simulink signals using Matlab's inbuilt function library. The measurements from the sensors are used to calculate the slips and tyre penetration and associated tyre forces and moments through Simulink blocks as shown in figure A.2.

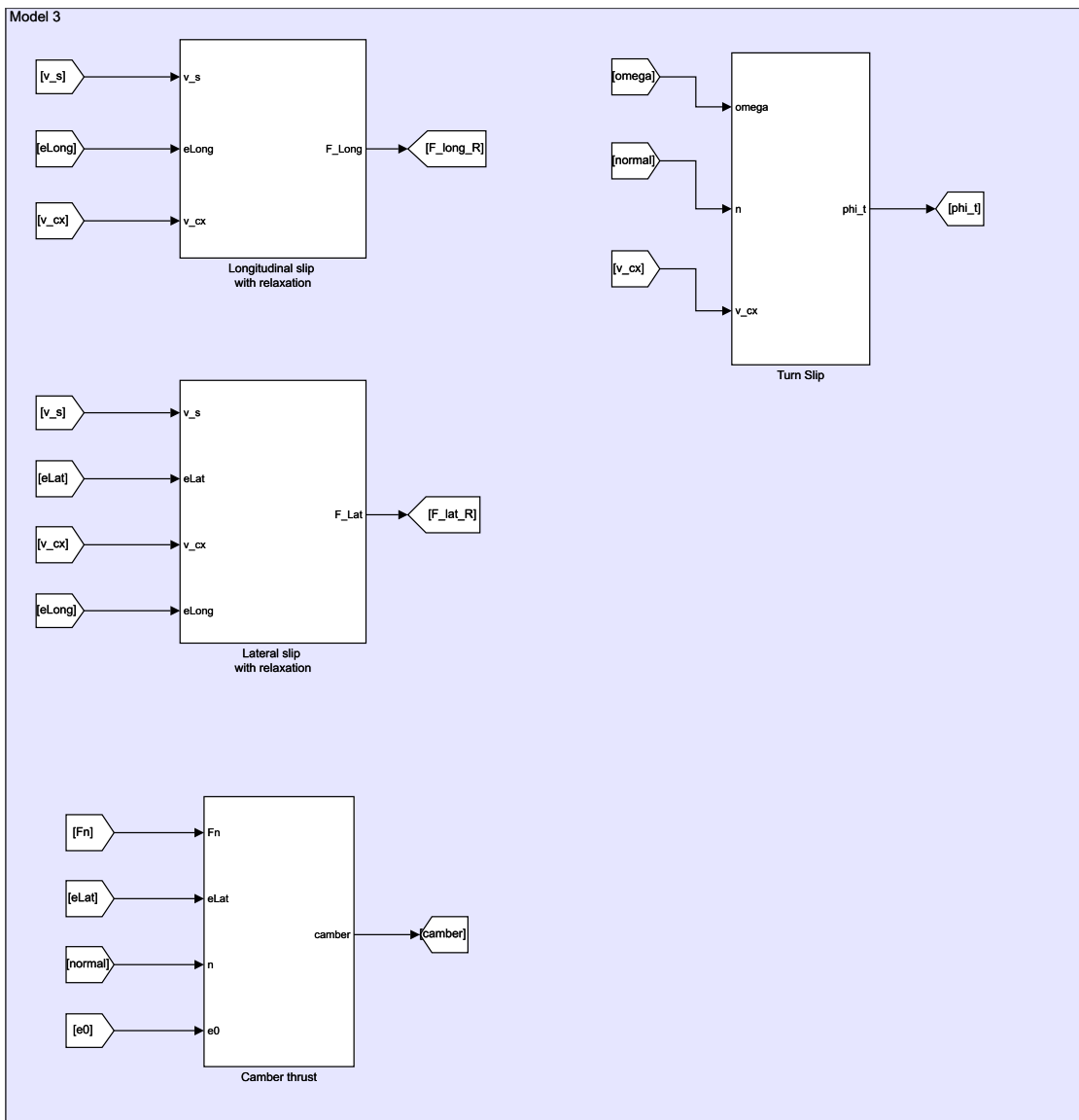


Figure A.2: Single Wheel: Tyre slips, forces and moment calculation

The slip velocity required for the slip calculation for  $\kappa$  and  $\alpha$  is calculated separately as shown in figure ???. Also calculating the wheel vector calculation from the

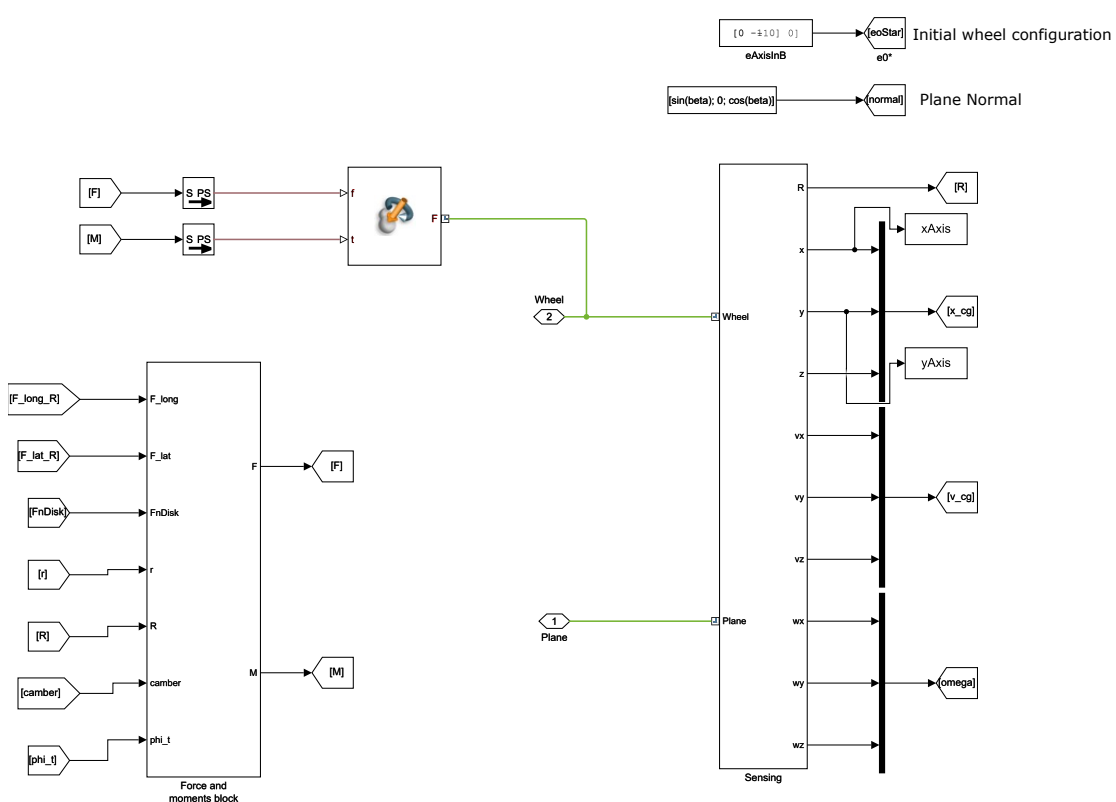


Figure A.3: Single Wheel: Forces and Moments actuation to body element using a Force element

initial wheel configuration as shown in figure A.4, in this block also the contact point vector  $\mathbf{r}$  is calculated.

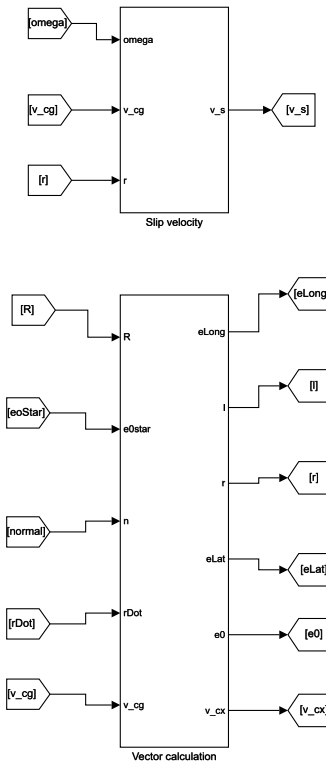


Figure A.4: Single Wheel: Wheel vector calculation and slip velocity

The calculated forces and moments are applied to the body element using a *External force and torque block* in SimMechanics as shown in figure A.3. The initial condition for the simulation is given at the joint state targets on velocities as shown in figure A.5.

Additionally, the wheel geometrical parameters and the tyre stiffness parameters including the relaxation length is given directly at the respective wheel and tyre library masks as shown in figures (A.6 and A.7). The friction at the wheel bearings is given as a damping in the spherical primitive of a six DOF joint as shown in figure A.8.

After running the simulations, the results can also be viewed directly from the Simulink scope block. Figure A.9, shows an example results from a test run at  $v_0 = 5m/s$ ,  $\varphi_0 = 5^\circ$  and a friction of  $1 \times 10^{-2}N - m/(rad/s)$ .

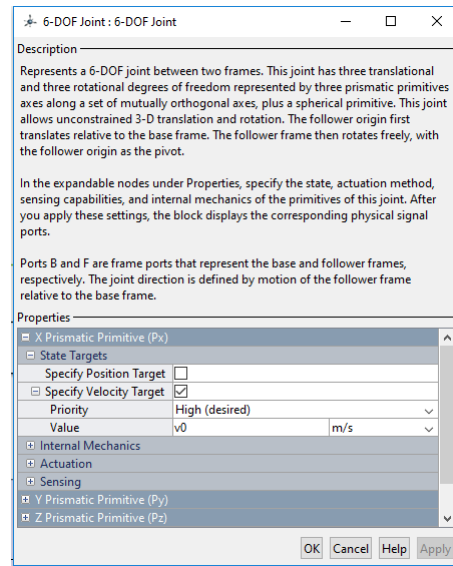


Figure A.5: Single Wheel: Initial conditions for the simulation

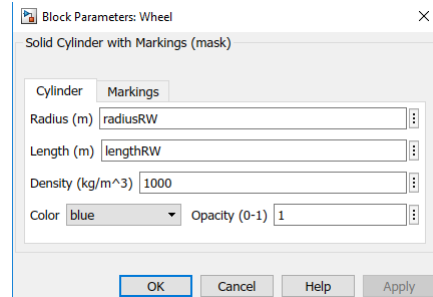


Figure A.6: Single Wheel: Initializing wheel geometrical parameters

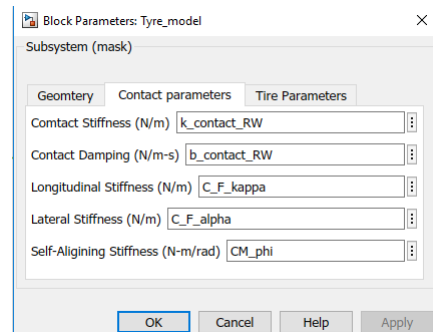


Figure A.7: Single Wheel: Initializing tyre parameters

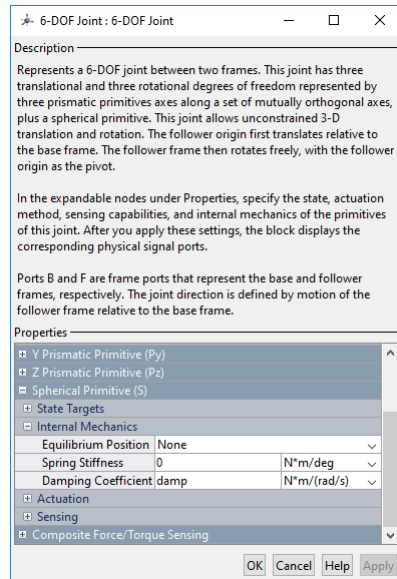


Figure A.8: Single Wheel: Initializing friction at the wheel bearings

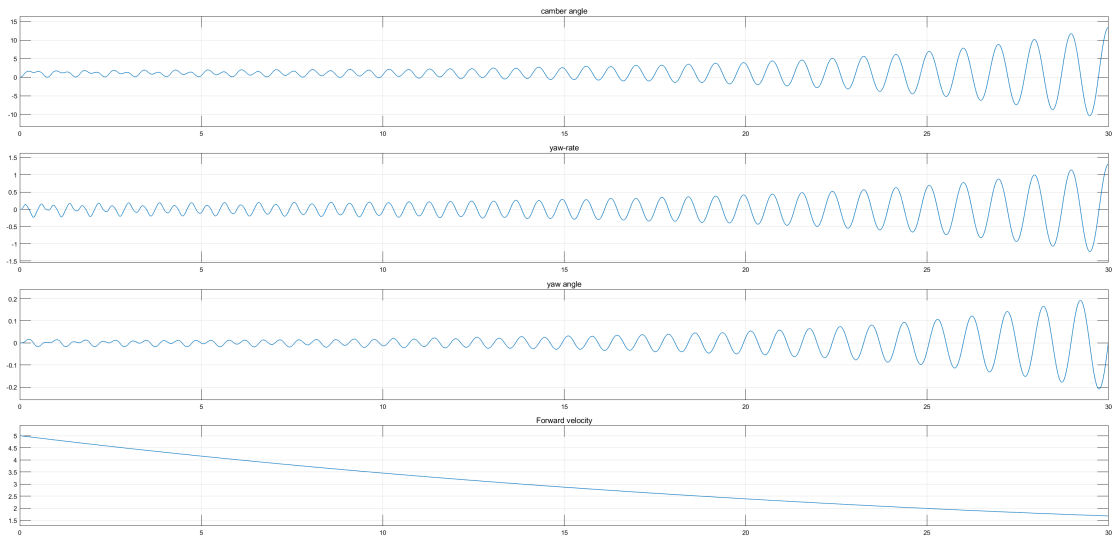


Figure A.9: Single Wheel: Results from the scope block



## B Appendix: Tricycle Simulator

A tricycle model is build on the tyre model as described in the section A. The frame of the tricycle is build on a six DOF joint which is later constrained by the constrains on three wheels applied individually by the tyre model library. The overview of the model can be seen in figure B.1.

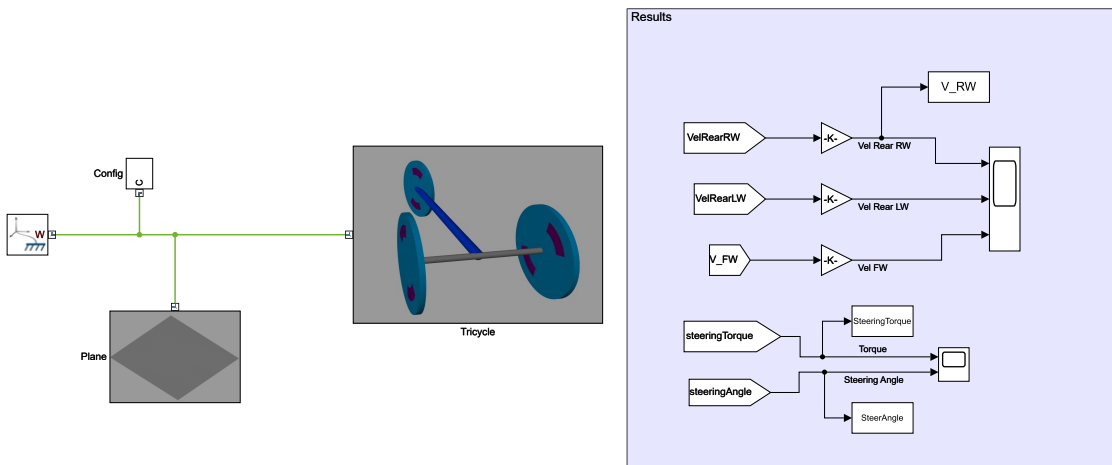


Figure B.1: Overview of a tricycle model built in SimMechanics

The initial conditions for the simulation in case of tricycle is given directly at this six DOF joint as shown in figure B.2.

Similar to the single wheel model, the wheel and tyre parameters can be initialized to each of the wheels independently directly in the wheel masks as shown in figure B.3.

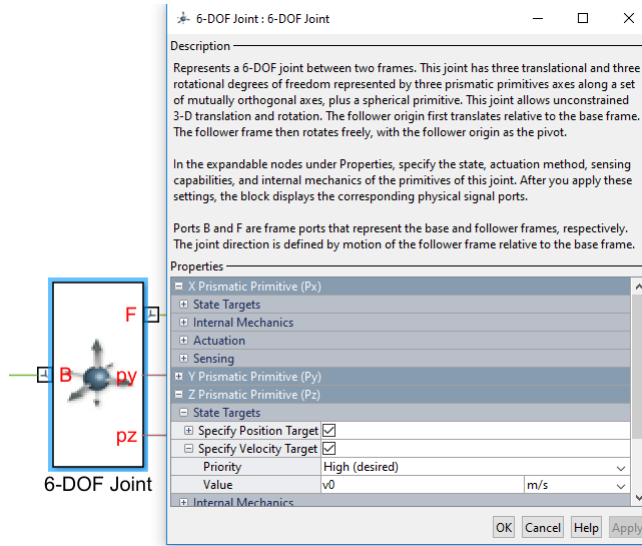


Figure B.2: Tricycle: Initializing simulation initial conditions

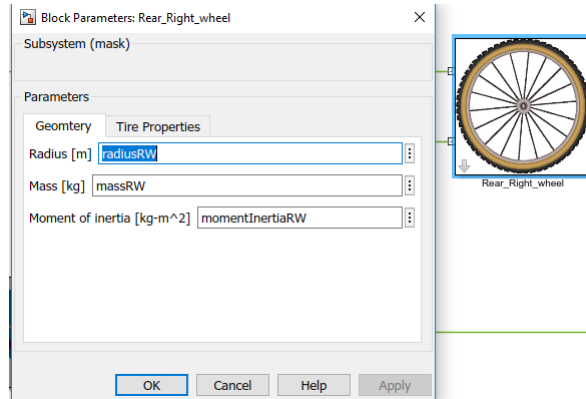


Figure B.3: Tricycle: Initializing tyre parameters

Additionally, for a tricycle, the steering is actuated in the steering joint in terms of external torque (figure B.4). The steering torque is applied using a signal builder as shown in figure B.5.

The simulation can be visualized in SimMechanics mechanics explorer, figure B.6 shows an example simulation for running the simulation at  $v_0 = 8\text{m/s}$  and with steering input torque as given in figure B.5.

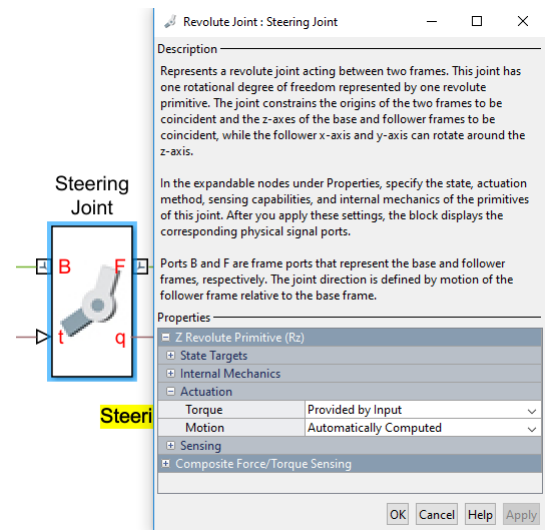


Figure B.4: Tricycle: Actuating steering

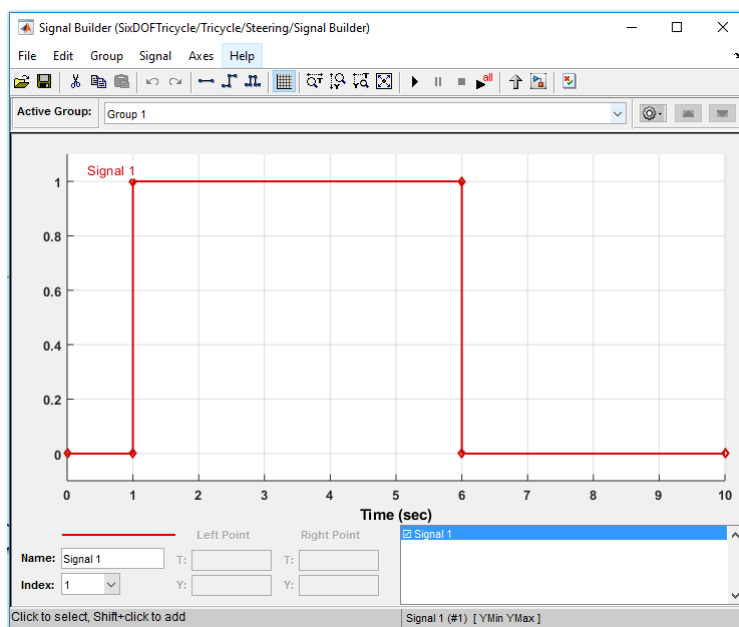


Figure B.5: Tricycle: Steering Torque

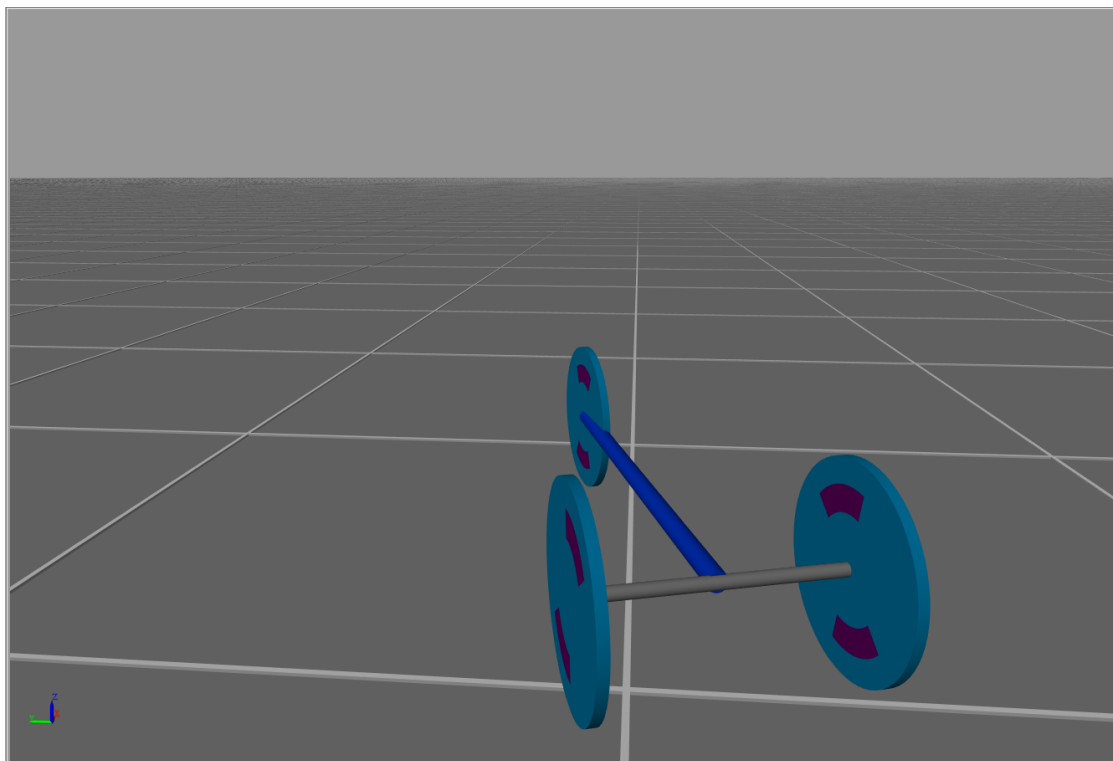


Figure B.6: Tricycle: Visualizing simulation in Mechanics explorer

# C Appendix: Bicycle Simulator

There are totally four different models available in the simulator for the bicycle. In a basic CAD model bicycle, a model is created that is easy to modify in terms of bicycle design parameters. These basic CAD models are used from the SimMechanics build-in CAD library for solid objects. The basic CAD models are used in *Investigation 1* and *Investigation 2*. In *Investigation 3* for blue and red bikes, a CAD model is imported from already built models. Additionally, a bicycle model is build to be implemented with the feedback using  $T_\varphi$  and  $T_\delta$ . In any case, the fundamental structure of the bicycle construction in SimMechanics environments remains the same. A fundamental overview of a bicycle construction can be seen through a model of a blue bike as shown in figure C.1.

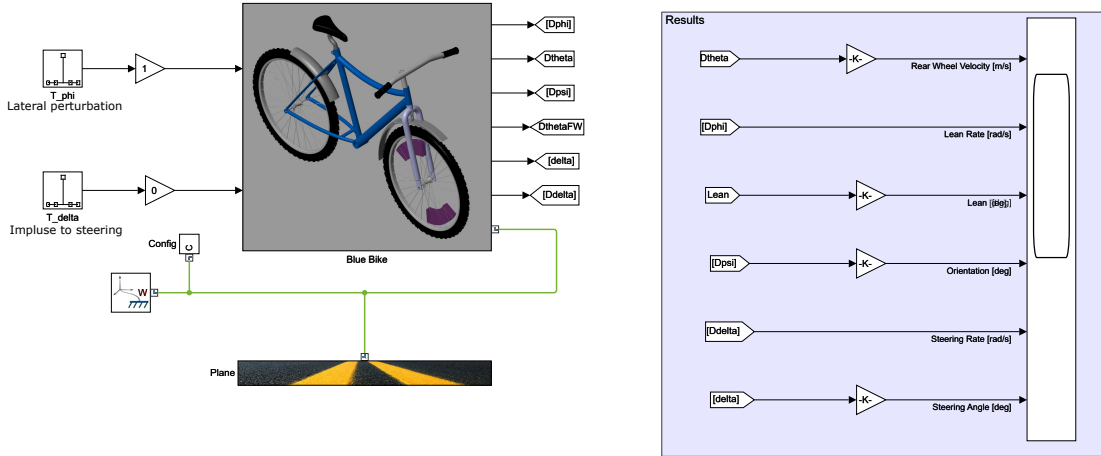


Figure C.1: Blue bike: Model overview

The construction of the bicycle is shown in figure C.2. The construction used six DOF joint for each wheel and revolute joints for each of the rear and front axles and the front steering. The ground parameters can be set directly at the ground mask as shown in figure C.3. For better visualizations, the ground block can be set with various colors from the drop-down menu. The tyre parameters can be set individually for each of the wheels including the friction at wheel bearings as shown in figure C.4.

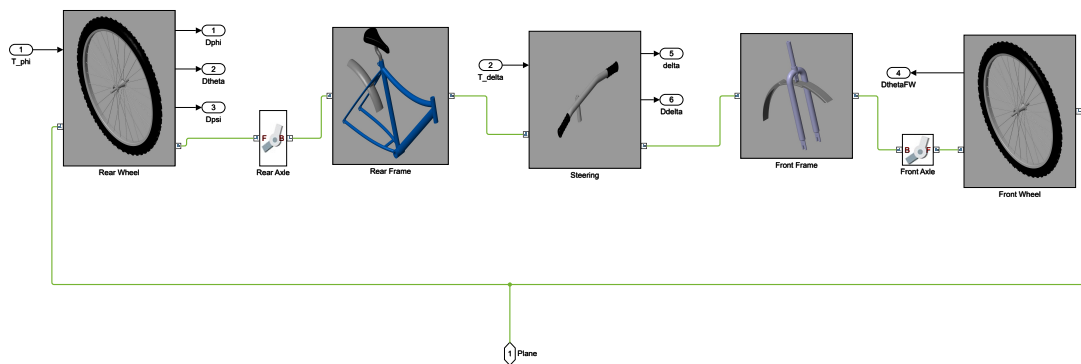


Figure C.2: Blue bike: Fundamental construction of a bicycle

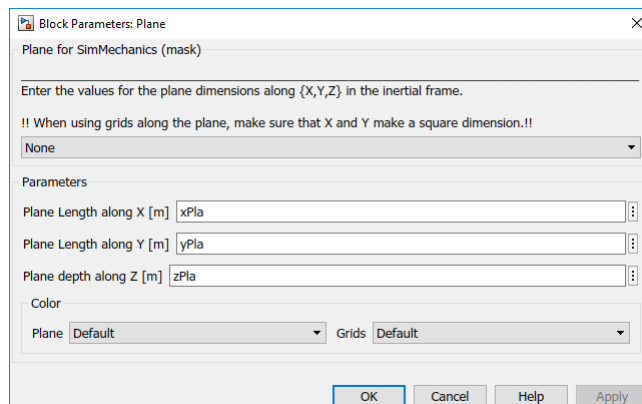


Figure C.3: Blue bike: Ground parameters

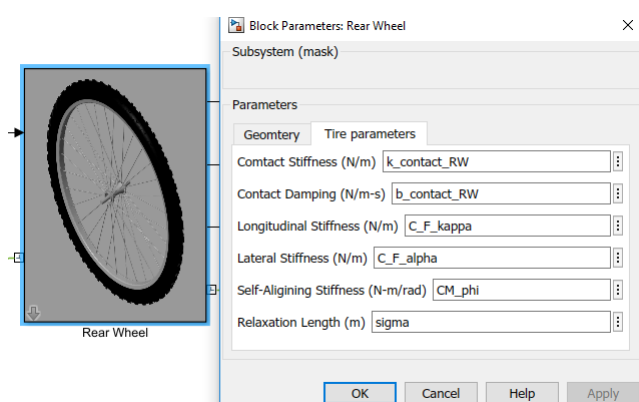


Figure C.4: Blue bike: Adjusting tyre parameters

The bicycle model has the following inputs: Initial simulation parameters and Inputs to the lateral disturbance and an impulse steering input. The simulation parameters are directly given at the joint blocks such as initial velocity as shown in figure C.5.

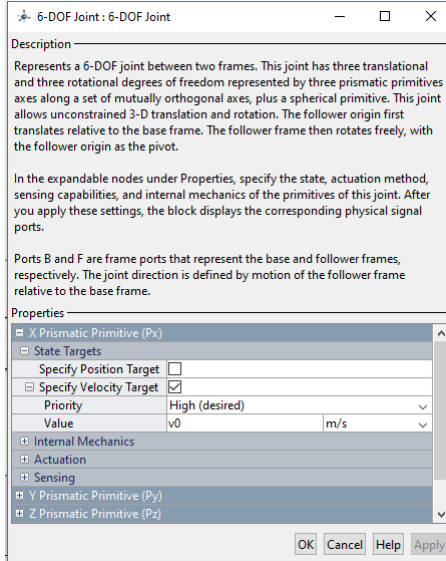


Figure C.5: Blue bike: Initial condition on velocity

Inputs in terms of lateral disturbances and steering impulse are given using a discrete impulse block from a digital signal processing toolbox (DSP) as shown in figure C.6. In case of a bicycle with feedback on  $T_\varphi$  and  $T_\delta$ , for balance control and riding in a curve respectively, these blocks are replaced with the inputs directly from the feedback  $T_\varphi$  and  $T_\delta$  as shown in figures (C.7 and C.8) respectively. The input  $T_\varphi$  is directly actuated to the rear wheel of the bicycle joint.

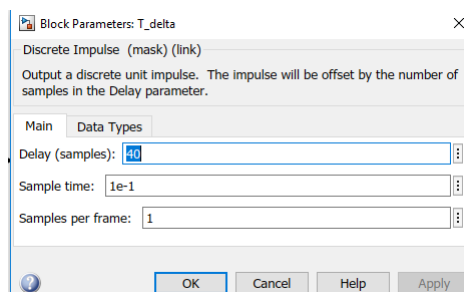
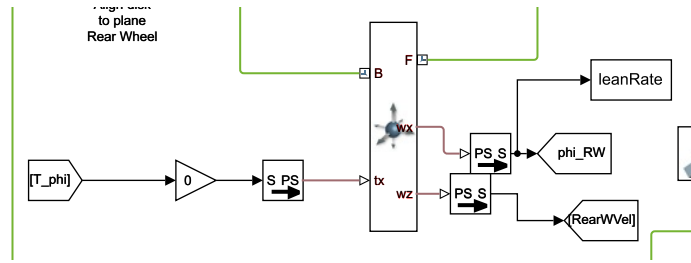
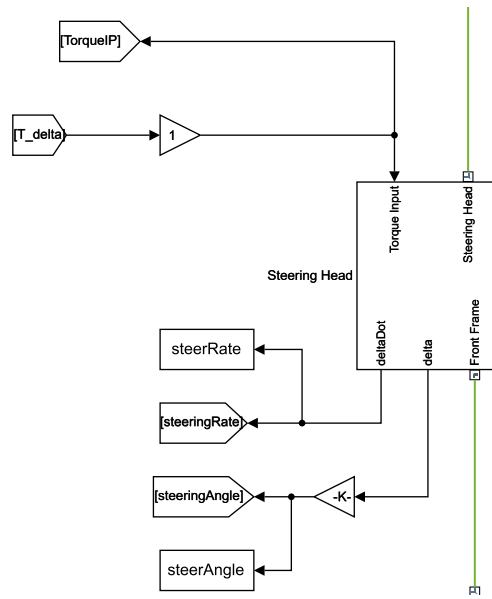


Figure C.6: Blue bike: Input lateral disturbance

Figure C.7: Bicycle: Feedback using  $T_\varphi$ Figure C.8: Bicycle: Feedback using  $T_\delta$ 

The feedback is implemented using Simulink blocks as shown in figures (C.9, C.10 and C.11). In figure C.9, a feedback  $T_\delta$  is used for balancing the bicycle at zero forward velocities. Figure C.10, shows a feedback using  $T_\varphi$  for hands-free riding in a curve. Similarly, figure C.11 shows the feedback using  $T_\delta$  on the steering for riding the bicycle in a curve.

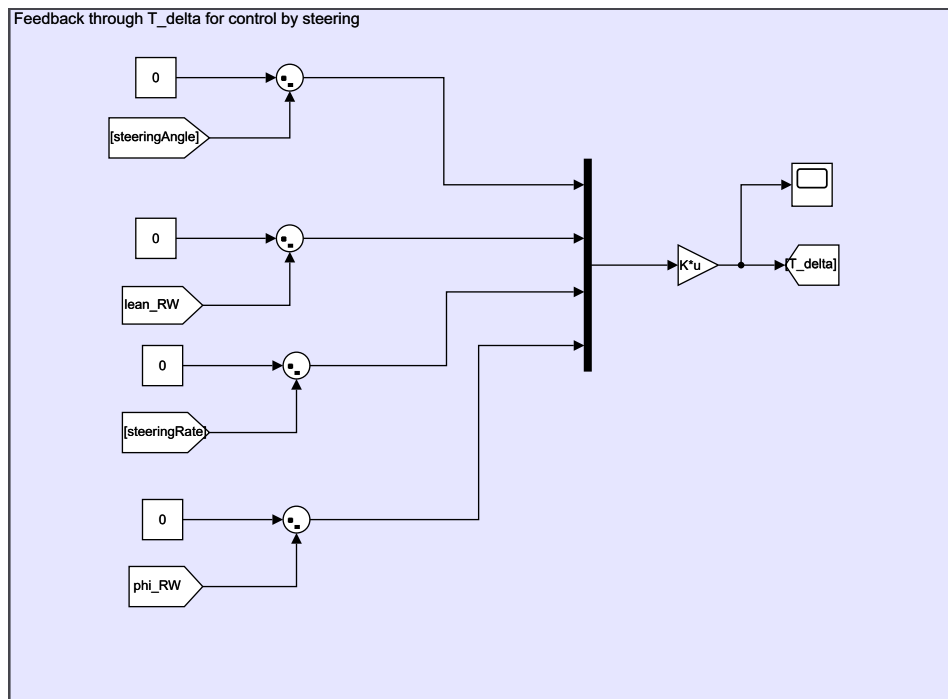


Figure C.9: Bicycle: Feedback using  $T_{\delta}$  for balance at  $v = 0m/s$

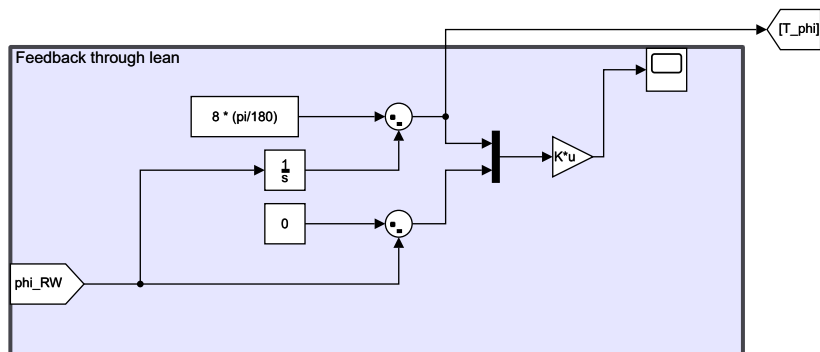


Figure C.10: Bicycle: Feedback using  $T_{\varphi}$  for hands free riding in a curve

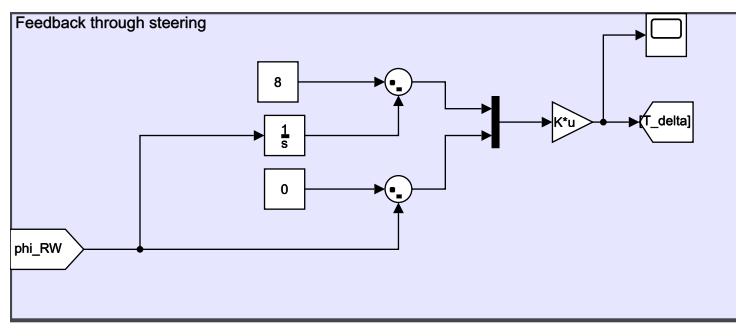


Figure C.11: Bicycle: Feedback using  $T_\delta$  for riding in a curve

All the outputs for measuring bicycle parameters are measured directly from the respective wheel and steering joints, except the measurement for leaning angle  $\varphi$  which is calculated separately inside the tyre model and is expressed as:

$$\varphi = \hat{n} \cdot e_{Axis} \quad (\text{C.1})$$

The respective Simulink block is shown in figure C.12. This is done in order to keep the consistency of parameters between the tyre model and the outputs displayed. Figure C.12 also shows the simulation terminating condition given when the lean angle reaches nearly  $90^\circ$ , indicating a bicycle which has fallen-over to the ground.

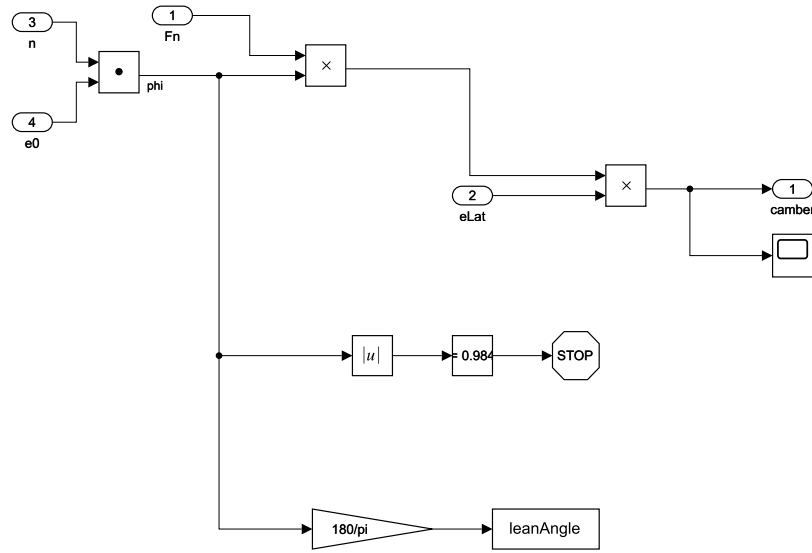


Figure C.12: Bicycle: Calculation of leaning angle  $\varphi$

Finally, the simulation can be directly visualized using mechanics explorer in SimMechanics as shown in figure C.13.

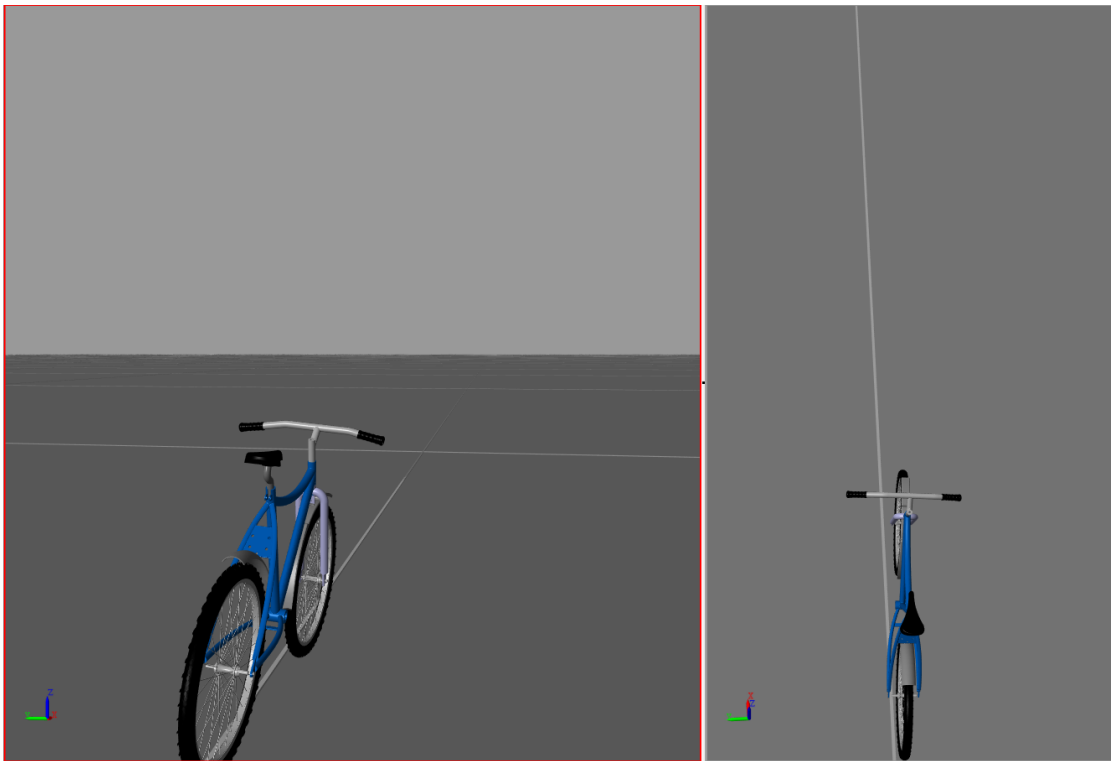


Figure C.13: Blue bike: Visualization in Mechanics explorer

# Bibliography

- [BDBK15] BULSINK, Vera E. ; DOIRA, Alberto ; BELT, Dorien van d. ; KOOPMAN, Bart: The effect of tyre and rider properties on the stability of a bicycle. In: *Advances in Mechanical Engineering* 7 (2015), Nr. 12, S. 1 – 19. <http://dx.doi.org/10.1177/1687814015622596>. – DOI 10.1177/1687814015622596
- [BH14] BLUNDELL, Micheal ; HARTY, Damian: *The Multibody Systems Approach to Vehicle Dynamics*. 1. Elsevier, 2014. – 768 S. – ISBN 9780080994253
- [DD10] DE VRIES, E J H. ; DEN BROK, J F A.: Assessing slip of a rolling disc and the implementation of a tyre model in the benchmark bicycle. (2010), S. 20–22
- [den] DEN BROK, J.F.A: *A SimMechanics Motorcycle Tyre Model for Real Time Purposes*, TU Delft, Diploma thesis
- [EL00] EVANGELOU, S ; LIMEBEER, DJN: Lisp programming of the 'sharp 1994'motorcycle model. In: ... /Research/Motorcycles/Reports (2000), 14. <http://portal-vip.cc.ic.ac.uk/pls/portallive/docs/1/50169.PDF>
- [Fra17] FRANCISCO, J. Garcia R.: *Development and implementation of pose estimation and localization for an autonomous bicycle*. Master Thesis Presentation, 2017
- [GM] GETZ, Neil H. ; MARDSEN, Jerrold E.: Control for an autonomous bicycl. IEEE International Conference on Robotics and Automation, Nagoya, , S. 1397 – 1402
- [JRLT17] JAVIER, Francisco ; ROSAS, Garcia ; LIU, S ; TURNWALD, Alen: Development and implementation of pose estimation and localization for an autonomous bicycle. (2017)
- [Lam] LAM, Pom Y.: *DESIGN AND DEVELOPMENT OF A SELF-BALANCING BICYCLE USING CONTROL MOMENT GYRO*, NATIONAL UNIVERSITY OF SINGAPORE, Masters thesis
- [Lu13] LU, Dang: Tire Model for Turn Slip Properties. In: *SAE Interna-*

- tional* (2013). <http://dx.doi.org/10.4271/2013-01-2371>. – DOI 10.4271/2013-01-2371
- [Mat18] MATHWORKS: *Six - DOF joint in SimMechanics*. <https://in.mathworks.com/help/physmod/sm/ref/6dofjoint.html>. Version: 2018
- [Mil] MILLER, Steve: *Simscape Multibody Contact Forces Library*. <https://www.mathworks.com/matlabcentral/fileexchange/47417>
- [MP97] MAURICE, J.P ; PACEJKA, H.B: Relaxation length behavior of tyres. In: *Vehicle System Dynamics Supplement S1* (1997), Nr. 27, S. 339–342. <http://dx.doi.org/10.1080/00423119708969668>. – DOI 10.1080/00423119708969668
- [MPRS07] MEIJAARD, J.P. ; PAPADOPOULOS, Jim M. ; RUINA, Andy ; SCHWAB, A.L.: Linearized dynamics equations for the balance and steer of a bicycle: a benchmark and review. In: *Proceedings of the Royal Society A: Mathematical, Physical and Engineering Sciences* (2007). <http://dx.doi.org/10.1098/rspa.2007.1857>. – DOI 10.1098/rspa.2007.1857. – ISBN 1364-5021
- [MT18] MESSNER, Bill ; TILBURY, Dawn: *Control tutorials for Matlab and Simulink*. <http://ctms.engin.umich.edu/CTMS/index.php?example=Introduction&section=SystemAnalysis>. Version: 2018
- [Pac] PACEJKA, H.B.: Tyre and Vehicle Dynamics.
- [Pac05a] PACEJKA, Hans B.: A bicycle model for education in multibody dynamics and real-time interactive simulation. In: *Vehicle system dynamics* 43 (2005), S. 3–17. <http://dx.doi.org/10.1080/00423110500140013>. – DOI 10.1080/00423110500140013
- [Pac05b] PACEJKA, Hans B.: Spin: camber and turning. In: *International Journal of Vehicle Mechanics and Mobility* 43 (2005), S. 3–17. <http://dx.doi.org/10.1080/00423110500140013>. – DOI 10.1080/00423110500140013
- [Rui18a] RUINA, Andy: *Bike test on Lateral perturbation - Andy Ruina*. <https://www.youtube.com/watch?v=j0i1P8kb8dM>. Version: 2018
- [Rui18b] RUINA, Andy: *Bike test on stable long run - Andy Ruina*. [https://www.youtube.com/watch?v=Fy\\_XRVO-j18](https://www.youtube.com/watch?v=Fy_XRVO-j18). Version: 2018
- [Sch03] SCHLÖTTER, Micheal: Multibody System Simulation with SimMechanics, University of Canterbury. (2003)
- [SMK12] SCHWAB, A.L ; MEIJAARD, J.P ; KOOIJMAN, J.D.G: Lateral dynam-

- ics of a bicycle with a passive rider model: stability and controllability. In: *Vehicle System Dynamics* 50 (2012), Nr. 8, S. 1209â1224
- [TA18a] TURNWALD, Alen ; AHMED, Rizwan: *GitHub: Blue bike model files.* [https://github.com/turnwald/CAE\\_Exercise/blob/master/BikeSimulator.zip](https://github.com/turnwald/CAE_Exercise/blob/master/BikeSimulator.zip). Version: 2018
- [TA18b] TURNWALD, Alen ; AHMED, Rizwan: *Youtube: Link to video description for SimMechanics wheel, tricycle and bicycle models.* <https://youtu.be/UStQpcYUEko>. Version: 2018
- [TL18a] TURNWALD, Alen ; LIU, Steven: A Nonlinear Bike Model for Pur- poses of Controller and Observer Design. In: *IFAC-Papers OnLine* (2018)
- [TL18b] TURNWALD, Alen ; LIU, Steven: Modeling of a bike in Hamiltonian and Lagrangian Framework. (2018), S. 1–19
- [TL18c] TURNWALD, Alen ; LIU, Steven: Modelling of a bike in Hamiltonian and Lagragnian Framework. In: *Month* 00 (2018), Nr. 20, S. 1–19
- [Tur18] TURNWALD, Alen: *Autonomes Zweirad projekt an der TU Kaiser- slautern.* [https://www.eit.uni-kl.de/liu/forschung/autobike\\_g.html](https://www.eit.uni-kl.de/liu/forschung/autobike_g.html). Version: 2018
- [Whi99] WHIPPLE, F.J.W: The stability of the motion of a bicycle. In: *Quart. J. Pure Appl. Math* 30 (1899), Nr. 120, S. 312–348